Thesis

Studies of the Chemical Reactions with Atomic Hydrogen on Si(100) Surfaces by Infrared Reflection Absorption Spectroscopy

Zhihong Wang

Doctor of Philosophy

Department of Structural Molecular Science
School of Mathematical and Physical Science
The Graduate University for Advanced Studies

2002

Abstract

Chemical reactions on silicon surfaces are very important and interesting from the viewpoint of both semiconductor technology and surface science. In this thesis we shall focus on (I) the hydrogen diffusion into silicon bulk causing infrared peak width broadening, (II) the reaction of water with ideally hydrogen terminated Si(100)-(2×1) surfaces and (III) the reaction of atomic hydrogen with water covered Si(100)-(2×1) surfaces.

Hydrogen reaction with Si(100) surface is an important model system in surface science studies. This system has been used extensively in semiconductor fabrication technology preventing the Si(100) surfaces from contamination and also employed as a precursor in several chemical vapor deposition reactions. Interaction of hydrogen with silicon surfaces has been extensively studied by several surface techniques such as temperature programmed desorption (TPD), scanning tunneling microscopy (STM), electron energy loss spectroscopy (EELS) as well as Fourier-transform infrared spectroscopy (FTIR). These investigations have thrown light on several aspects of hydrogen reaction with Si(100) surfaces. When silicon surface is exposed to atomic hydrogen, it generally forms (3×1), (2×1) and (1×1) surface structures depending on the adsorption conditions. However, very few reports have appeared on hydrogen diffusion into silicon bulk on nearly ideally hydrogen terminated silicon surfaces. Most of them have focused on theoretical and TPD studies.

We have investigated the dependence of the line width of the coupled monohydride symmetric stretching vibration on the H-terminated Si(100)-(2×1) surface as a function of temperature and hydrogen exposure by infrared reflection absorption spectroscopy (IRRAS) using $CoSi_2$ buried metal layer substrate (BML-IRRAS) (Fig. 1). We find that even for nearly ideally H-terminated Si(100) surface, the line width changes significantly depending on the hydrogen exposure and exposure temperatures. The minimum line width observed on the nearly ideally H-terminated surface at around 670 K and 500 L hydrogen exposure agrees or even better than the reported homogeneous line width determined by the dephasing effects. The dependence of line width broadening on hydrogen exposure and temperature on nearly ideal H-terminated regions can not be explained by either dephasing effects or inhomogeneities due to the coexistence of higher hydrides, or contamination by the residual water. The line width broadening is also not due to the surface roughness induced by the hydrogen etching. We suggest that the line width broadening is essentially caused by subsurface hydrogen.

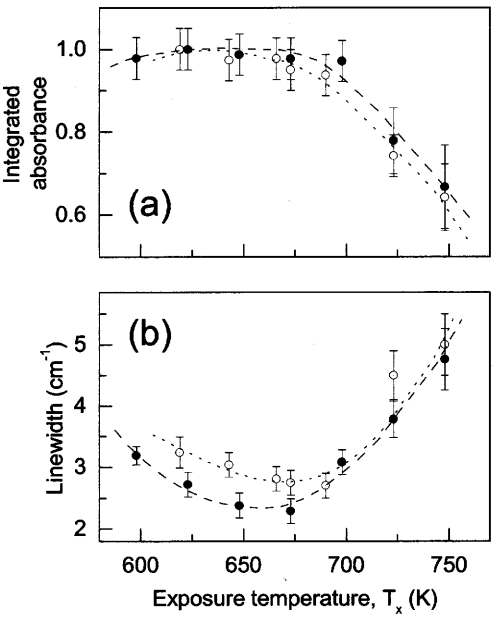

Fig. 1 Dependence of the normalized integrated absorbance (a) and the linewidth (b) on hydrogen exposure temperature for the hydrogen exposure of: (1) • : 500 L; (2) o:1000 L

We have carried out a number of experiments to investigate the presence of subsurface hydrogen and its effect on the infrared line width broadening. The Si(100) surface was initially cleaned by flashing it to high temperature (~ 1150 K) and exposed

to 5000 L atomic deuterium at about 670 K. Then the surface silicon deuterides were completely replaced by exposing 500 L atomic hydrogen at 620 K. The sample
was then annealed for one minute at fixed higher temperatures in order to check the reappearance of surface deuterium from silicon bulk by IR at 1525 cm^{-1}. We find that with increasing annealing temperatures, the decomposition rate of coupled monohydride (ν Si-H_{CM}) characterized by 2098 cm^{-1} becomes faster. This is simultaneously followed by the appearance of coupled monodeuteride peak at 1525 cm^{-1} which can only be explained by the diffusion of deuterium atoms from silicon bulk to the surface at higher annealing temperatures.

We have also measured the amount of deuterium incorporated into the Si bulk by conventional TPD experiment for the samples made by the similar process of deuterium exposure and replacement by hydrogen as described above. The ν Si-H_{CM} IR line width, separately measured for 500 L hydrogen exposure, is found to increase from 2.1 cm^{-1} at 673 K to 3.2 cm^{-1} at 598 K which is roughly in proportion to the amount of deuterium atoms incorporated in the Si bulk as determined by TPD measurements. Similarly, by keeping the exposure temperature constant, for example at 673 K, the IR peak width broadening occurs from 2.1 cm^{-1} at 500 L to 2.5 cm^{-1} at 1000 L of hydrogen exposure. We have carried out several measurements to confirm these trends.

The IR and TPD experiments clearly demonstrate that the diffusion of hydrogen atoms does occur into the Si(100) bulk and causes inhomogeneous broadening of the IR line width.

The interaction of water with Hydrogen-terminated Si(100) surface is another important topic for investigation by BML-IRRAS technique. For this purpose, nearly ideally H-terminated Si(100) surfaces were prepared by exposing the clean Si(100) surface to 500 L hydrogen at 650 K. These surfaces were exposed to controlled amount of water and the changes occurring on the surfaces were monitored by BML-IRRAS as a function of the water exposure. The surface oxidation of Si has been observed due to water adsorption and it is concluded that the nearly ideally H-terminated Si(100) surface is still quite reactive with water. However, it has also been noted that the reactivity of H-terminated surface has diminished due to the passivation effect of the surface hydride layer on Si against the background water in the ultrahigh vacuum.

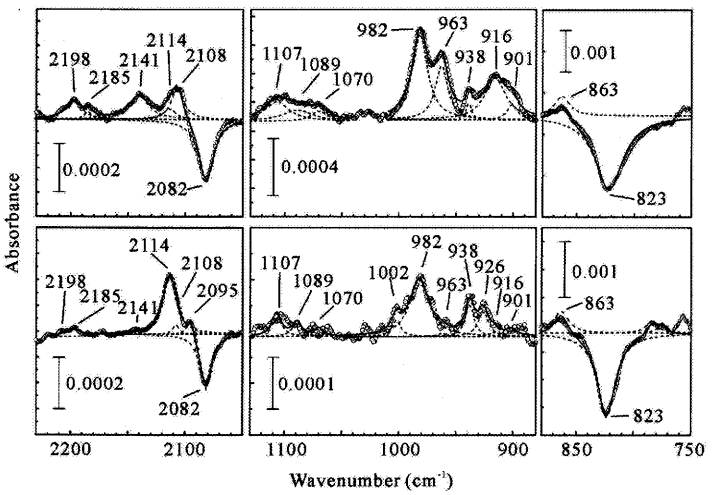

Fig. 2 Observed BML-IRRAS spectra (circles) of atomic H-exposed H_2O:Si(100)-(2×1) surfaces at Tm = 373 K for D=1000 L (top) and D=50 L (bottom). The results of curve-resolutions assuming a Lorenzian form are compared (solid and dotted lines).

The water-adsorbed Si(100) systems have received considerable attention due to its apparent simplicity and the widespread use of H_2O in industrial oxidation processes. In spite of many excellent scientific and technological studies, much remains to be understood about this system at microscopic level. Vibrational spectroscopy and *ab initio* quantum chemical cluster calculations have established that there is no barrier to dissociative chemisorption of H_2O on Si(100)-(2×1) surfaces forming stable Si-H and Si-OH bonds. Annealing of water exposed Si surfaces induces the insertion of oxygen atoms into Si back bonds or the formation of epoxides through dehydrogenation. It has also been reported that the initial Si(100)

surface is comprised of an array of isolated and intra-row coupled dimers, which are coupled by a hydrogen bonding between OH groups that reside on the same end of adjacent dimers in a dimer row. It is proposed that such inter-dimer coupling facilitates the subsequent transfer of oxygen between dimers forming oxygen agglomeration, so that the initial oxidized surface is comprised of an inhomogeneous array of zero-, one-, and two-oxygen containing dimers.

Recently the water-covered Si(100) surface exposed to atomic hydrogen at 220 K has been studied using external transmission (ET) infrared geometry method (Weldon et al. *J. Chem. Phys.* **113**, 2440, (2000)). These experiments conclusively show that the atomic hydrogen exposure induces oxygen insertion which is usually achieved by annealing the water-covered Si(100) surface. However, in this case, single O incorporation predominates which can be explained by the following mechanism. The first step is the elimination of H_2 into gas phase by the abstraction of hydrogen atom from the surface Si-OH group forming the SiO· radical species. The oxygen radical is preferentially inserted into the Si-Si dimer bond, thereby forming the single oxygen-inserted species. In spite of its scientific and technological importance, the investigation on atomic hydrogen induced-oxidation has only been performed over a limited range of temperature and hydrogen exposures.

In the present work, the BML-IRRAS has been used to investigate the atomic hydrogen-induced oxidation on the water-adsorbed Si(100)-(2 × 1) surface over a wide range of temperatures (268 ~ 373 K) and exposures of atomic hydrogen (Fig. 2). The BML-IRRAS has high sensitivity for the perpendicular component over a wide frequency range including less than 1000 cm^{-1} (the frequency cut off region of a multiple internal reflection (MIR) geometry). Owing to this unique characteristic of BML-IRRAS, a series of bending modes consisting of oxidized and nonoxidized SiH_2, which are not observed or very week by the ET geometry because of its low sensitivity to the perpendicular component, are observed clearly for the first time, and the new oxidation mechanism is proposed.

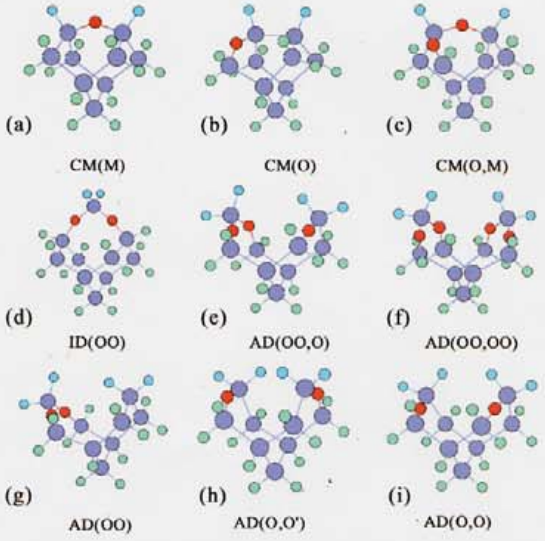

Fig. 3 Models of the different clusters investigated in this work. Atoms are represented as follows: dark blue denotes Si, red denotes O, light blue denotes H, and green denotes tritium. The meaning of the symbols are as follows: CM is coupled monohydride, ID is isolated dihydride, AD is adjacent dihydride, M in a bracket is an oxygen atom inserted into Si-Si dimer bond, and O is an oxygen atom singly inserted to Si back bond, and OO is doubly inserted oxygen atoms. O,O and O,O' are two singly inserted oxygen atoms at the *cis* and *trans* positions of back bonds with coupled or adjacent Si atoms, respectively.

Using the well-documented B3LYP gradient corrected density functional method with the polarized 6-31G** basis set for all atoms, we calculated the IR vibrational frequencies. The calculated harmonic frequencies are obtained by multiplying uniform frequency shift factors for each type of vibration, which were determined by using the assignment-established modes: $\upsilon\ SiH_{CM} = 2099\ cm^{-1}$, $\upsilon\ SiH_{CM(M)} = 993\ cm^{-1}$, and $\upsilon\ SiO^2_{CM(O,M)} = 1042\ cm^{-1}$ (Weldon et al. *Phys. Rev. Lett.* **79**, 2851, (1997)), $\upsilon\ SiH_{ID} = 2090\ cm^{-1}$, $\upsilon\ SiH_{AD} = 2107\ cm^{-1}$, $\delta\ SiH_{ID} = 902\ cm^{-1}$, and $\delta\ SiH_{AD} = 913\ cm^{-1}$ (Noda et al. *Chem. Phys. Lett.* **326**, 163 (2000)). By comparing the observed peaks with calculations many important peaks are

uniquely assigned. (The definitions of these symbols are given in the captions of Fig. 3). The most interesting observations are three pairs of doublet peaks, 901 and 916 cm^{-1}, 926 and 938 cm^{-1}, and 963 and 982 cm^{-1}. These are assigned to δSiH_{ID} and δSiH_{AD} with zero, one and two inserted oxygen atoms at Si back bonds, respectively. The perpendicular dynamic dipole moments of these modes make these peaks insensitive for the ET geometry (Even at 60 degree incidence, the δSiH_{ID} peak intensity observed on the H:Si(100)-(3×1) surface by ET geometry (Weldon et al. *Phys. Rev. Lett.* **79**, 2851, (1997)) is about 1/5 of the BML-IRRAS method (Noda et al. *Chem. Phys. Lett.* **326**, 163 (2000))). The small peaks observed at 990 ~ 1050 cm^{-1} range are assigned to the SiO stretching mode of coupled monohydrides with one to three oxygen atoms at the Si back bonds and/or the Si-Si dimer bond. The strong peak at 2114 cm^{-1} is assigned to the overlapping of the perpendicular components of $\nu SiH_{CM(M)}$ and $\nu SiH_{CM(O,M)}$. The peak at 2141 cm^{-1} observed in the high atomic dose region is assigned to the overlapping of the perpendicular components of $\nu SiH_{CM(OO,OO)}$ and $\nu SiH_{CM(OO,O)}$. The peaks at 2198 and 2185 cm^{-1} are assigned to the overlapping of the perpendicular components of $\nu SiH^{2}_{AD(OO,OO)}$ and $\nu SiH^{3}_{AD(OO,O)}$, and $\nu SiH^{2}_{AD(OO)}$, respectively. The 2108 cm^{-1} peak may be assigned to the overlapping of $\nu SiH_{CM(O,OO)}$ (calc. = 2108 cm^{-1}) and $\nu SiH_{CM(O,O)}$ (calc. = 2106 cm^{-1}). The band observed at ~ 1107 cm^{-1} is assigned to the overlapping of νSiO_{ID} and νSiO_{AD} with one to four oxygen atoms inserted into Si back bonds and νSiO_{CM} with three and four oxygen atoms inserted into Si-Si dimer and/or Si back bonds. From the studies, we have found that the atomic hydrogen-induced oxidation on water covered Si(100)-(2×1) surface has different reaction routes depending on the atomic hydrogen dose. At low atomic hydrogen dose region (< 100 L), the mechanism is well explained by the reaction H-Si-Si-OH + 2H → H-Si-O-Si-H or H-Si-Si(O)-H + H_2 proposed by Weldon et al. It is observed that the vibrational band at 982 cm^{-1} appears in IRRAS spectra only on Si(100) surface exposed to atomic hydrogen but not on the Si surface thermally annealed after water adsorption. The appearance of this peak, even in the lower hydrogen exposure region (< 100 L), suggests the existence of another hydrogen atom-induced oxidation channel, H-Si-Si-OH + 2H → SiH_2 +$Si(O)H_2$ which is followed by the formation of two oxygen atoms inserted SiH_2 through the inter-dimer oxygen atom migration. The increase of 982 cm^{-1} peak intensity with decreasing 2114 cm^{-1} peak intensity at hydrogen exposures greater than 100 L suggests that the O-inserted dihydride species are also formed by the hydrogen atom-induced reaction of O-inserted dimer species such as H-Si-O-Si-H + 2H → SiH_2 + $Si(O)H_2$. The observed IRRAS spectra show that double oxygen insertion is clearly favored over single oxygen insertion. This is also reasonable from the thermo-dynamical point of view. The calculated energy of AD(OO) is 0.449 eV and 0.438 eV lower than those of AD(O,O) and AD(O,O'), respectively. Also, CM(OO) is 0.561 eV and 0.509 eV more stable than the respective energies of CM(O,O) and CM(O,O').

Contents

List of Figures

List of Tables

Chapter 1

Introduction

1.1 Background

Chemical reactions on silicon surfaces are very important and interesting from the viewpoint of both semiconductor technology and surface science. Many studies have been carried out on silicon surfaces for more than 30 years [1–55].

Silicon crystals have diamond structure. The bulk silicon atoms are sp^3 hybridized and bonded to four nearest atoms in the tetrahedral coordination. The covalent bonds are 2.35 Å long with a bond strength of 226 kJ/mol and bond angle of 109.4^o [56]. When the crystal is cut or cleaved, those bonds are broken, creating dangling bonds at the surface. The number and direction of these dangling bonds will depend on the macroscopic direction of the surface, as shown schematically in Figure 1.1. The surface energy is lowered by reducing the number of dangling bonds by rebonding, and this leads to a wide variety of surface reconstructions on silicon surface. These dangling bonds are the source of the silicon surface chemical activity. Depending on the cutting angle and reconstruction, the silicon surfaces will form different surface structures. The most important surfaces are Si(100) with (2×1) reconstruction [57–59] and Si(111) with (7×7) reconstruction [57, 60, 61].

Hydrogen reaction with silicon surfaces is an important model system in surface science studies. The surface structures after atomic hydrogen adsorption have been investigated and well understood [1–11, 13, 14]. This system has been used extensively in semiconductor fabrication technology preventing the silicon

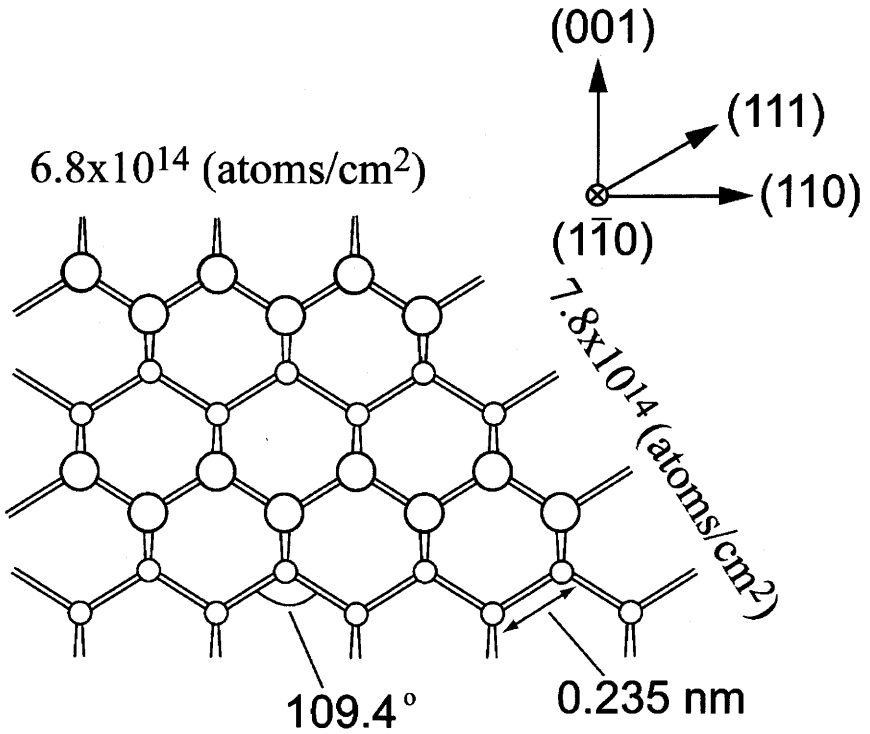

Figure 1.1: The dangling bond formation on the unreconstructed silicon surface. Each Si atom in the bulk is tetrahedrally bonded to four nearest atoms [60].

surfaces from contamination and also employed as a precursor in several chemical vapor deposition (CVD) [12, 19, 21–23, 28, 37, 40]. In 1990, it was found that the silicon surfaces were terminated by hydrogen atoms instead of fluorin atoms when treated by HF solution [22]. During the same period, ideally hydrogen terminated Si(111)-(1×1) surfaces were obtained by treating the clean Si(111) surface with buffered NH_4F solution [23, 27]. It attracted many researchers interest since it gives flat silicon surfaces on atomic level scale.

Interaction of hydrogen with silicon surfaces has been extensively studied by several surface techniques such as temperature programmed desorption (TPD) [16, 18, 20, 26, 30, 31], scanning tunneling microscopy (STM) [24, 25, 28, 32, 37], electron energy loss spectroscopy (EELS) [1, 3, 8, 10, 13, 14, 41], reflective high-energy electron diffraction (RHEED) [15, 17], low energy electron diffraction

(LEED) [11, 26, 57] as well as infrared spectroscopy (IR) [4–7, 9, 11, 12, 19, 21, 23, 27, 29, 33–35, 40, 46]. These investigations have thrown light on several aspects of hydrogen reaction with silicon surfaces. A number of theoretical studies have been reported clarifying various aspects of silicon surface chemistry [42, 45, 51, 54, 55].

1.2 Chemical reaction studies of atomic hydrogen on Si(100) surfaces

The Si(100) surface is of great significance in the semiconductor industry and has been the subject of extensive theoretical and experimental investigations. After Si(100) surface was cleaned at high temperatures, top silicon atoms will reconstruct to form a 2×1 structure [57]. The surface dangling bonds will reconstruct to form dimers (surface Si-Si bond) to reduce the surface energy. This surface is very active since the dangling bonds connected to the top silicon atoms are unsaturated (Fig. 1.2).

When such surface is exposed to atomic hydrogen, it will mainly form three types of surface structures depending on the adsorption/annealing condition as shown in Fig. 1.3. The Si(100)-(2×1) monohydride phase is formed after the saturation exposure at 600 K [26, 28, 62, 63] or after the high exposure at lower temperatures followed by annealing above 575 K [11, 62, 64]. A clear (2×1) LEED pattern [11, 26] is observed and the vibrational spectroscopy also shows only the existence of Si-H species [9, 11, 64, 65]. The Si(100)-(3×1) phase is formed when the silicon surface is saturated with atomic H at 400 K [11]. The IR spectra showed the presence of both monohydride and dihydride species on the surface. The surface consists of alternate coupled monohydride and dihydride structure which is confirmed by STM [28]. The saturated adsorption of atomic H to silicon surface at 300 K forms (1×1) structure which is confirmed by LEED [62, 63]. The similar IR spectra of 300 K and 400 K adsorption were first reported by Chabal et al. [11], lead them to the conclusion that the (1×1) structure is merely a disordered (3×1) phase. Further investigations indicated that the (1×1) phase is a disordered mixture of mono-, di- and trihydride species [26, 28].

The TPD experiment done on a hydrogen terminated Si(100) sample prepared at room temperature, shows three H_2 desorption peaks called β_1, β_2 and β_3 cen-

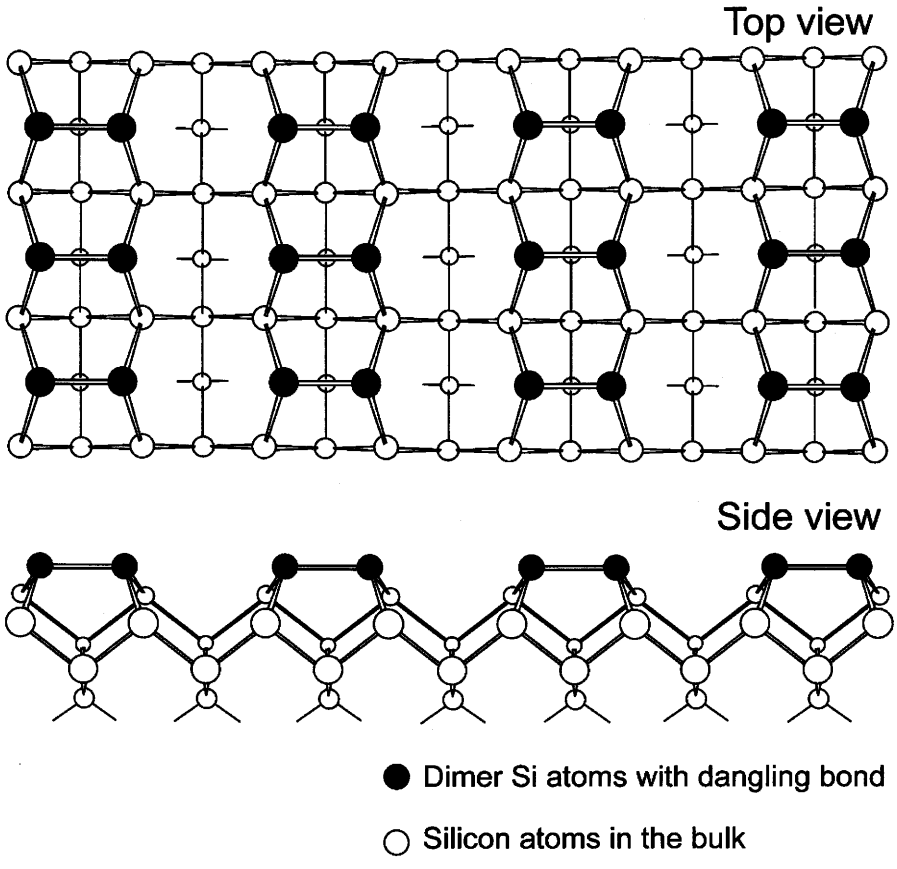

Figure 1.2: Si(100)-(2×1) reconstructed structure after cleaning at high temperature.

tering at 760 K, 630 K and 450 K, respectively [18, 26, 30, 31]. The β_1 peak has been assigned to the H_2 desorption from coupled monohydride species. The β_2 and β_3 peaks are assigned respectively to the H_2 desorption from dihydride and trihydride species [26]. From these studies, it is clear that the thermal stability for these three species is in the order of monohydride > dihydride > trihydride.

Hill et al. employed the STM atom-tracking technique to follow the individual diffusive hops of single H and D atoms on the Si(100) surface in ultrahigh vacuum [66]. They reported that H on the bare Si(100) surface has two diffusive modes: intradimer and intrarow diffusion. The diffusion rate increased with increasing surface temperature. From their studies, attempt frequencies and activation energies for diffusion along the dimer row (intrarow) and between the atoms of a

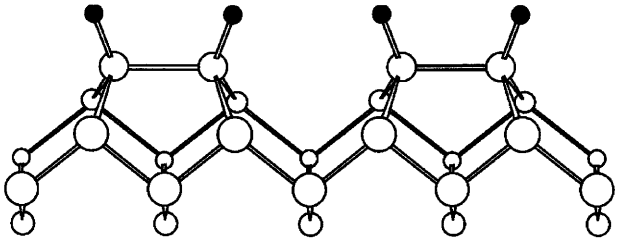

H/Si(100)-(2X1) phase
(coupled monohydride structure)

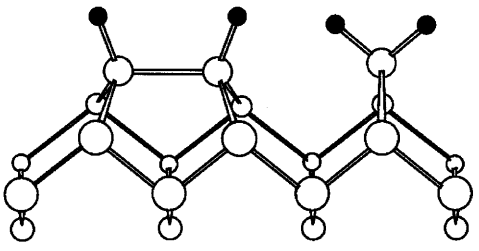

H/Si(100)-(3X1) phase
(alternating coupled monohydride and dihydride structure)

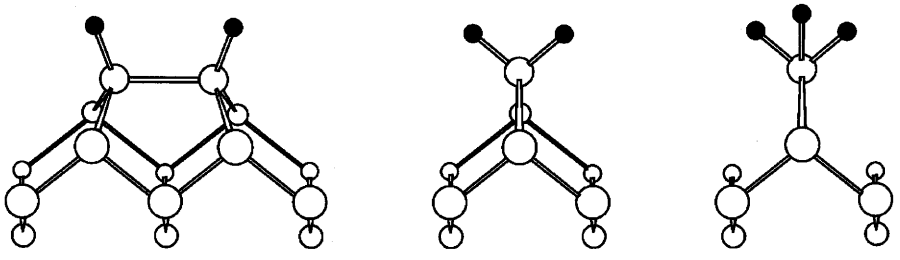

monohydride dihydride trihydride

H/Si(100)-(1X1)
(disordered mixture of mono-, di-, and trihydride)

Silicon
Hydrogen

Figure 1.3: Surface structures of Si(100) after atomic hydrogen adsorption at different conditions.

single Si dimer (intradimer) have been extracted. For the intrarow H diffusion, an activation energy of 1.75 ± 0.10 eV and an attempt frequency of $10^{14.5\pm0.8}$ Hz

are found. For the intradimer H diffusion, an activation energy of 1.01 $\pm$ 0.05 eV and a low attempt frequency of $10^{10.3\pm0.5}$ Hz are found.

Van de Walle et al. studied the behavior of hydrogen in crystalline silicon by state-of-the-art theoretical techniques, based on density-functional theory in the local-density approximation and *ab initio* norm-conserving pseudopotentials in a supercell geometry [67]. They concluded that the bond-center site (between Si-Si bond) is the globe minimum for the neutral and positive charge states. In the negative charge state, the tetrahedral interstitial site is preferred. These conclusions have also been supported by ion-channeling experiments [68]. The diffusion mechanism of hydrogen in amorphous silicon had been discussed by using *ab initio* molecular dynamics simulation method by Su and Pantelides[69]. Using the first-principles finite-temperature simulations, they demonstrated vividly that H is not released spontaneously, but awaits the arrival of a floating bond (FB). The "migrating species" is a FB-H complex, with H jumping from Si to Si and FB floating in the vicinity. Migration stops when the FB veers away.

1.3 Chemical reaction studies of water on Si(100) surfaces

The phenomenal progression in microelectronics miniaturization has now reached the point where gate oxide thicknesses of $\sim$ 1 nm are being grown for the 60 nm transistor that will be the standard at the end of the next decade. Consequently, the need for precise understanding and control of the Si/SiO_2 interface homogeneity is of paramount importance. However, despite the plethora of studies of this critical interface over the past thirty years, very little is known about the growth of the first monolayer (which will comprise 1/3 of the total oxide thickness in a 1 nm film). This dearth of detailed information about the microscopic oxidation processes results largely from the absence of both suitable experimental probes with the requisite sensitivity and theoretical approaches with sufficient accuracy at reasonable computational cost. Recently, these limitations have been overcome and the pathways for initial oxygen insertion and agglomeration have been identified [38, 70]. In short, it was found that for the model $H_2O/Si(100)$-(2×1) system, oxidation occurs inhomogeneously leading to the formation of epoxide

species at temperatures above 800 K.

Gurevich et al. have utilized broadband infrared (IR) spectroscopy in combination with comprehensive *ab initio* quantum cluster calculations to study the long-range coupling between dissociated water molecules [42]. They show that, upon exposure to water, the dimer structure of the clean surface is transformed into an array of "isolated" and "coupled" dimer units, with the coupling occurring by the interaction of neighboring surface hydroxyl groups. It has been found that this interdimer bonding is $\sim$ 2 kcal/mol more stable than the isolated dimer case. They propose that such interdimer coupling facilitates the subsequent transfer of oxygens between dimers and that the coupled dimer units consequently act as nucleation sites for oxidation.

The adsorption and subsequent reaction of water on Si(100) surfaces has been the subject of detailed investigations by many groups [36, 71–75]. Surface vibrational spectroscopy has been used as a probe in the investigation of water on Si(100). EELS as well as Fourier transform infrared spectroscopy (FT-IR) have unambiguously established that dissociation into H and OH takes place on the clean Si(100) surface [36, 74–76]. STM techniques have also been used to investigate the adsorption characteristics of H_2O on Si(100)-(2×1) surfaces [77]. These studies show a 2×1 structure consisting of Si-H and Si-OH obtained at saturation, but there is no long-range order in the arrangement of H and OH group. A detailed understanding of H_2O dissociation is also investigated combined with the first-principle quantum chemical cluster calculations [36]. The pathway for adsorption of H_2O on Si(100) surfaces and further reactions have also been studied using density functional theory [45, 78].

Weldon et al. investigated the water covered Si(100)-(2×1) surface and subsequently annealed at high temperatures and reacted with atomic hydrogen at 220 K by using external transmission (ET) infrared geometry technique [49]. They proposed that one and two oxygen-containing dimers are formed almost simultaneously during the thermal decomposition of water on this surface. The oxygen agglomerations seem to play an important role upon further annealing. For the atomic hydrogen reaction with water covered Si(100)-(2×1) surface, only single oxygen insertion into silicon back bond has been proposed.

1.4 Purpose and brief summary of the present studies

Because the importance of chemical reactions on Si(100) surface both from the surface science and semiconductor fabrication, tremendous number of chemical and physical detective methods have been used. Despite these huge amount of investigations, microscopic, namely, molecular science level knowledge for chemical reactions on Si(100) surfaces is very little. Based on this consideration, I have made the following guiding principles for my Ph. D thesis studies.

(1) The reaction of hydrogen atom with Si(100) surfaces is the most simple model system to investigate the chemical reaction on Si(100) surfaces.

(2) Water adsorbed Si(100) surfaces and the further oxidation or chemical reactions are important systems in semiconductor microfabrication processes.

(3) The *in situ* high resolution surface vibration spectroscopy is the most suitable technique for getting microscopic knowledge for these systems.

(4) Since a lot of vibrational frequencies are located at the $700 \sim 1200$ cm^{-1} region, infrared reflection absorption spectroscopy (IRRAS) using buried metal layer substrates (BML-IRRAS), which has a sufficient sensitivity in the finger print region, is the most suitable technique.

(5) When using BML-IRRAS, we must first confirm the surface is well defined after the epitaxial growth of the thin silicon layer on the surface.

Based on these ideas, I have carried out the following series of experiments.

The IR line width (full width at half maximum (FWHM)) is an important parameter which reflects the adsorbate-surface and intermolecular interaction conditions. The line width broadening contain two parts called homogeneous and inhomogeneous line width broadening. In general, we define here homogeneous line width as being caused by damping of the vibration due to interaction of the vibration molecule with the silicon surface such as phonon coupling or electron-hole pair creation. On the other hand, inhomogeneous broadening is caused by inhomogeneous distribution of individual oscillator frequencies determined by the molecule's adsorption site of intermolecular interaction. Homogeneous broadening due to pure dephasing and dipole-dipole coupling have been investigated and the observed theoretical line widths are 0.6 cm^{-1} and 1.2 cm^{-1} respectively

at 300K and 373 K [79]. However, no detailed investigations based on the well defined surface structures are available on inhomogeneous broadening. The investigation of the inhomogeneity is also very important since the BML-Si substrate is used. In the present work, the dependence of the line width of the coupled monohydride symmetric stretching vibration with the H-terminated Si(100)-(2×1) surface on the exposure temperature and the hydrogen exposure is investigated by using BML-IRRAS. Even for nearly ideally H-terminated Si(100) surface, the line width significantly changes depending on the exposure temperature and the hydrogen exposure. Combined with the TPD experiment, the reason of the line width broadening is discussed. These studies provide in depth knowledge of how to get the ideal H-terminated Si(100)-(2×1) surface which is very important for further studies.

The chemical reactivity of the hydrogen terminated Si(100) surface with water is another interesting and important topic not only for the theoretical studies but also for semiconductor processes. These studies are important to know the passivation effect of hydrogen terminated Si(100) surfaces and the initial mechanisms of the surface oxidation.

The water adsorbed Si(100) system has received considerable attention due to its apparent simplicity and widespread use of H_2O in industrial oxidation process. Recent experiments of exposing the water-covered surface to atomic hydrogen at 220 K by the ET infrared geometry showed that atomic hydrogen also induces the oxygen insertion like annealing, but in this case single O incorporation predominates [49, 70]. Concerning this atomic hydrogen induced-oxidation, however, investigation is only with a limited temperature and a hydrogen exposure in spite of its scientific and technological importance. In this work, the atomic hydrogen-induced oxidation on the water adsorbed Si(100)-(2×1) surface is investigated for a wide range of temperatures (268 $\sim$ 373 K) and exposures of atomic hydrogen by BML-IRRAS technique, which has high sensitivity for the perpendicular component at the wide frequency range including less than 1000 cm^{-1} (the frequency cut off region of a multiple internal reflection (MIR) geometry). Combined with cluster model theoretical calculation using density functional theory, a series of bending modes consisting of oxidized and nonoxidized SiH_2, which can't be observed by the ET geometry due to its insensitiveness to the perpendicular com-

ponent, are observed clearly for the first time, and the new oxidation mechanisms are also proposed.

All of these investigations give us fundamental knowledge of molecular science with chemical reactions on Si(100) surfaces and will establish a new starting point to explore more complex systems of semiconductor materials.

Bibliography

[1] H. IBACH and J. E. ROWE, *Surf. Sci.* **43**, 481 (1974).

[2] E. G. MCRAE and C. W. CALDWELL, *Phys. Rev. Lett.* **46**, 1632 (1981).

[3] H. WAGNER, R. BUTZ, U. BACKES, and D. BRUCHMANN, *Solid-State Commun.* **38**, 1155 (1981).

[4] T. S. SHI, S. N. SAHU, G. S. OEHRLEIN, A. HIRAKI, and J. W. CORBETT, *Phys. Stat. Sol.* **74**, 329 (1982).

[5] Y. J. CHABAL, G. S. HIGASHI, and S. B. CHRISTMAN, *Phys. Rev. B* **28**, 4472 (1983).

[6] Y. J. CHABAL, *Phys. Rev. Lett.* **50**, 1850 (1983).

[7] M. CARDONA, *Phys. Stat. Sol.* **118**, 463 (1983).

[8] H. KOBAYASHI, K. EDAMOTO, M. ONCHI, and M. NISHIJIMA, *J. Chem. Phys.* **78**, 7429 (1983).

[9] Y. J. CHABAL and K. RAGHAVACHARI, *Phys. Rev. Lett.* **53**, 282 (1984).

[10] J. A. SCHAEFER, F. STUCKI, J. A. ANDERSON, G. J. LAPEYRE, and W. GOPEL, *Surf. Sci.* **140**, 207 (1984).

[11] Y. J. CHABAL and K. RAGHAVACHARI, *Phys. Rev. Lett.* **54**, 1055 (1985).

[12] Y. J. CHABAL, G. S. HIGASHI, K. RAGHAVACHARI, and V. A. BURROWS, *J. Vac. Sci. Technol. A* **7**, 2104 (1985).

[13] H. FRIOITZHEM, U. KÖHLER, and H. LAMMERING, *Surf. Sci.* **149**, 537 (1985).

[14] M. NISHIJIMA, K. EDAMOTO, Y. KUBOTA, H. KOBAYASHI, and M. ONCHI, *Surf. Sci.* **158**, 422 (1985).

[15] A. ICHIMIYA and S. MIZUNO, *Surf. Sci.* **191**, 765 (1987).

[16] B. G. KOEHLER, C. H. MAK, D. A. ARTHUR, P. A. COON, and S. M. GEORGE, *J. Chem. Phys.* **89**, 1709 (1988).

[17] N. OHSE and K. YAGI, *Surf. Sci.* **217**, 430 (1989).

[18] S. M. GATES, R. R. KUNZ, and C. M. GREENLIEF, *Surf. Sci.* **207**, 364 (1989).

[19] U. JANSSON and K. J. URAM, *J. Chem. Phys.* **91**, 7978 (1989).

[20] C. M. GREENLIEF, S. M. GATES, and P. A. HOLBERT, *Chem. Phys. Lett.* **159**, 202 (1989).

[21] K. J. URAM and U. JANSSON, *J. Vac. Sci. Technol. B* **7**, 1176 (1989).

[22] G. W. TRUCKS, K. RAGHAVACHARI, G. S. HIGASHI, and Y. J. CHABAL, *Phys. Rev. Lett.* **65**, 504 (1990).

[23] G. S. HIGASHI, Y. J. CHABAL, G. W. TRUCKS, and K. RAGHAVACHARI, *Appl. Phys. Lett.* **56**, 656 (1990).

[24] J. J. BOLAND, *Surf. Sci.* **244**, 1 (1991).

[25] K. MORTENSEN, D. M. CHEN, P. J. BEDROSSIAN, J. A. GOLOVCHENKO, and F. BESENBACHER, *Phys. Rev. B* **43**, 1816 (1991).

[26] C. C. CHENG and J. T. Y. JR., *Phys. Rev. B* **43**, 4041 (1991).

[27] T. I. S. WATANABE, N. NAKAYAMA, *Appl. Phys. Lett.* **59**, 1458 (1991).

[28] J. J. BOLAND, *Surf. Sci.* **261**, 17 (1992).

[29] P. DUMAS, Y. J. CHABAL, and P. JAKOB, *Surf. Sci.* **269** (1992).

[30] S. F. SHANE, K. W. KOLASINSKI, and R. N. ZARE, *J. Chem. Phys.* **97**, 1520 (1992).

[31] M. C. FLOWERS, N. B. H. JONATHAN, Y. LIU, and A. MORRIS, *J. Chem. Phys.* **99**, 7038 (1993).

[32] Y. WEI, L. LI, and I. S. T. TSONG, *Appl. Phys. Lett.* **66**, 1818 (1995).

[33] A. YOSHIGOE, K. MASE, Y. TSUSAKA, T. URISU, Y. KOBAYASHI, and T. OGINO, *Appl. Phys. Lett.* **67**, 2364 (1995).

[34] A. YOSHIGOE, M. NAGASONO, K. MASE, and T. URISU, *Jpn. J. Appl. Phys.* **34**, 6894 (1995).

[35] Y. KOBAYASHI and T. OGINO, *Surf. Sci.* **368**, 102 (1996).

[36] K. RAGHAVACHARI, Y. J. CHABAL, and L. M. STRUCK, *Chem. Phys. Lett.* **252**, 230 (1996).

[37] D. ROGERS and T. TIEDJE, *Phys. Rev. B* **53**, 13227 (1996).

[38] M. K. WELDON, B. B. STEFANOV, K. RAGHAVACHARI, and Y. J. CHABAL, *Phys. Rev. Lett.* **79**, 2851 (1997).

[39] L. M. STRUCK, J. E. JR., B. E. BENT, G. W. FLYNN, Y. J. CHABAL, S. B. CHRISTMAN, E. E. CHABAN, K. RAGHAVACHARI, G. P. WILLIAMS, K. RADERMACHER, and S. MANTL, *Surf. Sci.* **380**, 444 (1997).

[40] S. WATANABE, *J. Chem. Phys.* **108**, 5965 (1998).

[41] F. S. TAUTZ and J. A. SCHAEFER, *J. Appl. Phys.* **84**, 6636 (1998).

[42] A. B. GUREVICH, B. B. STEFANOV, M. K. WELDON, Y. J. CHABAL, and K. RAGHAVACHARI, *Phys. Rev. B* **58**, 13434 (1998).

[43] Y.-S. KIM, Y.-G. JIN, J.-W. JEONG, and K. J. CHANG, *Semicond. Sci. Technol.* **14**, 1042 (1999).

[44] B. TUTTLE, C. G. V. DE WALLE, and J. B. ADAMS, *Phys. Rev. B* **59**, 5493 (1999).

[45] Y. OKAMOTO, *Phys. Rev. B* **60**, 10632 (1999).

[46] S. WATANABE, *J. Chem.Phys.* **113**, 2423 (2000).

[47] H. NODA and T. URISU, *Chem. Phys. Lett.* **326**, 163 (2000).

[48] H. NODA, T. URISU, Y. KOBAYASHI, and T. OGINO, *Jpn. J. Appl. Phys.* **39**, 6985 (2000).

[49] M. K. WELDON, K. T. QUEENEY, A. B. GUREVICH, B. B. STEFANOV, Y. J. CHABAL, and K. RAGHAVACHARI, *J. Chem. Phys.* **113**, 2440 (2000).

[50] A. YOSHIGOE and Y. TERAOKA, *Surf. Sci.* **482** (2001).

[51] K. T. NICHOLSON and M. M. B. HOLL, *Phys. Rev. B* **64**, 155317 (2001).

[52] Z.-H. WANG, H. NODA, Y. NONOGAKI, N. YABUMOTO, and T. URISU, *Surf. Sci.* **502** (2002).

[53] Z.-H. WANG, H. NODA, Y. NONOGAKI, N. YABUMOTO, and T. URISU, *Jpn. J. Appl. Phys.* **41**, 4275 (2002).

[54] N. MIURA and M. TSUKADA, *Jpn. J. Appl. Phys.* **41**, 306 (2002).

[55] Y. S. HIRAOKA, *Jpn. J. Appl. Phys.* **41**, 784 (2002).

[56] R. WALSH, *Acc. Chem. Res.* **14**, 246 (1981).

[57] R. E. SCHLIER and H. E. FARNSWORTH, *J. Chem. Phys.* **30**, 917 (1959).

[58] J. D. LEVINE, *Surf. Sci.* **34**, 90 (1973).

[59] D. J. CHADI, *Phys. Rev. Lett.* **43**, 43 (1979).

[60] D. HANEMAN, *Rep. Prog. Phys.* **50**, 1045 (1987).

[61] K. TAKAYANAGI, Y. TANISHIRO, S. TAKAHASHI, and M. TAKAHASHI, *Surf. Sci.* **164**, 367 (1985).

[62] T. SAKURAI and H. D. HAGSTRUM, *Phys. Rev. B* **14**, 1593 (1976).

[63] K. OURA, J. YAMANE, K. UMEZAWA, M. NAITOH, F. SHOJI, and T. HANAWA, *Phys. Rev. B* **41**, 1200 (1990).

[64] H. FROITZHEIM, U. KOHLER, and H. LAMMERING, *Surf. Sci.* **149**, 537 (1985).

[65] Y. M. WU, J. BAKER, P. HAMILTON, and R. M. NIX, *Surf. Sci.* **295**, 133 (1993).

[66] E. HILL, B. FREELON, and E. GANZ, *Phys. Rev. B* **60**, 15896 (1999).

[67] C. G. V. DE WALLE, P. J. H. DENTENEER, Y. BAR-YAM, and S. T. PANTELIDES, *Phys. Rev. B* **39**, 10791 (1989).

[68] N. B. NIELSEN, *Phys. Rev. B* **37**, 6353 (1988).

[69] Y.-S. SU and S. T. PANTELIDES, *Phys. Rev. Lett.* **88**, 165503 (2002).

[70] B. B. STEFANOV, A. B. GUREVICH, M. K. WELDON, K. RAGHAVACHARI, and Y. J. CHABAL, *Phys. Rev. Lett.* **81**, 3908 (1998).

[71] J. A. SCHAEFER and GÖPEL, *Surf. Sci.* **155**, 535 (1985).

[72] C. U. S. LARSSON, A. L. JOHNSON, A. FLODSTRÖM, and T. E. MADEY, *J. Vacuum Sci. Technol. A* **5**, 842 (1987).

[73] Q. GAO, Z. DOHNALEK, C. C. CHENG, W. J. CHOYKE, and J. T. YATES, *Surf. Sci.* **312**, 261 (1994).

[74] Y. J. CHABAL and S. B. CHRISTMAN, *Phys. Rev. B* **29**, 6974 (1984).

[75] F. STUCKI, J. ANDERSON, G. J. LAPEYRE, and H. H. FARRELL, *Surf. Sci.* **143**, 84 (1984).

[76] H. IBACH, H. WAGNER, and D. BRUCHMANN, *Solid State Commum.* **42**, 457 (1982).

[77] M. CHANDER, Y. Z. LI, J. C. PATRIN, and J. H. WEAVER, *Phys. Rev. B* **48**, 2493 (1993).

[78] R. KONEČNÝ and D. J. DOREN, *J. Chem. Phys.* **106**, 2426 (1997).

[79] J. C. TULLY, Y. J. CHABAL, K. RAGHAVACHARI, J. M. BOWMAN, and R. R. LUCCHESE, *Phys. Rev. B* **31**, 1184 (1985).

Chapter 2

Principle of BML-IRRAS and Experiments

2.1 Vibrational spectroscopy on semiconductor surfaces

There is a need for a deep studies covering those aspects of vibrational spectroscopy that would bridge the gap between basic principles and practical aspects of vibrational spectroscopy and focus on structure-property relations on surfaces and interfaces. The primary motivation for identifying surface structures is to determine the relationship between surface species and their architecture and surface performance properties. The ability of surfaces and interfaces to participate in various chemical processes make the surface studies particularly useful not only from the fundamental point of view but also in practical applications. Ultimately, through the understanding of structures involved in various surface and interfacial chemical processes, one would like to control and tailor these processes in an effort to optimize the surface and interfacial properties.

In view of these simplified but practical considerations, it is therefore the objective of most studies to develop the basic understanding necessary to optimize the structures to produce improved properties. This can be accomplished by determining the bonding and structures that develop on surfaces and/or interfaces. One important and useful technique often used is vibrational spectroscopy, which

consists of two physically different yet conceptually complementary methods, infrared and Raman spectroscopies. Their increasing importance in the surface science and the surface modification analysis is due to the fact that in recent years there have been tremendous instrumental advances in both types of spectroscopies, giving increased sensitivity and speed of measurements, and surface selectivity. Although the instrumental advances play a significant role, it is of great importance to understand the origin of physical processes governing spectral detection and interpretation of vibrational spectra.

Silicon semiconductor surfaces have been investigated by several vibrational spectroscopic techniques. Figure 2.1 shows the comparison among the well known surface vibration spectroscopy techniques.

EELS [1, 2] can be used in a wide frequency range including the finger print region (< 1000 cm^{-1}). The sensitivity of the EELS is very high. The disadvantage is the low resolution (~ 10 cm^{-1}) which is insufficient to resolve many vibrational peaks on the silicon surfaces. Attenuated total (internal) reflection (ATR) or multiple internal reflection (MIR) method is another powerful method for surface vibration analyses [3, 4]. The IR beam enters the prism and is incident on the surfaces of the prism at angles greater than the critical angle. If the geometry of the experiment is arranged correctly, then multiple internal reflection occurs as shown in Fig. 2.2. This method provides very high sensitivity and resolution, but the cut-off frequency locates at about 1000 cm^{-1} in the case of using Si prisms [5]. The transmission IR using Brewster's angle can be used in the wide frequency region. But the sensitivity is relatively low, and especially it is almost insensitive for the perpendicular component of the dynamic dipole moments.

To overcome these disadvantages, the BML-IRRAS technique which gives a high resolution and a high sensitivity for the surface vibration in a wide frequency range including the finger print region had been developed recently [6–8].

2.2 Principle of BML-IRRAS

The principle of the BML-IRRAS is shown in Fig. 2.3. The currently used BML substrates are made by the ion implantation. The silicon wafer is ion

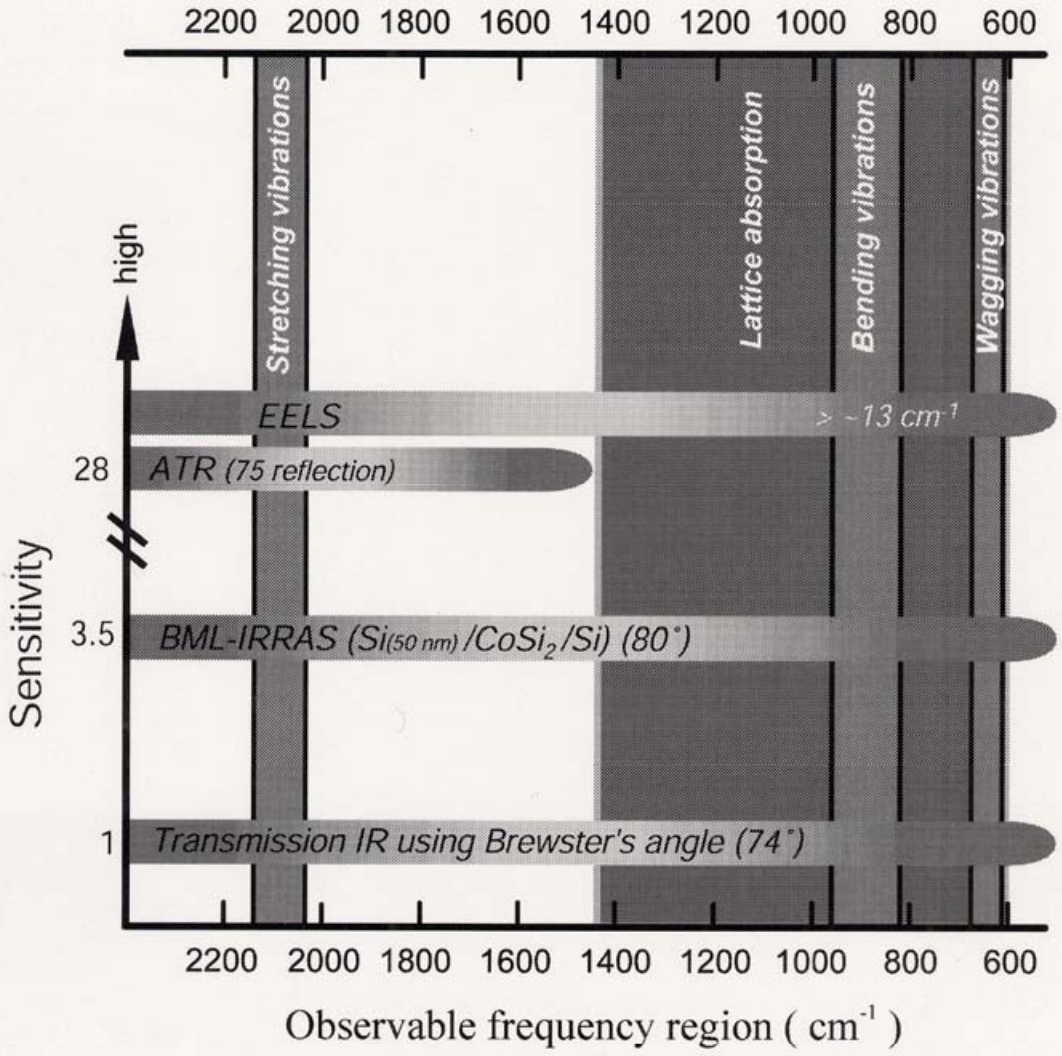

Figure 2.1: Comparison of the surface vibration spectroscopy techniques.

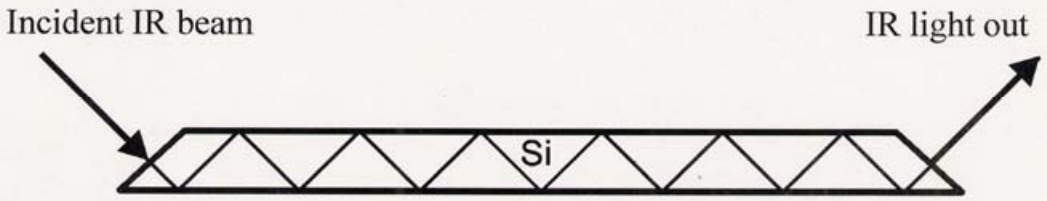

Figure 2.2: Arrangements of ATR or MIR method.

implanted by Co^+. Then this sample is annealed at high temperatures to form an uniform buried $CoSi_2$ layer giving the $Si/CoSi_2/Si$-base structures [7, 8]. The $CoSi_2$ layer works as a metal layer to reflect IR beam.

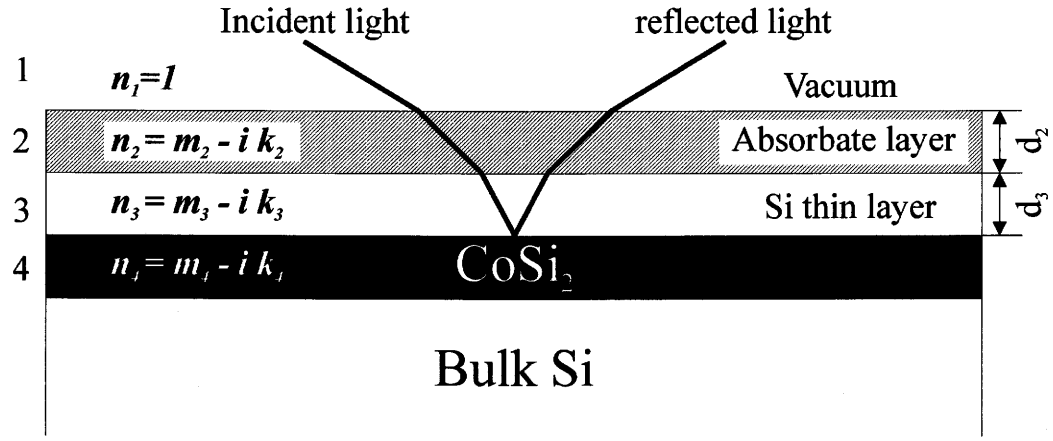

Figure 2.3: The principle of the BML-IRRAS. 1, 2, 3 and 4 represent the vacuum region 1, the layer 2, the layer 3 and the layer 4, respectively.

Since the surface silicon layer is very thin (< 100 nm), the silicon phonon effect can be ignored. Kobayashi et al. at NTT Basic Research Laboratories studied the relationship between the incident angle and the surface silicon layer thickness [8]. The results are shown in Fig. 2.4.

The top layer of the layer structure in Fig. 2.3 is an adsorbate layer (eg. hydrogen or others) , the third layer is the surface silicon single crystal layer and the forth layer is the cobalt siliside layer. The interaction of the light with the surface is described by the Fresnel equation, which incorporates the appropriate boundary conditions in the electromagnetic wave equations of the incident, reflected, and refracted wave fronts. The superscript suffix "s" and "p" represent parallel and perpendicular parts of reflective index. The 1, 2, 3, and 4 represent the different types of layer of the model structure.

$$
\begin{aligned}
n_1^s &= 1 \\
n_2^s &= m_2^s - ik_2^s \\
n_2^p &= m_2^p - ik_2^p \\
n_3^s &= m_3^s - ik_3^s
\end{aligned}
$$

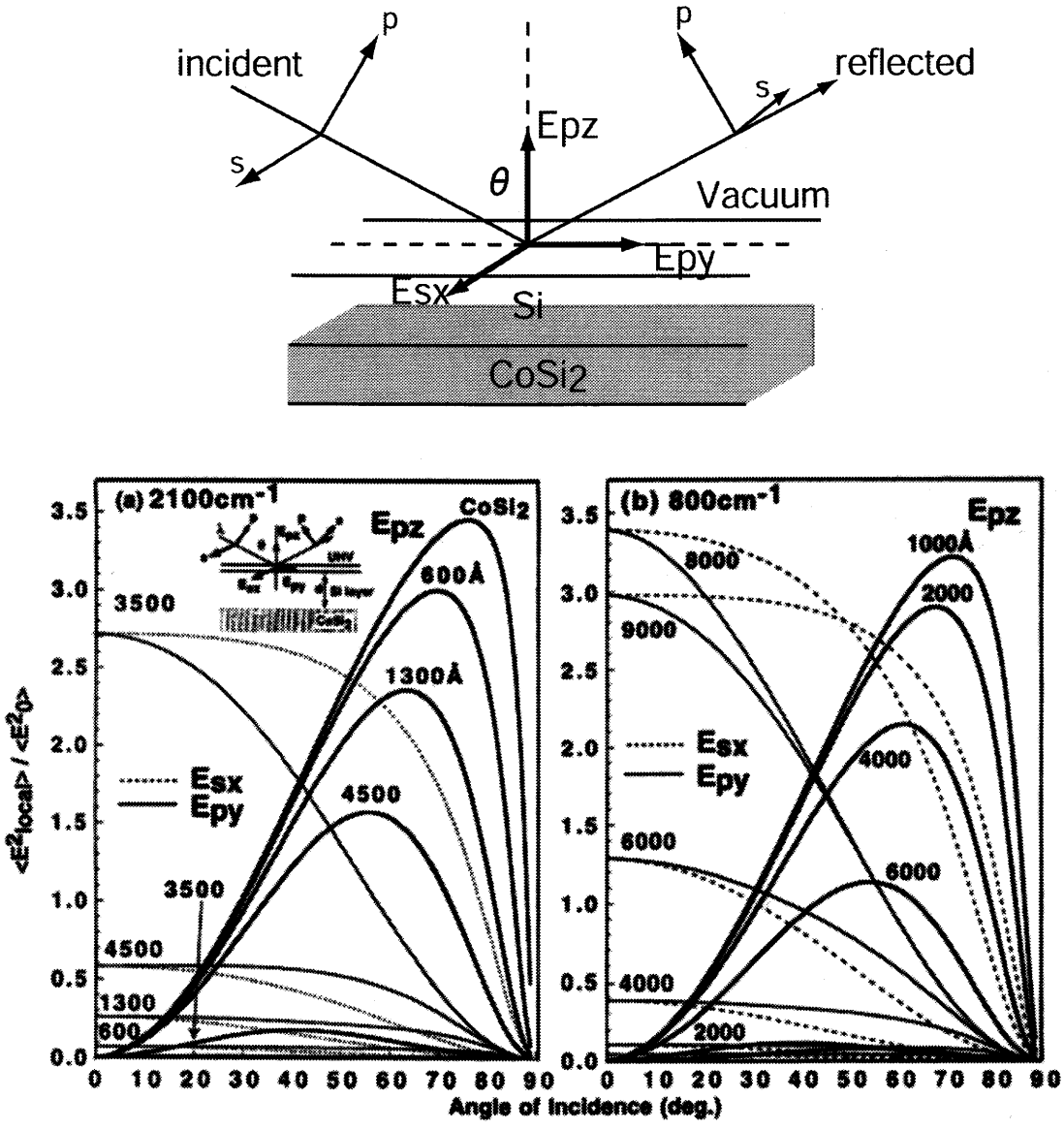

Figure 2.4: The relationship between IR incident angle and surface silicon layer thickness.

$$
\begin{aligned}
n_3^p &= m_3^p - ik_3^p \\
n_4^s &= m_4^s - ik_4^s \\
n_4^p &= m_4^p - ik_4^p \\
sin(i_2^s) \times n_2^s &= sin(i_1) \times n_1 \\
sin(i_2^p) \times n_2^p &= sin(i_1) \times n_1 \\
sin(i_3^s) \times n_3^s &= sin(i_2^s) \times n_2^s \\
sin(i_3^p) \times n_3^p &= sin(i_2^p) \times n_2^p \\
sin(i_4^s) \times n_4^s &= sin(i_3^s) \times n_3^s \\
sin(i_4^p) \times n_4^p &= sin(i_3^p) \times n_3^p
\end{aligned}
$$

i_1 is incident angle. C is light speed. λ is IR wavelength. d_2 and d_3 are the thickness of the second and the third layers, respectively.

From the effective Fresnel coefficient equation, we can get:

$$
\begin{aligned}
\Delta_2^s &= 2\pi d_2^s n_2^s cos(i_2^s)/\lambda \\
\Delta_2^p &= 2\pi d_2^p n_2^p cos(i_2^p)/\lambda \\
\Delta_3^s &= 2\pi d_3^s n_3^s cos(i_3^s)/\lambda \\
\Delta_3^p &= 2\pi d_3^p n_3^p cos(i_3^p)/\lambda
\end{aligned}
$$

$$
r_{12}^s = \frac{n_1^s cos(i_1^s) - n_2^s cos(i_2^s)}{n_1^s cos(i_1^s) + n_2^s cos(i_2^s)}
$$

$$
r_{12}^p = \frac{n_2^p cos(i_1^p) - n_1^p cos(i_2^p)}{n_1^p cos(i_2^p) + n_2^p cos(i_1^p)}
$$

$$
r_{23}^s = \frac{n_2^s cos(i_2^s) - n_3^s cos(i_3^s)}{n_2^s cos(i_2^s) + n_3^s cos(i_3^s)}
$$

$$
r_{23}^p = \frac{n_3^p cos(i_2^p) - n_2^p cos(i_3^p)}{n_2^p cos(i_3^p) + n_3^p cos(i_2^p)}
$$

$$
r_{34}^s = \frac{n_3^s cos(i_3^s) - n_4^s cos(i_4^s)}{n_3^s cos(i_3^s) + n_4^s cos(i_4^s)}
$$

$$r_{34}^{p} = \frac{n_4^p cos(i_3^p) - n_3^p cos(i_4^p)}{n_3^p cos(i_4^p) + n_4^p cos(i_3^p)}$$

$$r_{234}^{s} = \frac{r_{23}^{s} + r_{34}^{s} e^{-2i\Delta_3^s}}{1 + r_{34}^{s} r_{23}^{s} e^{-2i\Delta_3^s}}$$

$$r_{234}^{p} = \frac{r_{23}^{p} + r_{34}^{p} e^{-2i\Delta_3^p}}{1 + r_{34}^{p} r_{23}^{p} e^{-2i\Delta_3^p}}$$

$$r_{1234}^{s} = \frac{r_{12}^{s} + r_{234}^{s} e^{-2i\Delta_2^s}}{1 + r_{234}^{s} r_{12}^{s} e^{-2i\Delta_2^s}}$$

$$r_{1234}^{p} = \frac{r_{12}^{p} + r_{234}^{p} e^{-2i\Delta_2^p}}{1 + r_{234}^{p} r_{12}^{p} e^{-2i\Delta_2^p}}$$

$$R^s = \mid r_{1234}^{s} \mid^2$$
$$R^p = \mid r_{1234}^{p} \mid^2$$
$$R_0^s = \mid r_{1234}^{s} \mid^2 (d_2 = 0)$$
$$R_0^p = \mid r_{1234}^{p} \mid^2 (d_2 = 0)$$
$$Abs^s = -ln\frac{R^s}{R_0^s}$$
$$Abs^p = -ln\frac{R^p}{R_0^p}$$

Where, R^s and R_0^s (or R^p and R_0^p) are the reflectivities with adsorbate and without adsorbate, respectively, and Abs^s and Abs^p are the absorbance for s and p polarization, respectively.

2.3 Experimental configuration

The experimental configuration is shown in Fig. 2.5.

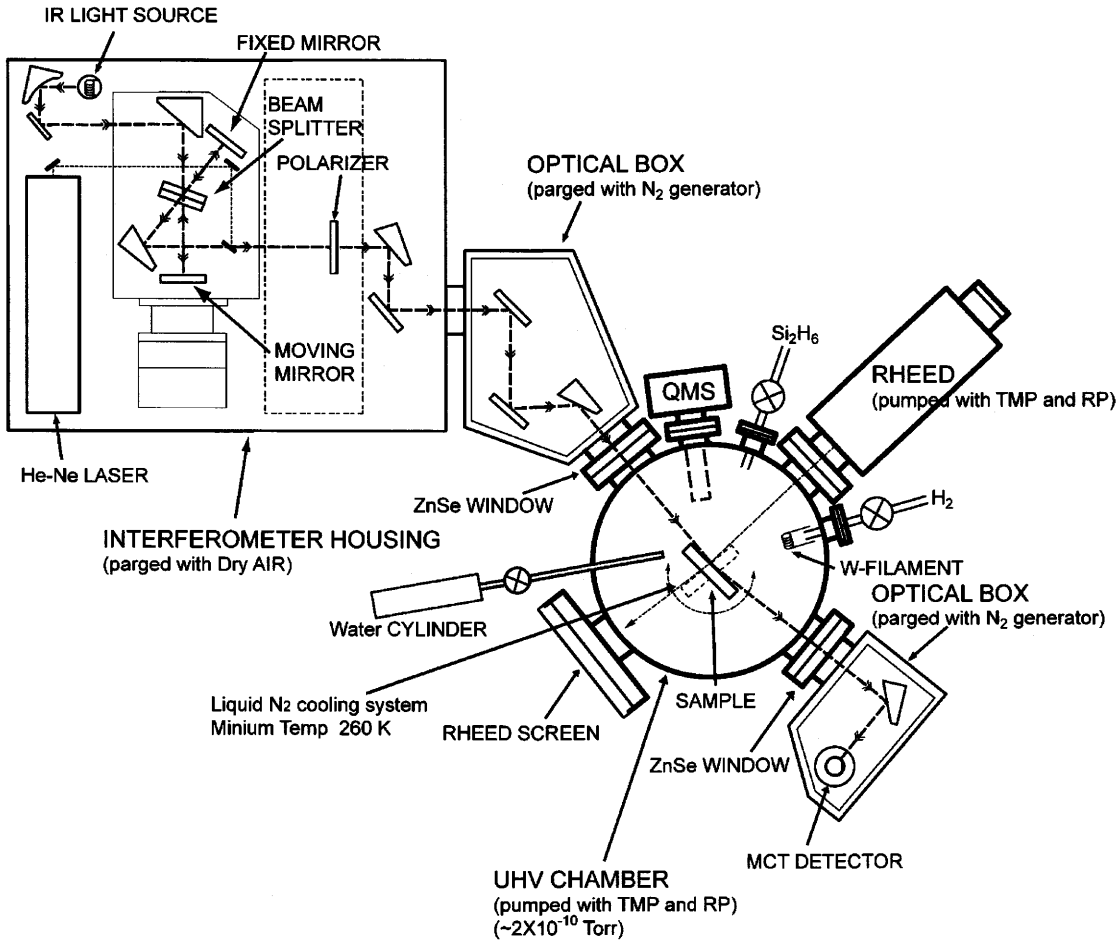

Figure 2.5: The experimental configuration.

The ultra-high vacuum (UHV) epitaxy chamber is pumped by the turbo molecular pump (TMP) with 500 L/s pumping speed. The vacuum is monitored by Phillips-Gravanell ion-gauge calibrated by the quadrupole mass spectrometer (Q-mass). The base pressure is less than 2×10^{-10} torr. The surface structure of the sample can be monitored by RHEED. The residual gas in the chamber is monitored by the Q-mass.

Samples are mounted and pass through the air-lock chamber which is connected to the epitaxy chamber. This air-lock chamber is pumped by 150 L/s TMP. After the vacuum is better than 1 $\times10^{-7}$ torr the sample is transferred to the epitaxy chamber by a magnetic type manipulater. All of this procedure

can be completed within 20 minutes after finishing the sample treatment. After the sample is mounted in the epitaxy chamber sample holder, it is heated by the PBN (Pyrolytic Graphaite/Pyrolytic Boron Nitride Ceramic Heater) heater. The heating current is controlled by PID (proportion-integral-differential) temperature controller. The temperature is monitored by a Re-W thermocouple which is in contact with the back side of the sample. A liquid nitrogen cooling system is also mounted which can reach 260 K. The temperature measured by the thermocouple is calibrated by the sample surface temperature measured by using the infrared pyrometer. The PID controlled heater keep the temperature error within 0.5 K at 373 K. At 870 K the temperature difference between the center and the edge of the sample is about 30 K. The sample holder and other parts are made by well-degased Mo, Ta or Nb materials. The sample can be rotated suitably using 3-D manipulator.

The disilane (Si_2H_6) is used to deposit a thin epitaxy layer on the surface of the as delivered Si-BML substrates which have a rough surface due to the ion implantation damage. Atomic hydrogen or deuterium is produced by cracking H_2 or D_2 by an incandescent tungsten filament. Water or deuterium water is supplied through a leak valve.

A FT-IR spectrometer (JEOL JIR 7000) is used in our experiment. IR light is produced by incandescent tungsten filament. A p-polarized IR beam was selected by a wire grid polarizer using KRS-5 and directed into the reaction chamber through a ZnSe viewing port with an incident angle of 85° on the sample surface. Therefore, only the perpendicular component of the dynamic dipole moment for the sample surface can be detected. The reflected IR beam is focused onto a mercury cadmium telluride (MCT) detector cooled by liquid nitrogen. The IR interferometer housing system is purged by dry air. The IR optical system outside of the UHV chamber is purged by nitrogen gas.

2.4 Preparation of Si(100) BML substrate

The Si(100)-$CoSi_2$ BML substrates, made by Co^+-ion implantation were purchased from Toray Research Center. Co^+ (200 KeV) was implanted by the density of $3\times10^{17}/cm^2$ at 673 K to form silicon and cobalt mixed layer under the silicon

surface. The thickness of the damaged layer was about 50 nm at this condition. After annealing at 970 K for 2 hours and 1170 K for 0.5 hour, a thin $CoSi_2$ layer was formed below the silicon surface layer (Fig. 2.6).

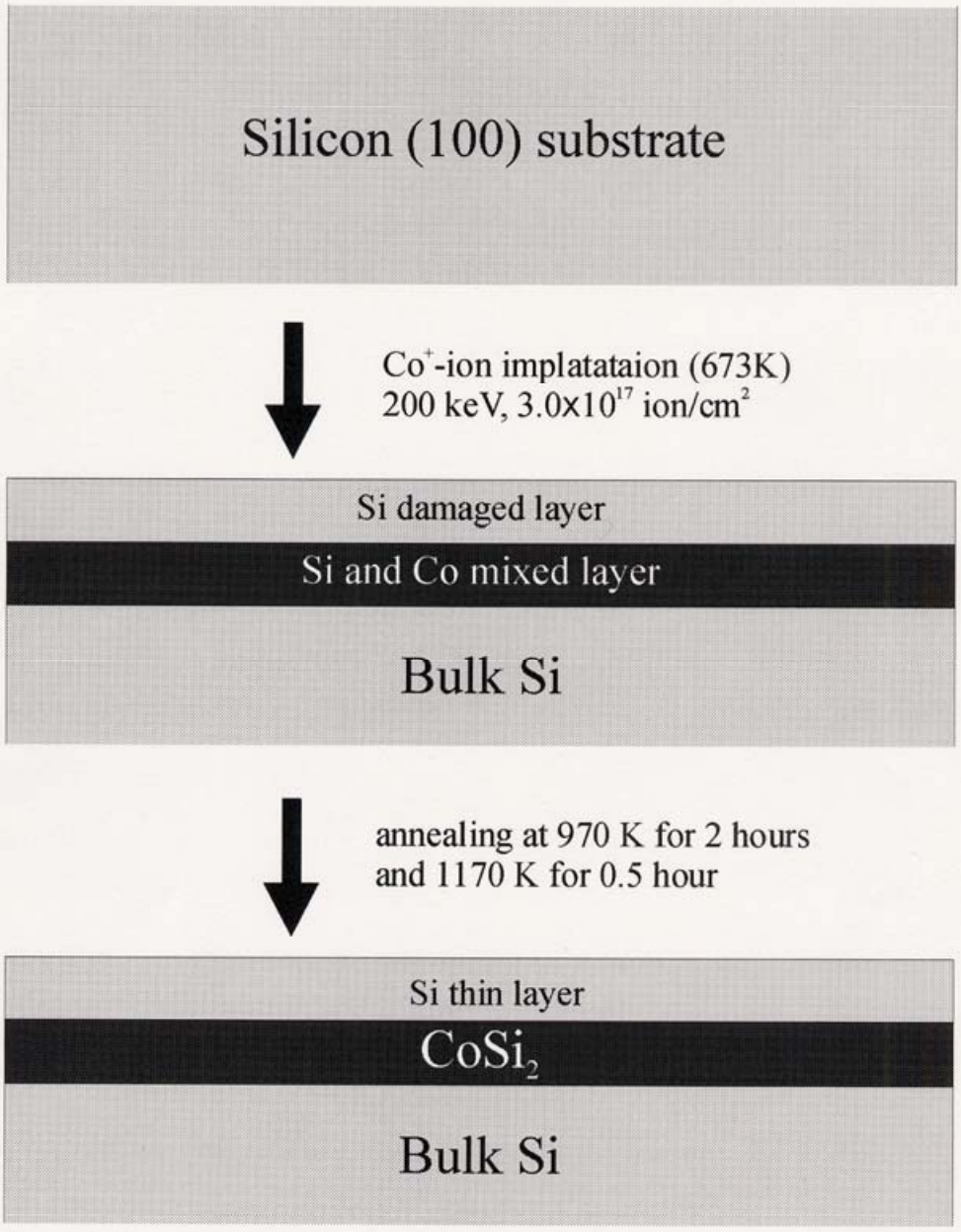

Figure 2.6: BML substrates fabrication procedure using ion implantation method.

Since the surface of the as delivered BML substrate was damaged by the ion

implantation, a thin silicon layer was grown by molecular beam epitaxy (MBE) method using disilane. The procedure is described below:

1. Cut the wafer as 14×14 mm^2
2. Ultrasonic cleaning using acetone (CH_3COCH_3) for 5 minutes
3. Rinse the sample at deionization water for 1 minute
4. Ultrasonic cleaning using methanol (CH_3OH) for 5 minutes
5. Rinse the sample in deionization water for 1 minute
6. Remove the oxidized surface layer by HF solution (H_2O : HF (46%) = 10 : 1)
7. Rinse the sample in the above solution, slowly pull out the sample from this solution after 15-30 seconds, then rinse the sample in deionization water
8. Oxidize the sample surface by HCl (35%) : H_2O_2 (30%) : H_2O = 4 : 1 : 1 solution for 5 minutes
9. Rinse the sample in deionized water for more than 5 minutes
10. Ultrasonic cleaning of the sample holder with acetone for more than 20 minutes
11. Dry the sample and sample holder using pure nitrogen gas
12. Fix the sample in sample holder and transfer to the airlock chamber
13. After the vacuum pressure of the airlock chamber become better than 1×10^{-7} torr, transfer the sample to the epitaxy chamber
14. Rise the Si-BML substrate temperature to 870 K slowly for keeping the epitaxy chamber vacuum better than 5×10^{-9} torr and keep annealing for more than 12 hours
15. Flash the sample at 1170 K to remove the surface oxidized layer

16. Lower the temperature to 950 K, deposit a thin silicon epitaxial layer by using Si_2H_6

After these procedures, we can get a well defined Si(100)-(2×1) surface. Figure 2.7 shows the RHEED pattern taken at different period.

We also checked the cross-sectional structure of this sample by using scanning electronic microscopy (SEM) as shown in Fig. 2.8.

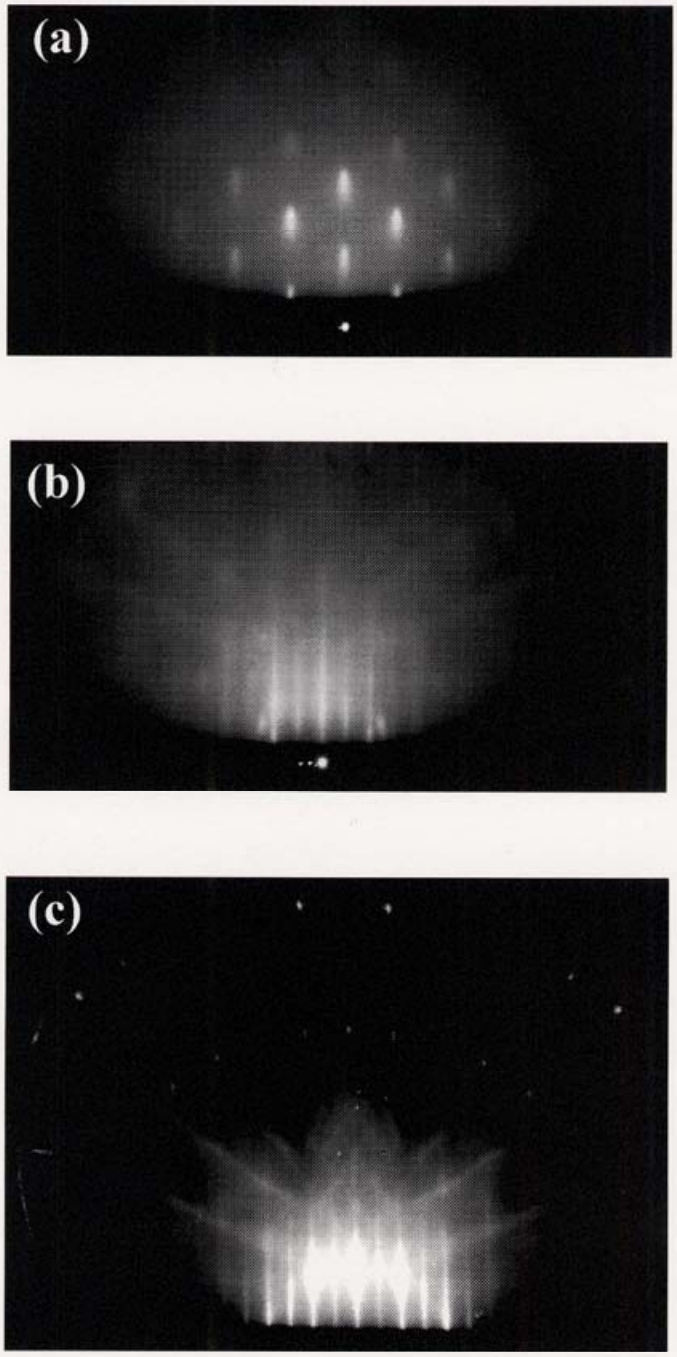

Figure 2.7: The RHEED patterns taken at different period. (a) before annealing; (b) after annealing; (c) after Si_2H_6 epitaxy.

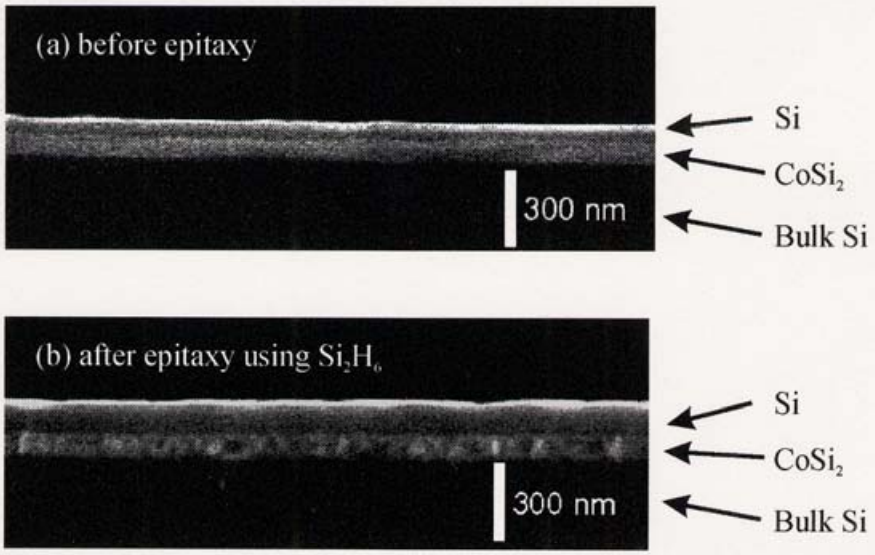

Figure 2.8: Cross-sectional structure observed by SEM of BML sample (a) before epitaxy and (b) after epitaxy using Si_2H_6

Bibliography

[1] H. Wagner, R. Butz, U. Backes, and D. Bruchmann, *Solid-State Commun.* **38**, 1155 (1981).

[2] F. S. Tautz and J. A. Schaefer, *J. Appl. Phys.* **84**, 6636 (1998).

[3] Y. J. Chabal, *Surf. Sci. Rept.* **8**, 211 (1988).

[4] P. Jakob, P. Dumas, and Y. J. Chabal, *Appl. Phys. Lett.* **59**, 2968 (1991).

[5] M. K. Weldon, B. B. Stefanov, K. Raghavachari, and Y. J. Chabal, *Phys. Rev. Lett.* **79**, 2851 (1997).

[6] V. M. Bermudez, *J. Vac. Sci. Technol. A* **10**, 152 (1992).

[7] A. Yoshigoe, K. Mase, Y. Tsusaka, T. Urisu, Y. Kobayashi, and T. Ogino, *Appl. Phys. Lett.* **67**, 2364 (1995).

[8] Y. Kobayashi and T. Ogino, *Surf. Sci.* **368**, 102 (1996).

Chapter 3

IR Line Width Broadening at Nearly Ideally H-terminated Region on Si(100) Surfaces

Surface Science 502-503 (2002) 86-90

3.1 Abstract

The dependence of the line width of the coupled monohydride symmetric stretching vibration of the H-terminated Si(100)-(2×1) surface on the exposure temperature and the hydrogen exposure has been investigated with BML-IRRAS. Even for nearly ideally H-terminated Si(100) surface, the line width significantly changes depending on the exposure temperature and the hydrogen exposure. The reason of the line width broadening is discussed, and it is strongly suggested that hydrogen diffusion into the subsurface of Si has a significant influence on the line width broadening. Using a new experimental approach, the evidence of hydrogen (deuterium) diffusion into the subsurface is investigated for the first time using an IRRAS measurement.

3.2 Introduction

Hydrogen terminated Si surfaces have attracted strong interest not only from the viewpoint of application to semiconductor device fabrication, but also for their importance as a model system for surface science phenomena. Although atomically flat and bulk-like Si(111) surfaces can be obtained by etching of the surfaces using pH controlled buffered HF solutions [1], it is a common understanding that atomically flat Si(100) surfaces are difficult to be obtained by the wet processes [2, 3]. Therefore the dry process is the method of choice for the Si(100) surface. In spite of the large number of reported works on the H-termination, there are still many unascertained details. One of the important topics is the hydrogen diffusion into the subsurface, which possibly causes the etching of the surface [4]. It is reported that hydrogen atoms incorporated by the hydrogen exposure when making the H-termination mainly locate at the bond-center site [5]. Due to the low density or low sensitivity for the IR absorption of the bond-center hydrogen atoms, this topic has not been addressed in the past by surface vibration analysis.

In the present work, the dependence of the IRRAS spectra on the substrate Si(100)-(2×1) surfaces have been measured for various hydrogen exposures and exposure temparature (T_x) using BML-IRRAS [6–8]. We find line width of the symmetric stretching of the coupled monohydride (CMH) significantly changes depending on the T_x and the hydrogen exposure, and broadens even for nearly ideally H-terminated (almost 100% CMH terminated) surfaces, which seems to be due to hydrogen diffusion into the subsurface.

3.3 Experiments

Experimental systems and sample treatments are described in detail in ref. [9] and Fig. 2.5. The optical path of the IRRAS system was purged by N_2 gas. A p-polarized IR beam from a FT-IR spectrometer (JEOL JIR7000) was selected by a wire grid polarizer using KRS-5 and directed into the reaction chamber through a ZnSe viewing port with an incident angle of 85^o on the sample surface. The reflected IR beam was focused onto an MCT detector cooled by liquid nitrogen. The temperature inhomogeneity in the IR illuminated area of the sample surface

was less than 30 K. Hydrogen was dosed using a leak valve and by monitoring the pressure in the chamber with a Granville-Phillips ion gauge. The base pressure in the chamber was less than 2×10^{-10} torr. The hydrogen dosing time for each deposition and measurement cycle was 20 seconds. The IRRAS spectrum of a completely deuterium covered surface just after the surface cleaning was used as the background (BG). The displayed spectra are obtained by dividing the signal spectrum (SG) by the BG. The substrate temperature for both the BG and SG measurements (T_m) was 373 K in the present work, if it is not otherwise stated. The line width in the present work corresponds to the value as measured without a deconvolution of the resolution function.

The usual procedure of an IR measurements cycle was: 1) thermal cleaning of the sample surface at around 1170 K, 2) saturation (5000 L) adsorption of deuterium at 673K, 3) a temperature decrease to 373K and the measurement of the BG IRRAS, 4) the thermal cleaning of the sample at about 1170 K followed by a decrease to the exposure temperature T_x and a saturation adsorption (500L or 1000L) of hydrogen, and 5) a temperature decrease to 373 K for the measurement of the SG.

All the samples showed a clear (2×1) RHEED pattern before and after the hydrogen (deuterium) exposure.

3.4 Results and discussion

It is well known that the structure of the hydrogen-adsorbed Si(100) surface changes characteristically depending on the temperature [9, 10]. At above 600K, higher hydride species almost completely decomposes and the surface is covered only by CMH. In our preliminary experiments [4, 9], we confirmed that the CMH saturation is achieved in the 200 $\sim$ 5000 L exposure range as in that region a sharp (2×1) RHEED pattern is observed. At higher exposures the (2×1) RHEED pattern becomes diffuse, indicating that the surface becomes rough due to hydrogen etching effects (Fig. 3.1). Based on this background knowledge, the vibrational spectra for the H saturated Si(100) surface made by 200 $\sim$ 1000 L H exposure have been investigated in detail.

The IRRAS spectra have been measured at different H exposure temperatures

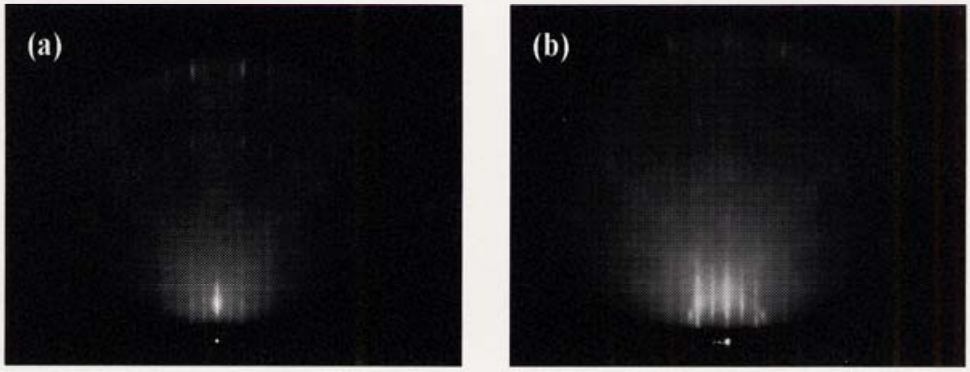

Figure 3.1: RHEED pattern at different hydrogen exposure at 623 K (a): before 5000 L hydrogen exposure; (b): 10000 L hydrogen exposure

T_x for an exposure of 500 L. Only three representative SG/BG IRRAS spectra are shown in Fig. 3.2, and the detailed dependence of the integrated absorbance and the line width of the CMH symmetric vibration peak on T_x are shown in Fig. 3.3. Furthermore, we have measured the change of the line width depending on the hydrogen exposure at T_x=673K as depicted in Fig. 3.4.

For nearly ideally H-terminated regions, which is known to locate at T_x=620 $\sim$ 670 K from Fig. 3.3, the homogeneous line width of the CMH symmetric stretching vibration can be determined by vibration dephasing [11]. The minimum line width obtained in our experiments at 500L exposure, 2.1 cm^{-1} at T_m=373 K or 1.75 cm^{-1} at T_m=300 K, almost agrees with that reported in literature (3.2 cm^{-1} for T_m=373 K [12] or 1.9 cm^{-1} at T_m=300K [11]). The detailed investigation of the line width, however, shows much more complex dependence on the temperature and the exposure than expected.

Concerning Fig. 3.3, the line width narrowing of the CMH symmetric stretching vibration with increasing T_x at around T_x=600K is explained by the increase in homogeneity due to the decomposition of higher hydrides, which is shown by the decrease of the peak intensity of SiH_2 bend scissors mode at about 900 cm^{-1} from 5 $\times 10^{-4}$ (Ref. [9] Fig. 3.2(b) T_x=400 K) to 1.3×10−4 (Fig. 3.2(a)) in absorbance. In the high temperature region, ($T_x > 675$), the line width broadens again with increase T_x, which can be explained by the increase of the inhomogeneity due to the decomposition of CMH, resulting in the inhomogeneous distribution

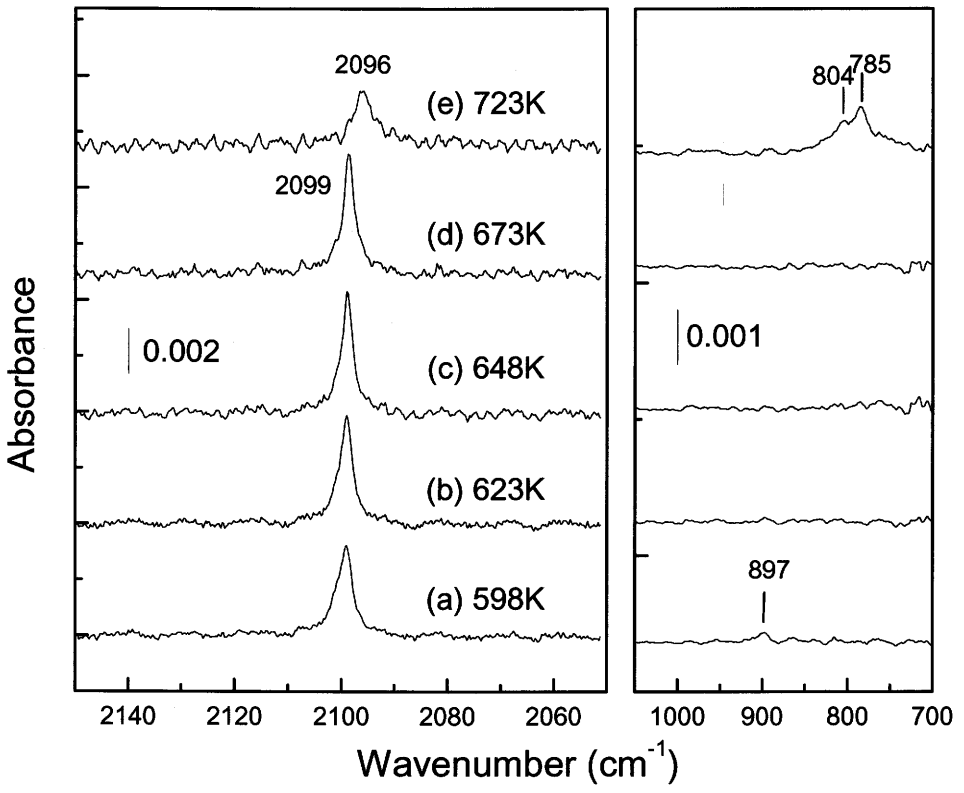

Figure 3.2: BML-IRRAS spectra of the Si(100)-(2×1)-H surfaces for different T_x : (a)-(e). Assignments of peaks are: 2099 and 2096 cm^{-1}, CMH symmetric stretching; 804 and 785 cm^{-1}, Si-OH stretching; and 897 cm^{-1}, SiH_2 bend scissors.

of CMH, and a contamination with water from the residual gas, which is ascertained by the 804 and 785 cm^{-1} peaks which are assigned to Si-OH stretching mode [13] as shown in Fig. 3.2(e). Concerning Fig. 3.4, the large line width at low exposure (<200L, not show in here) range can be attributed to a low coverage of the CMH resulting in the increase of the inhomogeneity of the CMH spatial distributions and in contamination by H_2O from the residual gas.

An interesting point is the line width broadening at higher exposure regions of >500 L in Fig. 3.4. Also it is interesting that the line width becomes narrow

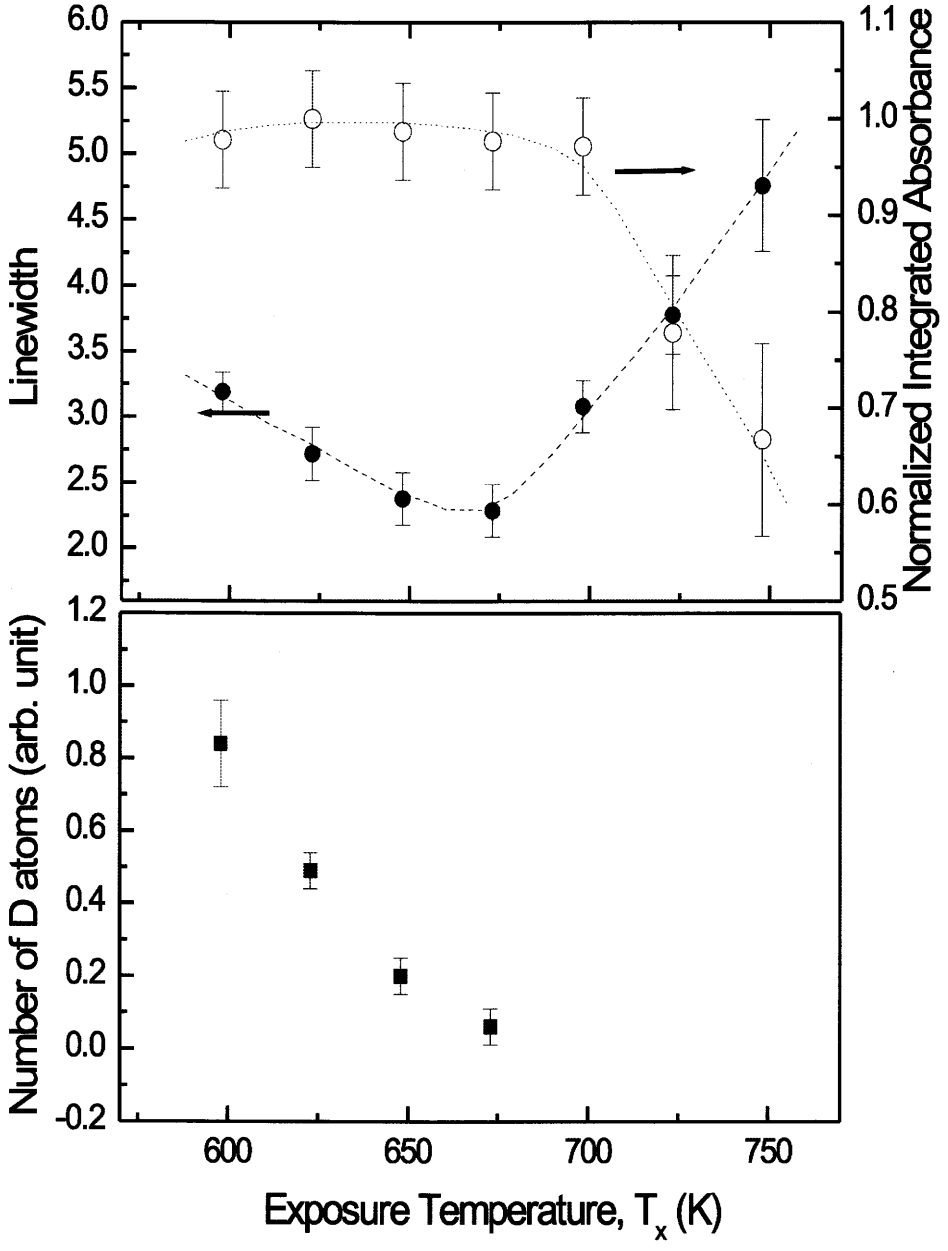

Figure 3.3: Dependence of the normalized integrated absorbance and the line width of the CMH symmetric stretching vibration peak (upper), and the relative number of D atoms incorporated into Si bulk (lower) on T_x. The hydrogen exposure (upper) was 500 L, and the deuterium exposure (lower) was 5000 L.

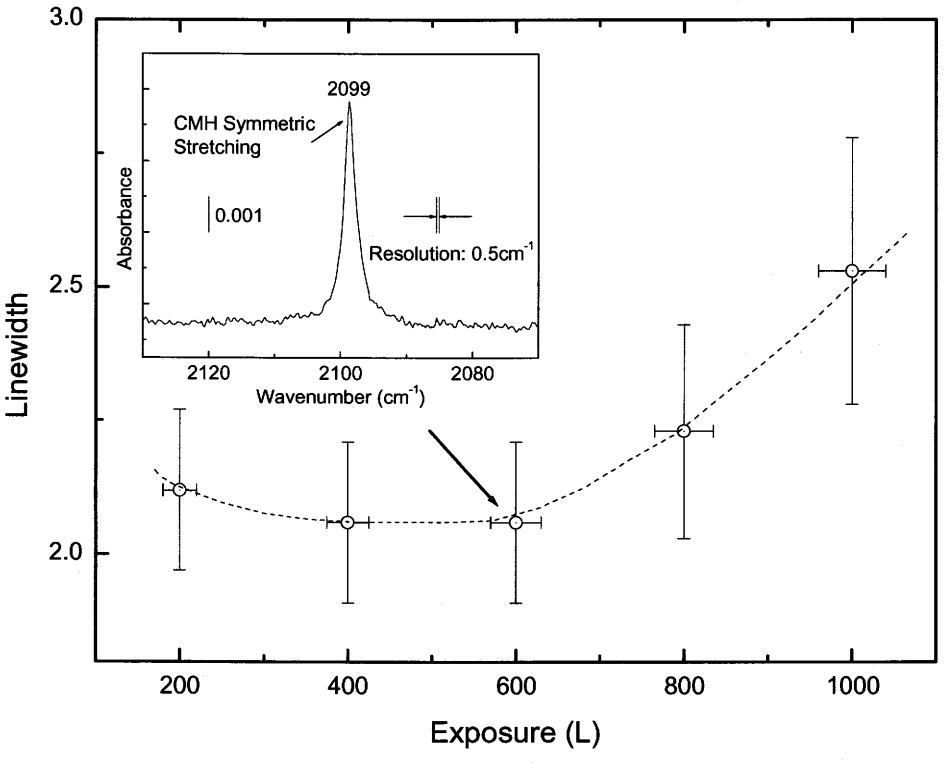

Figure 3.4: Dependence of the line width on the hydrogen exposure. T_x was 673 K.

with increasing T_x at $T_x = 620 \sim 670$K, where no higher hydride peaks are observed. These data shows that the line width sensitively changes depending on T_x and exposure even at nearly ideally H-terminated conditions, where both of the inhomogeneity due to the background water contamination and the CMH inhomogeneous distribution can be ignored. We have also ascertained that no peaks relating to the water contamination appear on the nearly ideal hydrogen termination surfaces even 10 h after the H-termination in the vacuum chamber.

Surface roughness induced by etching can be ruled out to explain these line width broadening: all RHEED patterns exhibit a sharp (2×1) pattern, further no defect-related vibration peaks such as isolated SiH are observed up to $\sim$ 5000 L.

The structural stability of the H-terminated Si(100)-(2×1) surface at high temperatures (∼ 600 K) for prolonged hydrogen exposure is assured also by STM [10]. As a possible origin we therefore suggest an exposure dependent accumulation of subsurface hydrogen.

Although the behavior of hydrogen in crystalline silicon has been the subject of previous experimental and theoretical investigations [14–16], the effect of the bulk hydrogen on the IR line width has not yet been investigated to the authors' knowledge.

To establish whether subsurface H could be present under our experimental conditions we have subsequently first exposed the Si(100) surface to the atomic deuterium (∼5000 L) at around 670 K just after the high temperature thermal cleaning. Then, after the surface silicon deuterides were completely replaced by hydrogen by exposing the surface to atomic hydrogen (500 L) at 620 K, the sample was annealed at fixed temperatures for one minute. After this treatment no Si-D coupled monodeuteride vibration peak was detected in our experiments. The BG of IRRAS was taken at 373 K after the hydrogen adsorption, and the sample spectra (SG) were also taken at temperature of 373 K after the one minute annealing, then the spectra of SG/BG were obtained as shown in Fig. 3.5. With increasing annealing temperatures, the decomposition rate for the CMH becomes fast, which results in a decrease of the intensity of the CMH peak as manifested in the negative peak at around 2100 cm^{-1} in Fig. 3.5. It further shifts to the lower frequency side (appearance of positive peak at around 2098-2099 cm^{-1} in Fig. 3.5) due to the decrease of the dipole-dipole coupling interaction. Remarkable is the appearance of the new peak at 1521 cm^{-1}, which corresponds to the Si-D coupled monodeuteride symmetric stretching mode, indicating that the deuterium atoms diffuse out on the surface from the bulk by the annealing. We have also measured the amount of deuterium incorporated into the Si bulk by a conventional temperature programmed desorption (TPD) experiment for samples made by the similar process of deuterium exposure (at the T_x) followed by hydrogen termination as mentioned above, and found that the line width increase from T_x = 673 L to 598 K roughly in proportion to the amount of incorporated deuterium atoms as shown in Fig. 3.3. From the present data, we suggest that a complex inhomogeneity due to the subsurface hydrogen introduced by the hydrogen

diffusion during the exposure caused the line width broadening.

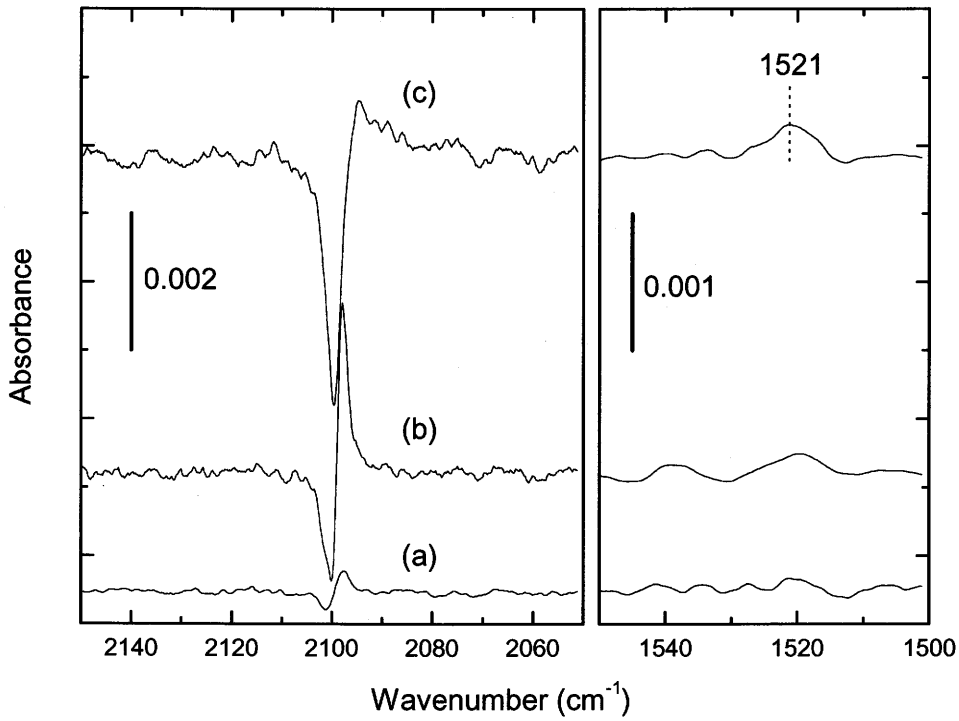

Figure 3.5: BML-IRRAS spectra after annealing. The 1521 cm^{-1} peak is assigned to the coupled monodeuteride symmetric stretching vibration. The sequence of the sample treatments and measurements was: (1) sample cleaning at 1170 K; (2) deuterium saturation adsorption (5000 L) at 673 K; (3) exposure to atomic hydrogen by 500 L at 620 K; (4) measurement of BG at 373 K; (5) annealing (a) 673 K, 1 min, (b) 723 K, 1 min, and (c) 773 K, 1 min; (6) measurement of SG at 373 K; and (7) SG/BG.

3.5 Conclusion

The complex dependencies of line widths and integrated absorbance on hydrogen exposure temperatures and exposures on Si(100) surfaces have been investigated in detail by using the BML-IRRAS. The minimum linewidth observed at the nearly ideally H-terminated surface, which is given at around the temperature 670 K and the hydrogen exposure 500 L, is almost agree with the reported homogeneous line width determined by the dephasing effects. The line width broadening with increasing hydrogen exposures and with decreasing exposure temperatures has been observed for nearly ideally H-termination regions where the broadening can not be explained by dephasing effects and inhomogeneities due to the coexistence of higher hydrides, contamination by the residual water or inhomogeneous distribution of CMH. This exposure dependence of the line width is also not due to the surface roughness induced by the hydrogen etching. From that the diffusion of the deuterium atoms to the subsurface of Si has been assured by the IRRAS spectrum. It is strongly suggested that the hydrogen diffusion into the subsurface of Si causes the inhomogeneous broadening of the line width.

Bibliography

[1] G. S. Higashi, Y. J. Chabal, G. W. Trucks, and K. Raghavachari, *Appl. Phys. Lett.* **56**, 656 (1990).

[2] P. Dumas, Y. J. Chabal, and P. Jakob, *Surf. Sci.* **269** (1992).

[3] Y. J. Chabal, G. S. Higashi, K. Raghavachari, and V. A. Burrows, *J. Vac. Sci. Technol. A* **7**, 2104 (1989).

[4] H. Noda, T. Urisu, Y. Kobayashi, and T. Ogino, *Jpn. J. Appl. Phys.* **39**, 6985 (2000).

[5] B. Tuttle, C. G. V. de Walle, and J. B. Adams, *Phys. Rev. B* **59**, 5493 (1999).

[6] A. Yoshigoe, K. Mase, Y. Tsusaka, T. Urisu, Y. Kobayashi, and T. Ogino, *Appl. Phys. Lett.* **67**, 2364 (1995).

[7] Y. Kobayashi and T. Ogino, *Surf. Sci.* **368**, 102 (1996).

[8] V. M. Bermudez, *J. Vac. Sci. Technol. A* **10**, 152 (1992).

[9] H. Noda and T. Urisu, *Chem. Phys. Lett.* **326**, 163 (2000).

[10] J. J. Boland, *Surf. Sci.* **261**, 17 (1992).

[11] J. C. Tully, Y. J. Chabal, K. Raghavachari, J. M. Bowman, and R. R. Lucchese, *Phys. Rev. B* **31**, 1184 (1985).

[12] S. Tsai, C. E. Lin, J. C. Lin, and J. K. Wang, *Chem. Phys. Lett.* **295**, 509 (1998).

[13] A. B. Gurevich, B. B. Stefanov, M. K. Weldon, Y. J. Chabal, and K. Raghavachari, *Phys. Rev. B* **58**, 13434 (1998).

[14] S. K. Jo, J. H. Kang, X. M. Yan, J. M. White, J. G. Ekerdt, J. W. Keto, and J. Lee, *Phys. Rev. Lett.* **85**, 2144 (2000).

[15] U. K. Das, T. Yashda, and S. Yamasaki, *Phys. Rev. Lett.* **85**, 2324 (2000).

[16] S. BEDARD and L. J. LEWIS, *Phys. Rev. B* **61**, 9895 (2000).

Chapter 4

Hydrogen Diffusion and Chemical Reactivity with Water on Nearly Ideally H-terminated Si(100) Surface

Jpn. J. Appl. Phys. 41 (2002) 4275-4278

4.1 Abstract

A nearly ideally H-terminated condition for a Si(100) 2×1 surface is determined from the dependence of the peak intensity and the line width of the coupled monohydride symmetric stretching vibration on the hydrogen exposure and exposure temperature, which has been investigated with BML-IRRAS. Even for nearly ideally H-terminated surfaces, the line width significantly changes depending on the hydrogen exposure and the exposure temperature. The concentration of deuterium atoms incorporated in the Si bulk is measured by temperature programmed desorption, and it is concluded that hydrogen diffusion into the subsurface of Si has a significant influence on the line width broadening. The chemical reactivity with water on the H-terminated Si surface is also investigated.

4.2 Introduction

Hydrogen-terminated Si surfaces have attracted strong interest not only from the viewpoint of application to semiconductor device fabrication, but also of their importance as a model system for surface science phenomena. It is well-known that atomically flat Si(100) surfaces are difficult to obtain by the wet process [1, 2]. Therefore, the dry process is the method of choice for the Si(100) surface. In spite of the large number of reported works on H-termination, there are still many undiscussed important topics. Such important topics are the hydrogen diffusion into the silicon bulk and its surface reactivity with water which possibly causes the initial oxidation of the silicon surface. Because of the difficulties due to limitations in the sensitivity and resolution of the available experimental techniques, these topics have only begun to be understood in detail [3–5]. In the present work, the dependencies of the IR spectra on the hydrogen exposure and exposure temperature have been measured for H-terminated Si(100)-(2×1) surfaces. A BML-IRRAS technique is used for IR measurements [6–8]. It is found that even at an almost ideally H-terminated region the line width of CMH changes significantly with the exposure temperature (T_x) and the hydrogen exposure. The condition for the nearly ideally H-terminated Si(100) surface has been determined. The reason for line width broadening has been discussed and it was ascertained that line width broadening is caused by the diffusion of hydrogen into the silicon subsurface. The chemical reactivity of the H-terminated surface with water is investigated in detail for the first time.

4.3 Experiments

Experiments were carried out using an UHV reaction chamber equipped with IRRAS optical systems and a RHEED apparatus. The optical path of the IRRAS system was purged by N_2 gas. A p-polarized IR beam from a FT-IR spectrometer (JEOL JIR7000) was selected by a wire grid polarizer using KRS-5 and directed into the reaction chamber through a ZnSe viewing port with an incident angle of 85^o on the sample surface. The reflected IR beam was focused onto an MCT detector cooled by liquid nitrogen. The sample was heated by a PBN heater

controlled by a feed-back temperature controller. A W-Re thermocouple gauge was attached to the rear side of the substrate. The thermocouple gauge was calibrated by an optical pyrometer using ε =0.8. The error of our temperature measurement was estimated to be less than $\pm$ 10 K by comparing our hydrogen TPD spectrum with published data. [9] The temperature inhomogeneity (difference between the center and the edge region observed using the pyrometer) in the IR-illuminated area of the sample surface was less than 30 K. Atomic hydrogen was produced by using an incandescent tungsten filament. Hydrogen was dosed using a leak valve and by monitoring the pressure in the chamber with a Granville-Phillips ion gauge. The base pressure in the chamber was less than 2×10^{-10} Torr. The hydrogen dosing time for each deposition and measurement cycle was 20 s. The IRRAS spectrum of a completely deuterium-covered surface immediately after the surface cleaning was used as the background (BG). The displayed spectra are obtained by dividing the signal spectrum (SG) by the BG. The substrate temperature (T_m) for both the BG and SG measurements was 373 K in the present work, if it is not stated otherwise. The line width in the present work corresponded to that measured without a deconvolution of the resolution function.

The Si(100)-$CoSi_2$ BML substrates, prepared by Co^+-ion implantation (200 keV, 3×10^{17} ions cm^{-2} followed by annealing at 1170K), were purchased from Toray Research Center. The 100-nm-thick $CoSi_2$ layer was buried under the 50-nm-thick overlayer. The BML wafer was cut to 14×14 cm^2, and after wet treatments using dilute HF and HCl/H_2O_2 solutions, it was put into the reaction chamber, where the surface oxide was desorbed by heating the wafer above 1100K. Since as-purchased wafers have significant ion implantation damage, a Si epitaxial layer of about 50 nm thickness, which gave a clear 2×1 RHEED pattern, was grown on the damaged surface by using disilane gas at 1020K. The total thickness of the overlayer measured by cross-sectional SEM was about 100 nm. A Rutherford backscattering (RBS) analysis revealed that no cobalt was present in the overlayer.

The usual procedures for one IR measurement cycle were: 1) thermal cleaning of the sample surface at about 1170 K, 2) saturation (5000 L) adsorption of deuterium at 673 K, 3) temperature decrease to 373 K for the measurement of

the BG IRRAS, 4) thermal cleaning of the sample at about 1170 K followed by a decrease to the exposure temperature T_x and saturation adsorption (500 L or 1000 L) of hydrogen, and 5) temperature decrease to T_m=373 K for the measurement of the SG.

All of the samples showed clear (2×1) RHEED patterns before and after the hydrogen (deuterium) exposure.

4.4 Nearly ideally H-terminated surface

It is well known that the structure of the hydrogen-adsorbed Si(100) surface changes characteristically depending on the temperature [10–12]. At above 600 K, the higher hydride species almost completely decomposes and the surface is covered only by CMH. In our preliminary experiments [12, 13], we confirmed that the CMH saturation is achieved in the 200 $\sim$ 5000 L hydrogen exposure range as in that region a sharp (2×1) RHEED pattern is observed. No higher hydride species existed since no such related peaks could be detected in our experiments. At a higher hydrogen exposure range, the (2×1) RHEED pattern becomes diffuse, indicating that the surface becomes rough due to hydrogen etching effects. Based on this background knowledge, the vibrational spectra for the H-saturated Si(100) surface obtained following 200 $\sim$ 1000 L hydrogen exposure have been investigated in detail.

The IRRAS spectra have been measured at different T_x for hydrogen exposure of 500 L and 1000 L (Fig. 4.1). The dependencies of the integrated absorbance and the line width of the CMH symmetric vibration peak on T_x are shown in Fig. 4.2. Furthermore, we have measured the change of the line width depending on the hydrogen exposure level at T_x=623 K and T_x=673 K as depicted in Fig. 4.3.

The homogeneous line width of the CMH symmetric stretching vibration can be determined by vibration dephasing [14]. The minimum line widths obtained in our experiments at the hydrogen exposure level of 500 L, which are 2.1 cm^{-1} at Tm=373 K and 1.75 cm^{-1} at T_m=300 K, almost agree with those reported in literature (3.2 cm^{-1} at T_m=373 K [15] and 1.9 cm^{-1} at T_m=300 K [14]). The detailed investigation of the line width, however, shows much more complex

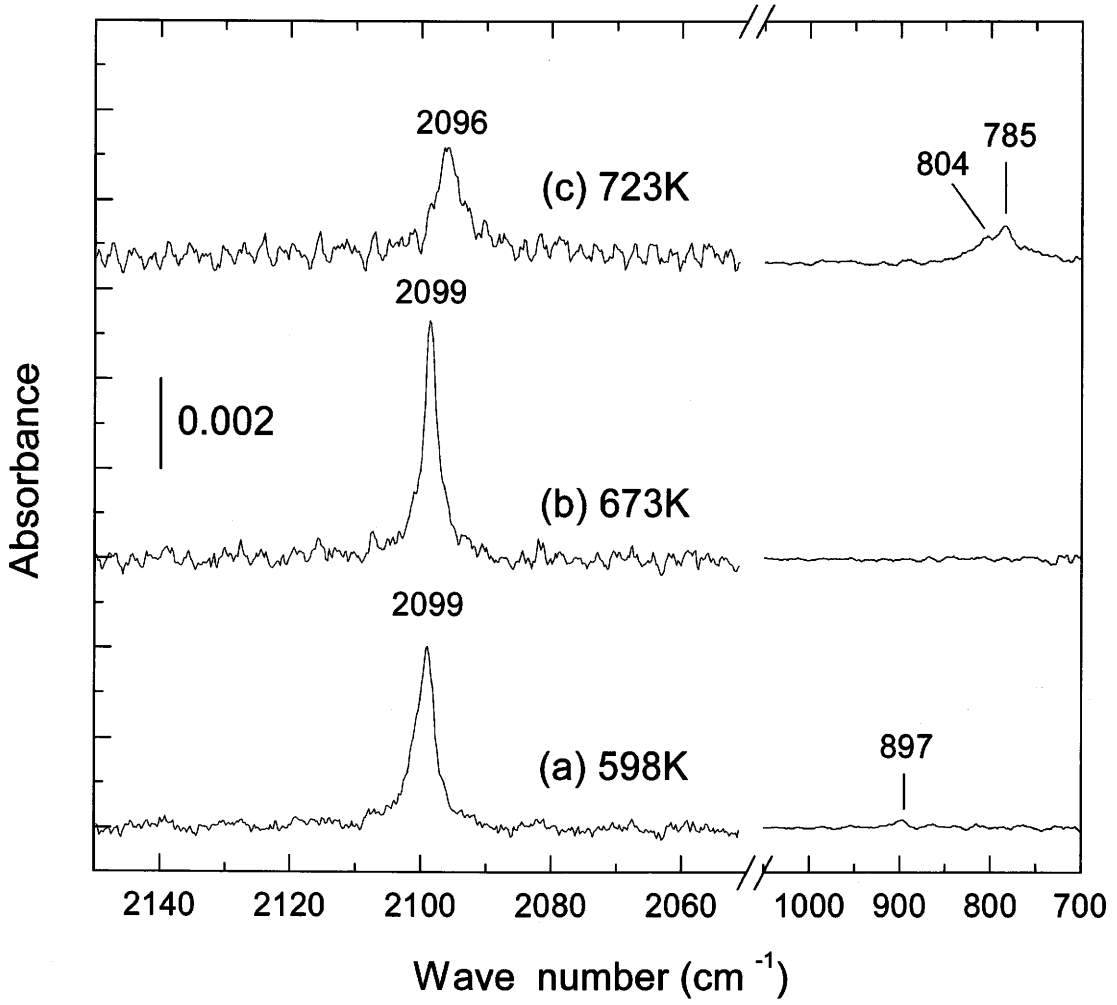

Figure 4.1: BML-IRRAS spectra of the Si(100) (2×1)-H surfaces prepared at different T_x (a) 598 K, (b) 673 K and (c) 723 K on 500 L hydrogen exposure. Assignments of the peaks: 2096 and 2099 cm^{-1}: CMH, 897 cm^{-1}: SiH_2 bend scissors, and 804 and 785 cm^{-1}: Si-OH stretching.

dependencies on the exposure temperature and the hydrogen exposure than those previously reported.

Concerning Fig. 4.2, the line width narrowing of the CMH symmetric stretching vibration with increasing T_x up to around T_x=600 K is explained by the increase in homogeneity due to the decomposition of higher hydride species, which is shown by the decrease of the peak intensity of the SiH_2 bend scissors mode from 5×10^{-4} (at T_x= 400 K, not shown) to 1.3×10^{-4} (Fig. 4.1(a)) in absorbance.

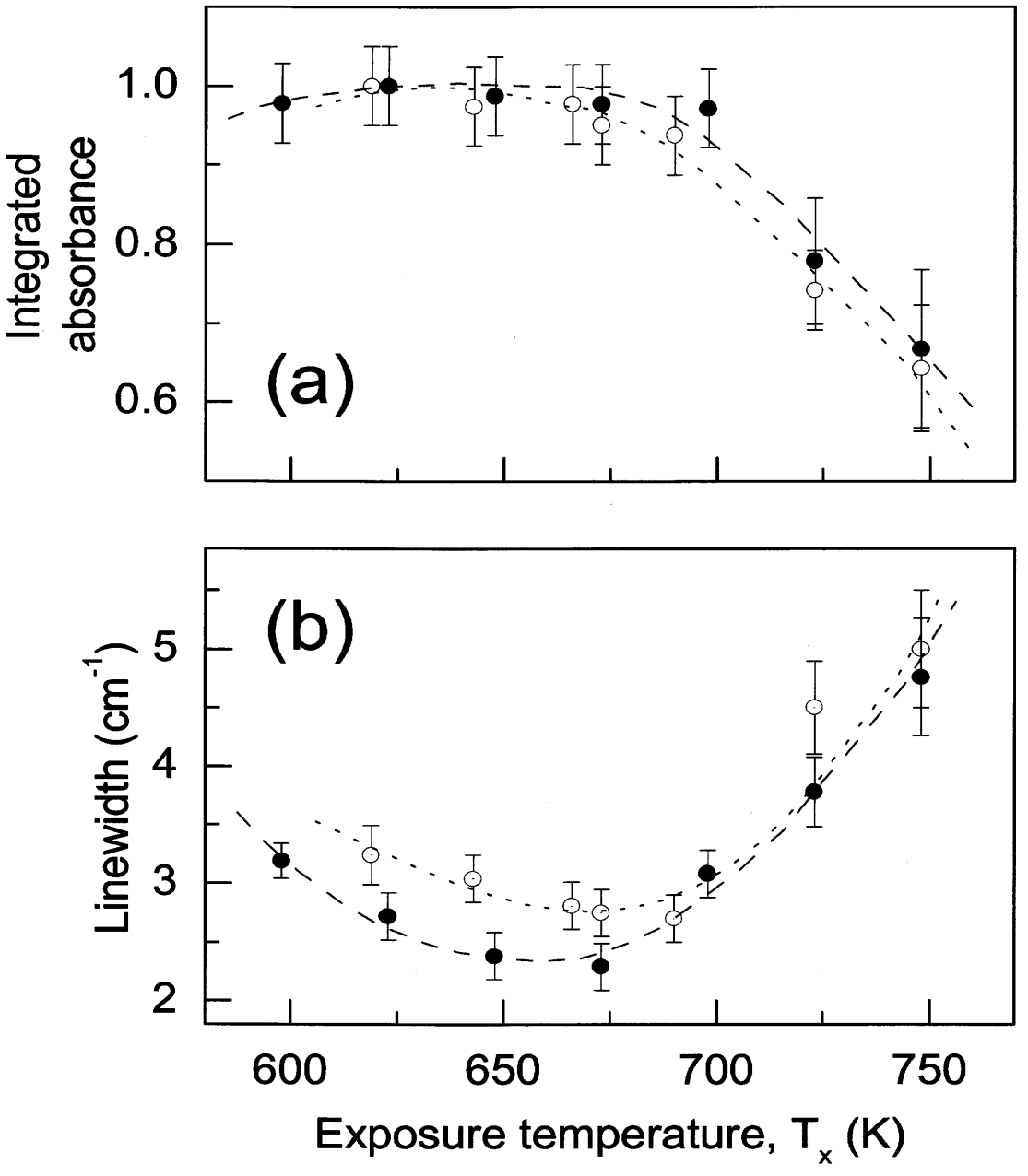

Figure 4.2: Dependencies of the normalized integrated absorbance (a) and the line width (b) on hydrogen T_x for the hydrogen exposure of 500 L (•) and 1000 L (○).

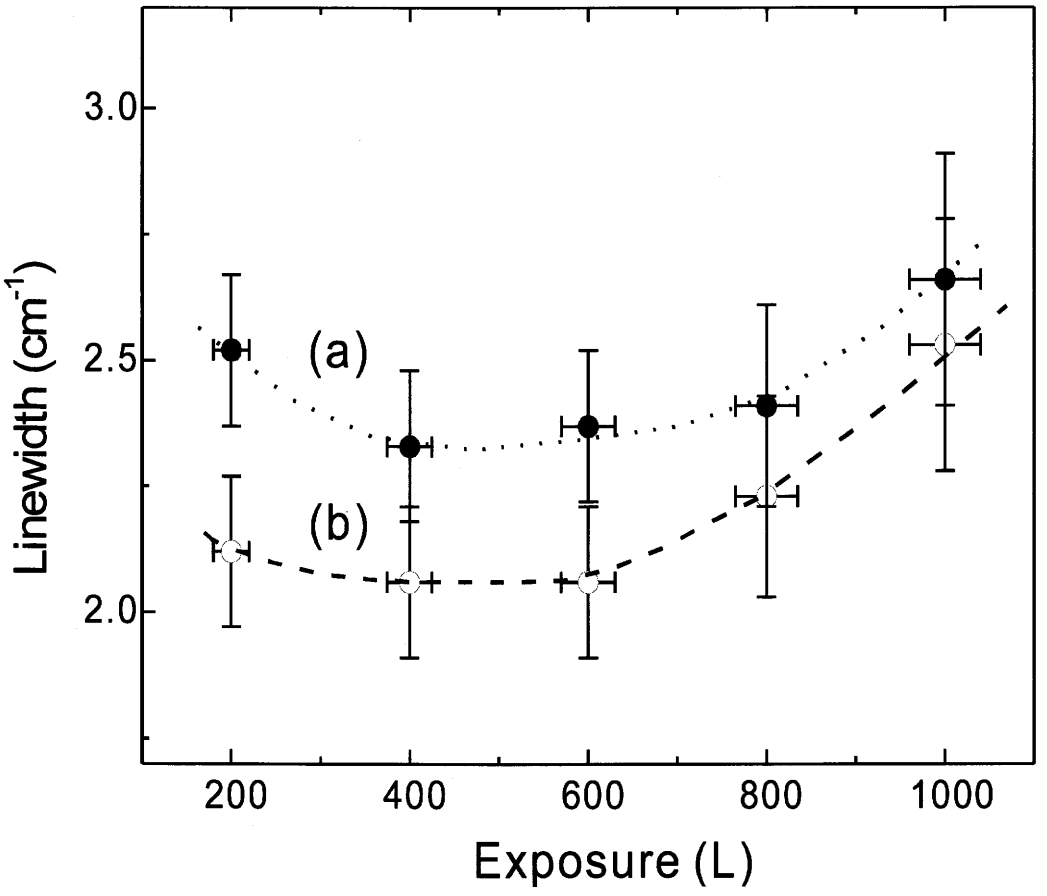

Figure 4.3: Dependence of the line width on the hydrogen exposure and T_x. •: T_x=623 K, and ○: T_x=673 K

At a high-temperature region, (T_x > 675 K), the line width broadens again with increase of T_x, which can be explained by the increase of the inhomogeneity due to the decomposition of CMH, resulting in the inhomogeneous distribution of CMH and contamination by water from the residual gas, which is revealed by the 804 and 785 cm^{-1} peaks which are assigned to the Si-OH stretching mode [16] as shown in Fig. 4.1(c). The almost similar line width curves for 500 L and 1000 L hydrogen exposure (Fig. 4.2) are consistent with this result, since at a high-temperature region, (T_x > 675 K), CMH decomposition effects induced a condition on the Si surface similar to that when equilibrium was reached after adsorption. Concerning Fig. 4.3, the large line width at a low hydrogen exposure range (< 200 L, data not shown here) can be attributed to a low coverage

of the CMH resulting in the increase of the inhomogeneity of the CMH spatial distributions and contamination by H_2O from the residual gas. One interesting point is the line width broadening at higher exposure regions of $>$ 500 L in Fig. 4.3 where no higher hydride species peaks can be observed. Also, it is interesting that the line width becomes narrow with increasing T_x at T_x=620 $\sim$ 670 K. These data show that the line width sensitively changes depending on T_x and hydrogen exposure even at completely H-terminated conditions, where both the inhomogeneity due to the background water contamination and the CMH inhomogeneous distribution can be ignored. We have also confirmed that no peaks related to the water contamination appear even after 10 h in the vacuum chamber on the nearly ideal H-terminated surfaces.

As a reason of this line width broadening, surface roughness induced by the etching could be ruled out: all RHEED patterns exhibit a sharp (2×1) pattern, and further more no defect-related vibration peaks such as isolated SiH are observed up to $\sim$ 5000 L hydrogen exposure. The nonexistence of higher hydride species and hydrogen etching defects, and the structural stability for prolonged hydrogen exposure of completely H-terminated Si(100) surfaces are also confirmed by STM [17]. As a possible explanation we therefore suggest that line width broadening is due to hydrogen diffusion into the silicon subsurface.

Although the behavior of hydrogen in crystalline silicon has been the subject of previous experimental and theoretical investigations [18–20], to our knowledge the effect of the bulk hydrogen on the IR line width has not yet been investigated.

To establish whether subsurface H could be present under our experimental conditions, we have subsequently first exposed the Si(100) surface to the atomic deuterium ($\sim$ 5000 L) at different T_x immediatedly after the high-temperature thermal cleaning. Then, after the surface silicon deuterides were completely replaced by hydrogen by exposing the surface to atomic hydrogen (500 L) at 620 K, the concentration of D atoms incorporated in the bulk Si was measured by the conventional TPD as shown in Fig. 4.4. The relative amount of the desorbed D atoms was found to increase in proportion to the line width increasing from T_x=673 K to T_x=598 K as shown in Figs. 4.2(b) and 4.4. This means that hydrogen (deuterium) incorporation becomes easier when T_x becomes lower. It is also clearly identified from Fig. 4.3 that the low-T_x line width is always larger

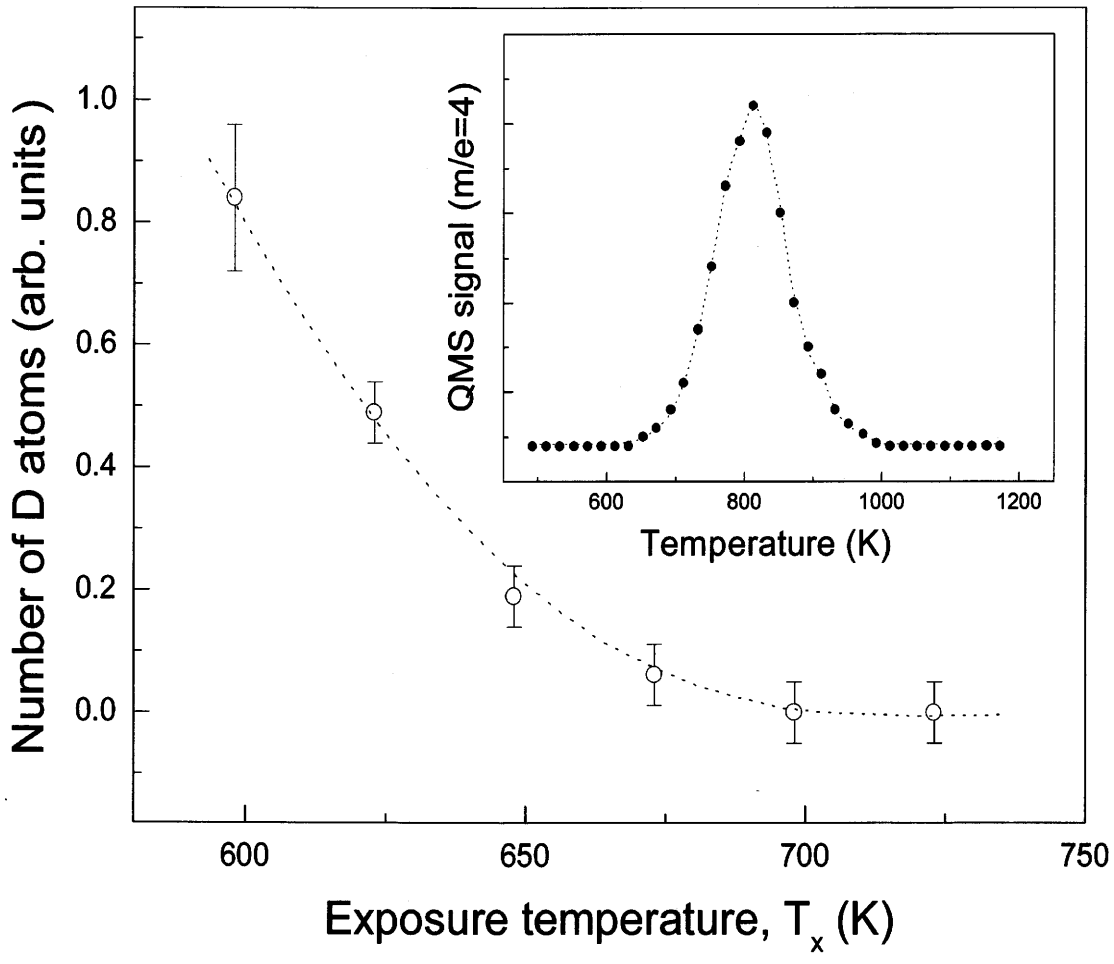

Figure 4.4: Dependence of the desorption of deuterium atoms incorporated into the Si bulk on the T_x. Desorption in the form of D_2 is measured by TPD. The TPD spectrum for the sample prepared at T_x=623 K is inserted. Sample preparation procedures are written in the text.

than the high-T_x line width.

From these data, it is concluded that the nearly ideally H-terminated surface can be obtained in the 400 $\sim$ 600 L hydrogen exposure range at T_x=620 $\sim$ 670 K.

4.5 Reactivity with water of H-terminated Si(100) surfaces

It is known that the Si(100) surface is extremely reactive with water [3, 21]. The surface is almost fully covered by Si-H and Si-OH groups by the dissociative adsorption of a water molecule on a single dimer unit [22–24]. In our experiments after high-temperature annealing, peaks related to the water adsorption (785 and 804 cm^{-1}) appear even at UHV (base pressure about 2×10^{-10} Torr) as shown in Fig. 4.1(c). Also it is known that the Si(100) surface will be contaminated by residual water on UHV chamber even the water partial pressure is at 10^{-11} torr level [25]. Figure 4.5 showed the trace of water decomposed to form Si-H and Si-OH at the same Si-Si dimer on Si(100) clean surface. It is interesting to know whether the H-terminated Si(100) surface reacts with water. This is also important from the viewpoint of application to the silicon device fabrication, since surface passivation plays an important role in the semiconductor process.

Nearly ideally H-terminated Si(100) surfaces were formed by exposing the clean Si(100) surface to 500 L hydrogen at 650 K. Then the change of the surface by exposing to water was monitored by BML-IRRAS as a function of the water exposure as shown in Fig. 4.6. The negative peak at 2098 cm^{-1} shows that the initial coupled monohydride is decomposed by irradiation of water. With increasing the water exposure the negative peaks became larger and the positive also keep the same trend. The peaks at 901 and 914 cm^{-1} are attributed to the scissoring modes of isolated and adjacent SiH_2 (δSiH_{ID} and δSiH_{AD}), respectively [12]. The peaks at 962 and 979 cm^{-1} are first observed in our experiment.

To explained the vibrational peaks we have been calculated two types of cluster model systems, which contain 9 and 10 silicon atoms, respectively. Almost all possible model sturctures have been used for calculation. The detailed assignment and discussion will be the topic of next paragraph. Here we only make simple assignment for several typical peaks. The doublet peaks at 962 and 979 cm^{-1} are assigned to δSiH_{ID} and δSiH_{AD} with two inserted oxygen atoms at Si back bonds. It means the oxidation processes will occur when water react with H-terminated Si(100) surface. The final products are highly oxidized species. This can be explained also by theoretical calculation analysis. Fig. 4.7 shows the

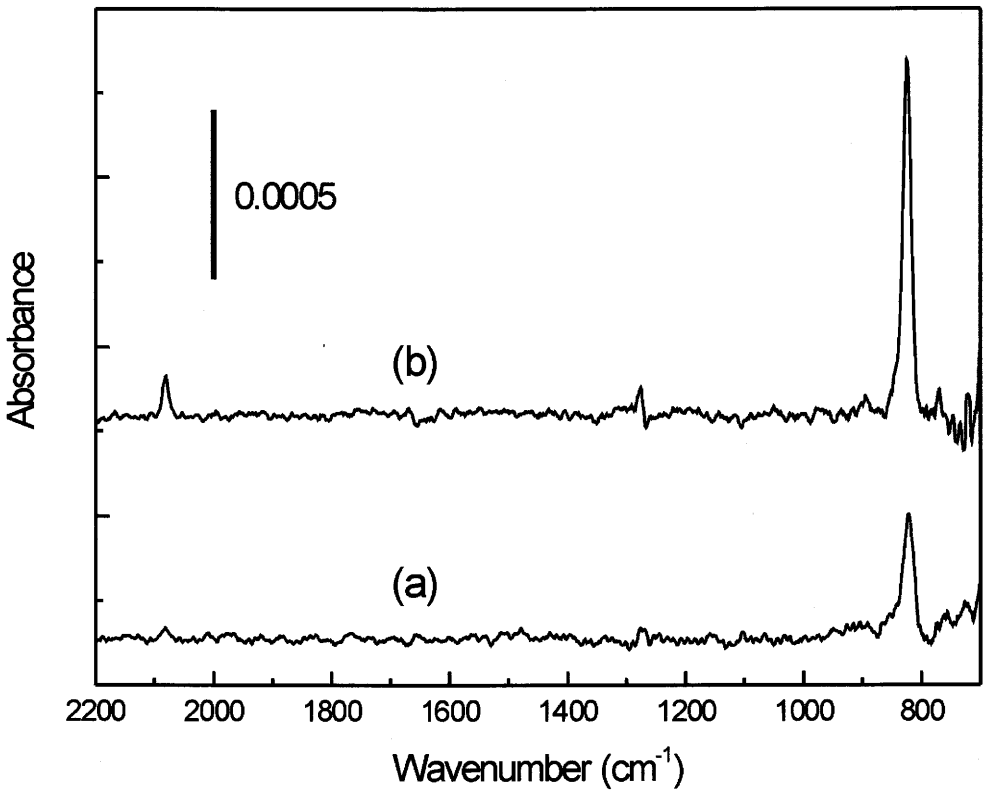

Figure 4.5: Change of the BML-IRRAS spectra after high temperature annealing for Si(100) sample at UHV chamber wiht base pressure 2×10^{-10} torr and water partial pressure 5×10^{-11} torr. (a) 1 hour after cleanning, about 0.2 L; (b) 5 L water exposure.

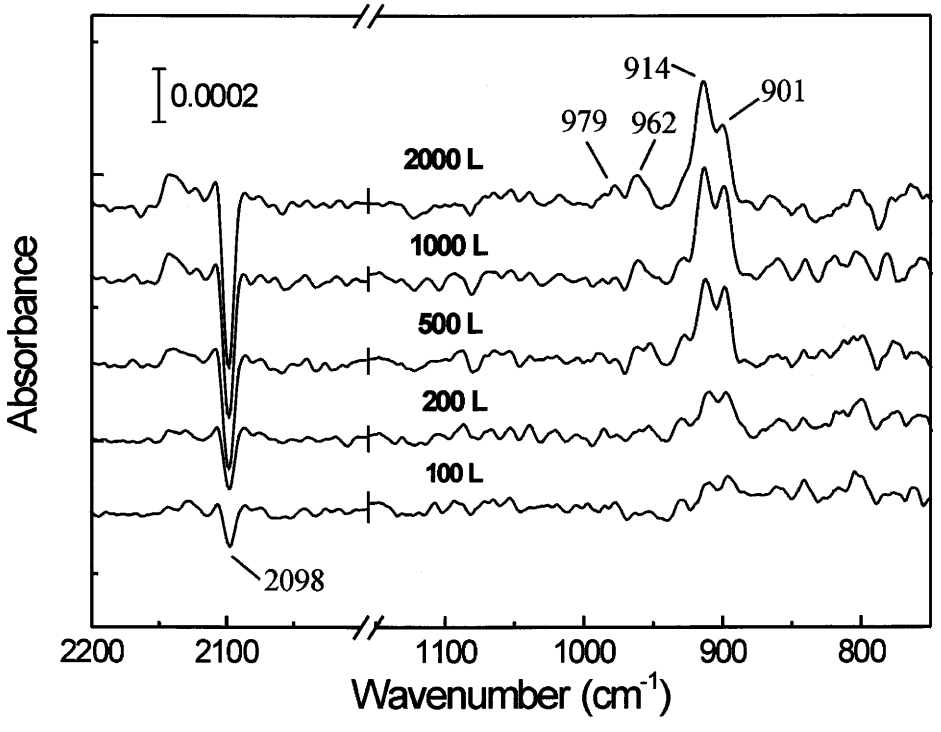

Figure 4.6: Change of the BML-IRRAS spectra by exposing to water at 373 K, on nearly ideally H-terminated Si(100)-(2×1) surface.

possible reaction path way for this system.

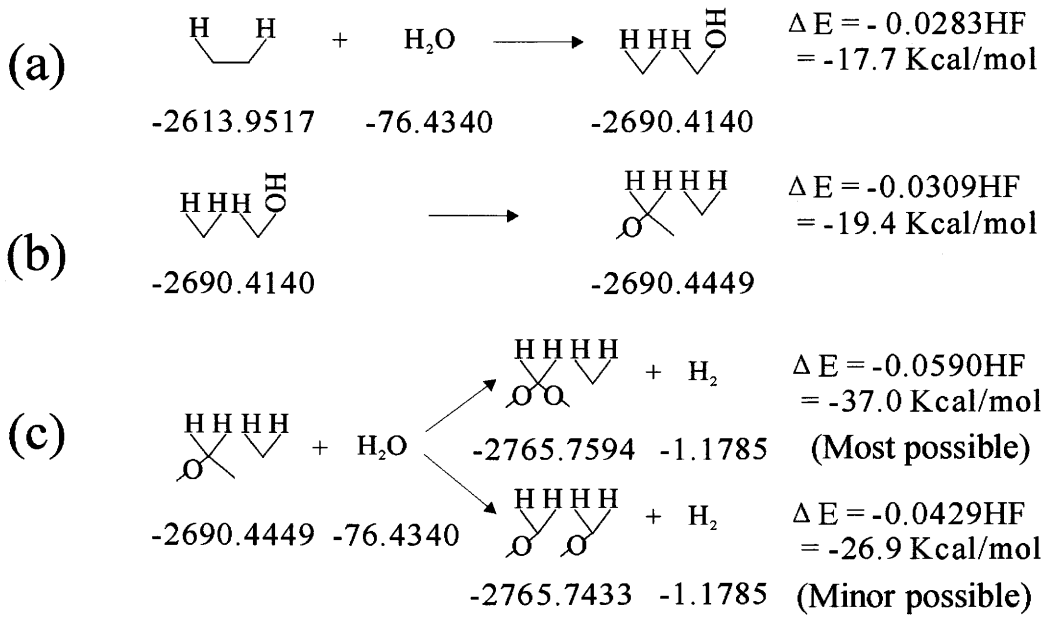

Figure 4.7: Possible reaction mechanism scheme for H_2O + H-terminated Si(100)-(2×1) system. The number below every model structures are calculated energies in HF unit.

From the Fig. 4.7 it is clear the most of final products are highly oxidized species with two oxygen atoms inserted into Si backbond. It si concluded that the nearly ideally H-terminated Si(100) surface is still quite reactive with water. However, it is also concluded that H-terminated surface works as the passivation layer on the basis of the comparison between Figs. 4.5 and 4.6. It is known that we can protect the Si(100) surface from the background water for more than 10 h at 10^{-10} Torr which we can easily attain by the conventional ultrahigh vacuum techniques.

4.6 Conclusions

The complex dependencies of line widths and integrated absorbance on T_x and hydrogen exposure for Si(100) surfaces have been investigated in detail by using the BML-IRRAS. Nearly ideally H-terminated Si(100) surfaces can be obtained in the 400 $\sim$ 600 L hydrogen exposure at T_x=620 $\sim$ 670 K. The IR line

width of CMH changes depending on the hydrogen exposure and T_x. This line width change is attributed to the hydrogen diffusion into the Si subsurface. The reactivity of the nearly ideally H-terminated Si(100) surface with water molecules was investigated, and it has been found that the surface is still quite reactive with water, but the H-termination has high passivation ability against the background water in the UHV chamber.

Bibliography

[1] P. DUMAS, Y. J. CHABAL, and P. JAKOB, *Surf. Sci.* **269** (1992).

[2] Y. J. CHABAL, G. S. HIGASHI, K. RAGHAVACHARI, and V. A. BURROWS, *J. Vac. Sci. Technol. A* **7**, 2104 (1989).

[3] M. K. WELDON, B. B. STEFANOV, K. RAGHAVACHARI, and Y. J. CHABAL, *Phys. Rev. Lett.* **79**, 2851 (1997).

[4] B. B. STEFANOV, A. B. GUREVICH, M. K. WELDON, K. RAGHAVACHARI, and Y. J. CHABAL, *Phys. Rev. Lett.* **81**, 3908 (1998).

[5] M. K. WELDON, K. T. QUEENEY, A. B. GUREVICH, B. B. STEFANOV, Y. J. CHABAL, and K. RAGHAVACHARI, *J. Chem. Phys.* **113**, 2440 (2000).

[6] V. M. BERMUDEZ, *J. Vac. Sci. Technol. A* **10**, 152 (1992).

[7] A. YOSHIGOE, K. MASE, Y. TSUSAKA, T. URISU, Y. KOBAYASHI, and T. OGINO, *Appl. Phys. Lett.* **67**, 2364 (1995).

[8] Y. KOBAYASHI and T. OGINO, *Surf. Sci.* **368**, 102 (1996).

[9] C. C. CHENG and J. T. Y. JR., *Phys. Rev. B* **43**, 4041 (1991).

[10] H. WAGNER, R. BUTZ, U. BACKES, and D. BRUCHMANN, *Solid-State Commun.* **38**, 1155 (1981).

[11] Y. J. CHABAL and K. RAGHAVACHARI, *Phys. Rev. Lett.* **54**, 1055 (1985).

[12] H. NODA and T. URISU, *Chem. Phys. Lett.* **326**, 163 (2000).

[13] H. NODA, T. URISU, Y. KOBAYASHI, and T. OGINO, *Jpn. J. Appl. Phys.* **39**, 6985 (2000).

[14] J. C. TULLY, Y. J. CHABAL, K. RAGHAVACHARI, J. M. BOWMAN, and R. R. LUCCHESE, *Phys. Rev. B* **31**, 1184 (1985).

[15] S. TSAI, C. E. LIN, J. C. LIN, and J. K. WANG, *Chem. Phys. Lett.* **295**, 509 (1998).

[16] A. B. GUREVICH, B. B. STEFANOV, M. K. WELDON, Y. J. CHABAL, and K. RAGHAVACHARI, *Phys. Rev. B* **58**, 13434 (1998).

[17] J. J. BOLAND, *Surf. Sci.* **261**, 17 (1992).

[18] S. K. JO, J. H. KANG, X. M. YAN, J. M. WHITE, J. G. EKERDT, J. W. KETO, and J. LEE, *Phys. Rev. Lett.* **85**, 2144 (2000).

[19] U. K. DAS, T. YASHDA, and S. YAMASAKI, *Phys. Rev. Lett.* **85**, 2324 (2000).

[20] S. BEDARD and L. J. LEWIS, *Phys. Rev. B* **61**, 9895 (2000).

[21] F. S. TAUTZ and J. A. SCHAEFER, *J. Appl. Phys.* **84**, 6636 (1998).

[22] Q. GAO, Z. DOHNALEK, C. C. CHENG, W. J. CHOYKE, and J. T. YATES, *Surf. Sci.* **312**, 261 (1994).

[23] L. M. STRUCK, J. E. JR., B. E. BENT, G. W. FLYNN, Y. J. CHABAL, S. B. CHRISTMAN, E. E. CHABAN, K. RAGHAVACHARI, G. P. WILLIAMS, K. RADERMACHER, and S. MANTL, *Surf. Sci.* **380**, 444 (1997).

[24] N. FRANCO, J. CHROST, J. AVILA, M. C. ASENSIO, C. MULLER, E. DUDZIK, A. J. PATCHETT, I. T. MCGOVERN, T. GIEBEL, R. LINDSAY, V. FRITZSCHE, A. M. BRADSHAW, and D. P. WOODRUFF, *Appl. Surf. Sci.* **123** (1998).

[25] H. NODA, *Thesis of the Doctor of Philosophy, The Graduated University for Advanced Studies* (2000).

Chapter 5

Assignment of surface IR absorption spectra observed in the oxidation reactions : H + H_2O/Si(100) and H_2O + H/Si(100)

Submitted to Physical Review B and Physical Review Letters

5.1 Abstract

Infrared reflection absorption spectroscopy using buried metal layer substrates (BML-IRRAS) and density functional cluster calculations have been employed to study the water related oxidation H + H_2O/Si(100)-(2×1), D + H_2O/Si(100)-(2×1) and H_2O + H/Si(100)-(2×1) systems. In addition to the oxygen inserted coupled monohydrides reported earlier in H + H_2O/Si(100)-(2×1) system, we report here several other oxidized Si hydride species in our BML-IRRAS experiments. We clearly identify three pairs of new doublet bands in the 900 ∼ 1000 cm^{-1} region. The vibrational frequencies have been calculated using Si9 and Si10 cluster models which include all possible structures from zero to five oxygen insertions into the top layer silicon atoms using B3LYP gradient corrected den-

sity functional method with polarized 6-31G** basic set to all atoms. The three doublet bands are assigned to the scissoring modes of adjacent and isolated SiH_2 with zero, one and two oxygen atoms inserted into the Si back bonds. All the other observed vibrational peaks related to Si oxidation have also been assigned in this study.

5.2 Introduction

Reaction of water with Si(100) surface has been receiving considerable attention due to its importance in industrial oxidation processes and the mechanic studies of the initial oxidation at Si surfaces [1–7]. Vibrational spectroscopy in combination with *ab initio* quantum chemical cluster calculations has been emerging as a powerful tool to investigate the atomic level picture of the Si oxidation process. This is essential for understanding and control of the extremely thin gate oxide film ($\sim$ 15 Å) for Si MOS transistors [3, 4, 7]. The reaction of water with Si(100) surface has been studied by IR external transmission (ET) method and the *ab initio* quantum chemical cluster calculations which clearly establish that there is no barrier to dissociative chemisorption of H_2O on Si(100)-(2×1) surface leading to the formation of stable Si-H and Si-OH bands on same Si-Si dimer unit [2]. Further annealing induces the insertion of oxygen atoms into the Si backbonds or the formation of epoxides through dehydrogenation [3, 4]. It has also been reported that the initial surface comprises of an array of isolated and intra row coupled dimers which are coupled by hydrogen-bonding interactions between the OH groups that reside on the same end of adjacent dimers in a dimer row [6]. Such inter dimer coupling facilitates the subsequent transfer of oxygen between dimers leading to the oxygen agglomeration. This initial oxidation of Si surface consists of an inhomogeneous array of zero-, one-, and two-oxygen containing dimers [3]. Recent experiments by external transmission (ET) infrared geometry on atomic hydrogen exposed water-covered surface (H_2O/Si(100)) at 220 K showed that the atomic hydrogen exposure can also induce oxygen insertion as in the case of annealing, but a single oxygen atom incorporation predominates in the former [7]. We have employed infrared reflection absorption spectroscopy (IRRAS) using $CoSi_2$ buried metal layer (BML) Si substrate which is sensitive

to the perpendicular dynamic dipole moment even in the finger print region to investigate the vibrational modes of various oxygen inserted Si species [8–10]. In this paper we report a comprehensive picture of Si oxidation with water and the occurence of new IR bands in the Si-H stretching region as well as new doublet bands in the 900 $\sim$ 1000 cm^{-1} region on H + H_2O/Si(100)-(2×1), D + H_2O/Si(100)-(2×1) and H_2O + H/Si(100)-(2×1) systems. The vibrational bands have not been observed earlier both in multiple internal reflection (MIR) and ET IR measurements. They have been assigned to appropriate surface species present on the highly oxidized Si surface based on the model cluster calculations using B3LYP gradient corrected density functional method with polarized 6-31G** basic set to all atoms.

5.3 Experiments

The BML Si(100) sample was mounted in an ultrahigh-vacuum (UHV) reaction chamber (base pressure less than 2×10^{-10} torr) equipped with IRRAS optical system and reflective high-energy electron diffraction (RHEED) apparatus. A FT-IR spectrometer (JEOL JIR 7000) was used for measurements. IR light was produced by incandescent tungsten filament and p-polarized IR beam was selected by a wire grid polarizer using KRS-5 transmissive lens and directed into the reaction chamber through a ZnSe view port at an incident angle of 85° with respect to Si surface normal. The reflected IR beam is focused onto a mercury cadmium telluride (MCT) detector cooled by liquid nitrogen. The IR interferometer housing system is purged by dry air and the IR optical system outside the UHV chamber is purged by pure nitrogen gas.

The BML Si(100) sample was heated by the PBN (Pyrolytic Graphaite/Pyrolytic Boron Nitride) ceramic heater. The heating current is controlled by PID (proportion-integral-differential) temperature controller. The temperature is monitored by a Re-W thermocouple which is in contact with the back side of the Si sample. The thermocouple temperature is calibrated with respect to the Si sample surface temperature measured by using the infrared pyrometer (ϵ = 0.8). The sample temperature is controlled within 0.5 K at 373 K. The temperature variation from the center to the edge of the sample is about 30 K at 870 K.

The disilane (Si_2H_6) gas has been used to grow thin Si epitaxial layer on the rough surfaces of the ion implanted Si-BML substrates. Atomic hydrogen or deuterium has been produced in the UHV chamber by cracking H_2 or D_2 molecules with incandescent tungsten filaments. Water exposures were given through a high precision needle valve. The hydrogen (deuterium or water) exposures were given in Langmuir units (1L = 10^{-6} Torr-sec) measured by an uncalibrated ion gauge. The Si(100) surface was always cleaned by flashing it above 1100 K for 30 sec and cooled to the desired temperatures for exposures. Water adsorbed Si(100) surfaces were prepared by exposing the clean Si(100) surface to 5 L H_2O at 373 K and H-terminated Si(100) surfaces by exposing Si(100) to 1000 L atomic H at 650 K. The 2×1 RHEED pattern were checked on the Si(100) surfaces before and after exposures. The IRRAS spectrum measured on water covered surfaces has been used as a background (BG) to the signal (SG) spectrum obtained from the H or D exposed H_2O/Si(100) surface. For H_2O + H/Si(100)-(2×1) system, the IR spectrum of H-terminated Si(100) surface was used as a background. All the spectra are presented as -log(SG/BG) with good reproducibility. In the case of H/Si(100)-(2×1) surfaces, we have confirmed the homogeneous line width (2.1 cm^{-1} at 373 K) of the symmetric stretching vibration mode ($\nu_s SiH_{CM}$) of the coupled monohydride (CM) indicating the nearly ideally H-terminated surface [11].

5.4 Theoretical method

The infrared spectral features observed in this study are assigned by quantum chemical calculations. The vibrational frequencies of all the possible modes have been calculated by employing two types of cluster model systems containing 9 and 10 silicon atoms. We have used more than 30 cluster systems in order to calculate the stretching vibrations of the various species involved in the silicon oxidation process and some of them are presented in Fig. 5.1. The 9 silicon atom cluster model structures contain two subtypes which are called coupled monohydride (CM) and adjacent dihydride (AD). The 10 silicon atom cluster model structures have been used for the isolated dihydride (ID) species. The cluster structures in this work include models with one to five oxygen atoms inserted into the top Si

back bonds and/or Si dimer bonds. In the model systems, the dangling bonds of Si atoms other than the top silicon atoms have been terminated by tritium atoms to avoid artifacts due to excess spin or charge. Unlike the reported theoretical methods in which the third and forth layer silicon atoms are fixed at the ideal bulk crystalline positions [2–5, 7], all atoms of the clusters in this study are allowed to fully relax with no constraints. The termination with tritium atoms has been found very effective in localizing all the surface vibrations which makes the identification of appropriate final vibrations easier from the calculations. The tritium and the third and forth layer silicon atoms in the clusters are nearly fixed when the final calculation is made for a given vibrational structure. The calculated Si-Si bond lengths in the third and forth layers are varied from 2.35 to 2.38 Åwhich are close to the experimental value 2.35 Å[12]. The minimized total energy geometry is then obtained for each cluster via gradient corrected density functional calculations using the B3LYP method. This combines the gradient corrected 3-parameter exchange function due to the Becke with the Lee-Yang-Parr correlation function [13]. We have used the polarized 6-31 G** basis set for all the atoms and the calculations are performed with Gaussian 98 [14].

5.5 Results and discussion

Figure 5.2 shows the observed BML-IRRAS spectra for 50 L and 1000 L H-exposures to H_2O/Si(100)-(2×1) surface at 373 K. The deconvoluted curves using Lorenzian function are also shown as solid and dotted lines. The negative peaks at 823 cm^{-1} and 2082 cm^{-1} in Fig. 5.2 are assigned to the stretching vibration modes of Si-OH and Si-H, respectively, formed by the dissociative adsorption of H_2O on the same Si-Si dimer present on the Si(100)-(2×1) surface [3, 7, 15]. Since we use H_2O/Si(100) IR spectrum as a background, the negative peaks indicate the decomposition of Si-OH and Si-H groups due to the exposure of atomic hydrogen to water covered Si(100) surface. The positive peaks in Fig. 5.2 essentially demonstrate the reactivity of water covered Si surface with atomic hydrogen. Higher exposure of atomic hydrogen develops clear IR peaks for various surface species. Figure 2 shows clear vibrational bands at 863, 901, 916, 926, 938, 963 and 982 cm^{-1} in the SiH_2 scissoring mode region. The peaks at 863 cm^{-1}, 901

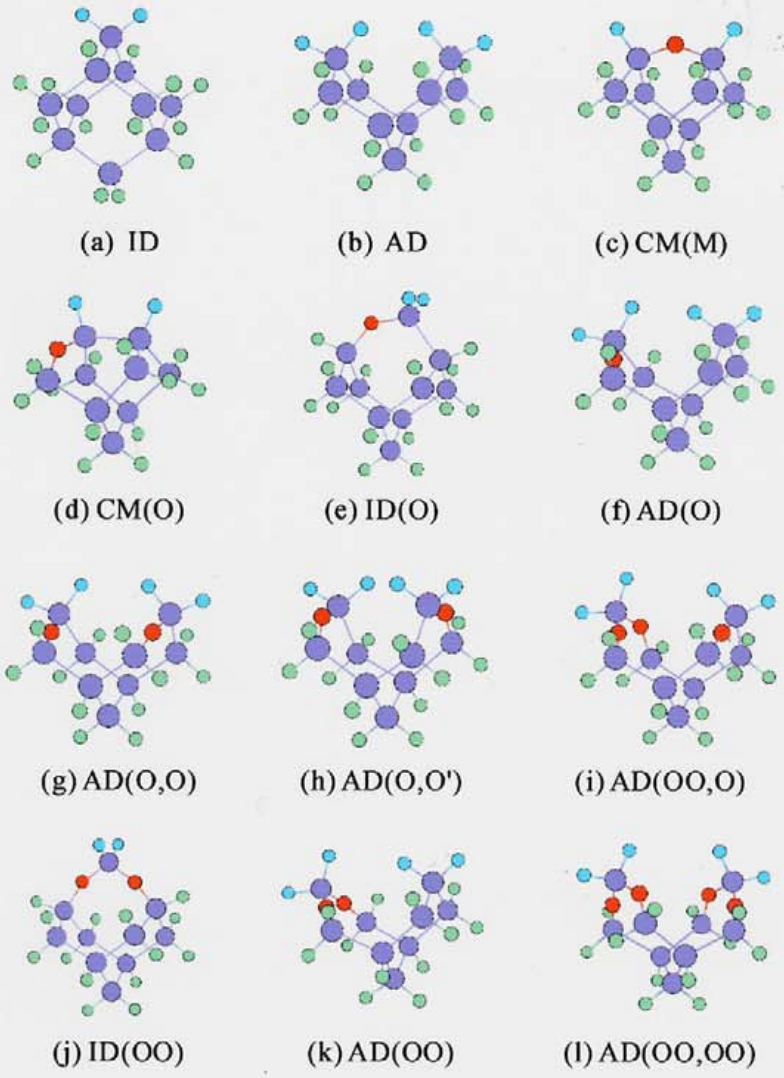

Figure 5.1: Models of different clusters investigated in this work. In the figure, dark blue denotes Si atom, red denotes O atom, light blue denotes H atom and green denotes tritium atom. The cluster models are denoted as ID (isolated dihydride), AD (adjacent dihydride) and CM (coupled monohydride). M in parenthesis represents the oxygen in the dimer bond (Si-O-Si), O and OO in parenthesis represent single oxygen (Si(O)) and double oxygen atoms (Si(OO)) inserted into the Si back bonds. In the cluster models (g) and (h) the single oxygen atoms in the back bonds are present in the *cis* (O,O) and *trans* (O,O') positions.

cm^{-1} and 916 cm^{-1} have been attributed earlier to the symmetric deformation mode of SiH_3 species, the scissoring modes of isolated SiH_2 (δSiH_{ID}, Fig. 5.1(a)) and adjacent SiH_2 (δSiH_{AD}, Fig. 5.1(b)) species respectively [16]. The other vibrational bands observed in the IR spectra of Fig. 5.2 include 1070, 1089, 1107 cm^{-1} in the Si-O stretching region and also 2108, 2114, 2141, 2185, 2198 cm^{-1} in the Si-H stretching region along with the small peaks at 990 $\sim$ 1050 cm^{-1} region. The vibrational peak at 2108 cm $^{-1}$ is assigned to Si-H stretching mode for adjacent dihydride species as shown in Fig. 5.1(b) [7, 16]. The vibrational mode at 2114 cm^{-1} in the stretching region is similar to those observed in earlier studies and assigned to the asymetric and symmetric ν(Si-H) modes respectively of the single-oxygen inserted coupled monohydride (H-Si-O-Si-H : Fig. 5.1(c) or H-Si-Si(O)-H : Fig. 5.1(d)) [7]. In the present study we have assigned the remaining vibrational bands in the Si-O stretch, Si-H stretch and the scissoring regions to various surface species supported by the cluster calculations described above.

The calculated vibrational frequencies along with experimental values for various silicon oxide species are summarized in Table 1 and Table 2. In order to obtain absolute frequency values from the calculated frequencies appropriate frequency scaling factors (SF) have been used. The scaling factors for various surface silicon species are determined from the established experimental vibrational frequencies already reported. The SF is obtained as the ratio of the selected experimental frequency to the calculated frequency. The selected species and their frequencies include H-Si-Si-H (CM) $\nu(\text{Si-H})_{CM}$ = 2100 cm^{-1}, H-Si-O-Si-H (CM(M)) $\nu(\text{Si-H})_{CM(M)}$ = 2118 cm^{-1}, H-Si-O-Si(O)-H (CM(O,M)) $\nu(\text{Si-O})^2_{CM(O,M)}$ = 1043 cm^{-1} [7], H-Si-H (ID) $\nu(\text{Si-H})_{ID}$ = 2090 cm^{-1} and $SiH_2 \cdots SiH_2$ (AD) $\nu(\text{Si-H})_{AD}$ = 2107 cm^{-1}, H-Si-H (ID) $\delta(\text{Si-H})_{ID}$ = 901 cm^{-1} and $SiH_2 \cdots SiH_2$ (AD) $\delta(\text{Si-H})_{AD}$ = 916 cm^{-1} [16]. For all the vibrations classified as $\nu(\text{Si-H})_{CM}$ SF is 0.9538. Similarly SF is 0.9599 for $\nu(\text{Si-H})_{CM(M)}$, 0.9532 for $\nu(\text{Si-H})_{ID}$, 0.9564 for $\nu(\text{Si-H})_{AD}$, 0.9768 for ν(Si-O), 0.9638 for $\delta(\text{Si-H})_{ID}$ as well as for $\delta(\text{Si-H})_{CM}$ and 0.98 for $\delta(\text{Si-H})_{AD}$. All possible vibrational frequencies expected to be observed by IR-RAS experiment which is sensitive only for the perpendicular component of the dynamic dipole moment have been calculated and depicted in Fig. 5.3.

The unassigned bending modes observed at 926, 938, 963 and 982 cm^{-1} in

Table 5.1: Some calculated and experimental vibrational frequencies for the coupled monohydride and isolated dihydride silicon oxide species.

Structure/species	Vibrational mode	Frequency (cm^{-1}) Calc.	Exp.	Ref.
H-Si-Si-H	ν(Si-H)$_{CM}$	2100	2098	2098 [3, 7, 16]
H-Si-H	ν(Si-H)$_{ID}$	2090	2095	2090 [16]
	δ(Si-H)$_{ID}$	901	901	901 [7, 16]
H-Si-O-Si-H	ν(Si-H)$_{CM(M)}$	2118	2114	2118 [3, 7]
	δ(Si-H)$_{CM(M)}$	791	785	799 [7]
H-Si-Si(O)-H	ν(Si-H)$^{1}_{CM(O)}$	2088	2095	2088 [7]
	ν(Si-H)$^{2}_{CM(O)}$	2112	2114	2109 [7, 16]
	ν(Si-O)$_{CM(O)}$	997	1002	This work *
	δ(Si-H)$_{CM(O)}$	777	775	779 [7]
H-Si(O)-O-Si-H	ν(Si-H)$^{1}_{CM(O,M)}$	2120	2114	2109 [7]
	ν(Si-H)$^{2}_{CM(O,M)}$	2164	2164	2165 [7]
	ν(Si-O)$^{1}_{CM(O,M)}$	1004	1002	1011 [7]
	ν(Si-O)$^{2}_{CM(O,M)}$	1043	1043	1038 [7]
	δ(Si-H)$^{1}_{CM(O,M)}$	796	803	799 [7]
	δ(Si-H)$^{2}_{CM(O,M)}$	821	817	This work
H-Si(O)-Si(O)-H	ν(Si-H)$_{CM(O,O)}$	2106	2108	This work
	ν(Si-O)$_{CM(O,O)}$	1039	1043	This work
H-Si(O)-H	ν(Si-H)$_{ID(O)}$	2107	2108	This work
	ν(Si-O)$_{ID(O)}$	1057	1058	This work
	δ(Si-H)$_{ID(O)}$	928	926	This work
H-Si(O)$_2$-H	ν(Si-H)$_{ID(OO)}$	2160	2164	This work
	ν(Si-O)$_{ID(OO)}$	1097	1089	This work
	δ(Si-H)$_{ID(OO)}$	962	963	This work

* This vibrational mode was reported experimentally at 967 cm^{-1} and correlated to theoretical value at 979 cm^{-1} [7]. However, we have assigned it differently.

Table 5.2: Calculated and experimental vibrational frequencies for the adjacent dihydride silicon oxide species.

Structure/species	Vibrational mode	Calc. (cm^{-1})	Exp. (cm^{-1})
$H_2Si\cdots SiH_2$	$\nu(\text{Si-H})_{AD}$	2107	2108
	$\delta(\text{Si-H})_{AD}$	917	916
$H_2Si\cdots Si(O)H_2$	$\nu(\text{Si-H})^1_{AD(O)}$	2104	2108
	$\nu(\text{Si-H})^2_{AD(O)}$	2113	2114
	$\nu(\text{Si-H})^3_{AD(O)}$	2114	2114
	$\nu(\text{Si-O})_{AD(O)}$	1092	1089
	$\delta(\text{Si-H})^1_{AD(O)}$	916	916
	$\delta(\text{Si-H})^2_{AD(O)}$	942	938
$H_2Si(O)_2\cdots SiH_2$	$\nu(\text{Si-H})^1_{AD(OO)}$	2106	2108
	$\nu(\text{Si-H})^2_{AD(OO)}$	2169	2164
	$\nu(\text{Si-O})_{AD(OO)}$	1125	1121
	$\delta(\text{Si-H})^1_{AD(OO)}$	916	916
	$\delta(\text{Si-H})^2_{AD(OO)}$	976	982
$H_2Si(O)\cdots Si(O)H_2$	$\nu(\text{Si-H})_{AD(O,O)}$	2116	2114
	$\nu(\text{Si-O})_{AD(O,O)}$	1102	1107
	$\delta(\text{Si-H})_{AD(O,O)}$	946	938
$H_2Si(O)\cdots Si(O)H_2$	$\nu(\text{Si-H})_{AD(O,O')}$	2116	2114
	$\nu(\text{Si-O})_{AD(O,O')}$	1087	1089
	$\delta(\text{Si-H})_{AD(O,O')}$	946	938
$H_2Si(O)_2\cdots Si(O)H_2$	$\nu(\text{Si-H})^1_{AD(OO,O)}$	2115	2114
	$\nu(\text{Si-H})^2_{AD(OO,O)}$	2149	2141
	$\nu(\text{Si-H})^3_{AD(OO,O)}$	2182	2185
	$\nu(\text{Si-O})_{AD(OO,O)}$	1110	1107
	$\delta(\text{Si-H})^1_{AD(OO,O)}$	944	938
	$\delta(\text{Si-H})^2_{AD(OO,O)}$	973	982
$H_2Si(O)_2\cdots Si(O)_2H_2$	$\nu(\text{Si-H})^1_{AD(OO,OO)}$	2155	2141
	$\nu(\text{Si-H})^2_{AD(OO,OO)}$	2180	2185
	$\nu(\text{Si-O})_{AD(OO,OO)}$	1115	1107
	$\delta(\text{Si-H})_{AD(OO,OO)}$	978	982

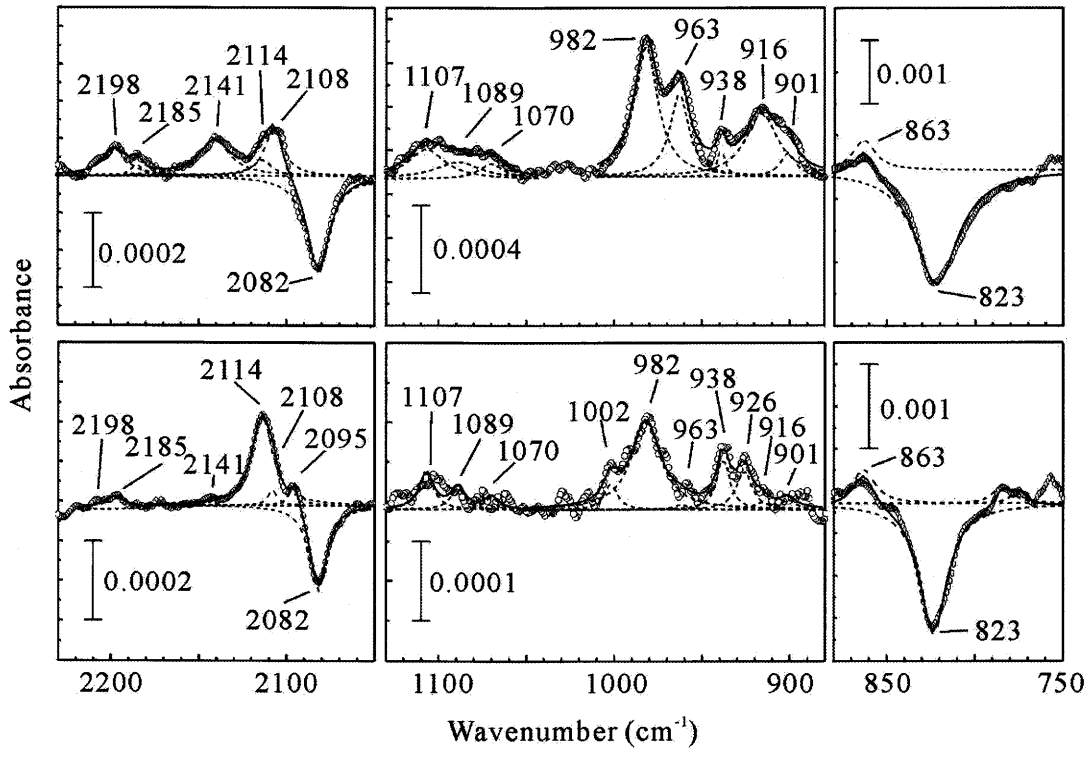

Figure 5.2: The BML-IRRAS spectra for the H + H_2O/Si(100)-(2×1) reaction system. The 50 L (lower panel) and 1000 L (upper panel) atomic hydrogen exposures are given at 373 K. The spectra are deconvoluted using Lorenzian function (solid and dotted lines).

the Si-H scissoring region can definitively be assigned to specific surface species as given in the Table 1 and Table 2. Accordingly, the vibrational excitation at 926 cm^{-1} is due to the isolated dihydride with one oxygen inserted into Si back bond as shown in Fig. 5.1(e) (H-Si(O)-H). The 938 cm^{-1} vibration appears to be a combination of four different adjacent dihydride species with an oxygen atom inserted into the silicon back bonds (Fig. 5.1(f)-1(i)). The Fig. 5.1(g) and 5.1(h) are *cis* and *trans* forms of the species H-Si(O)$\cdots$Si(O)-H. The mode at 963 cm^{-1} is correlated to the isolated dihydride species (H-Si$(O)_2$-H) with two oxygen atoms in the silicon back bonds as shown in Fig. 5.1(j). Further the mode at 982 cm^{-1} is related to the three adjacent dihydride species with two oxygen atoms inserted into the back bonds of the same silicon atom (Fig. 5.1(i), 5.1(k) and 5.1(l)).

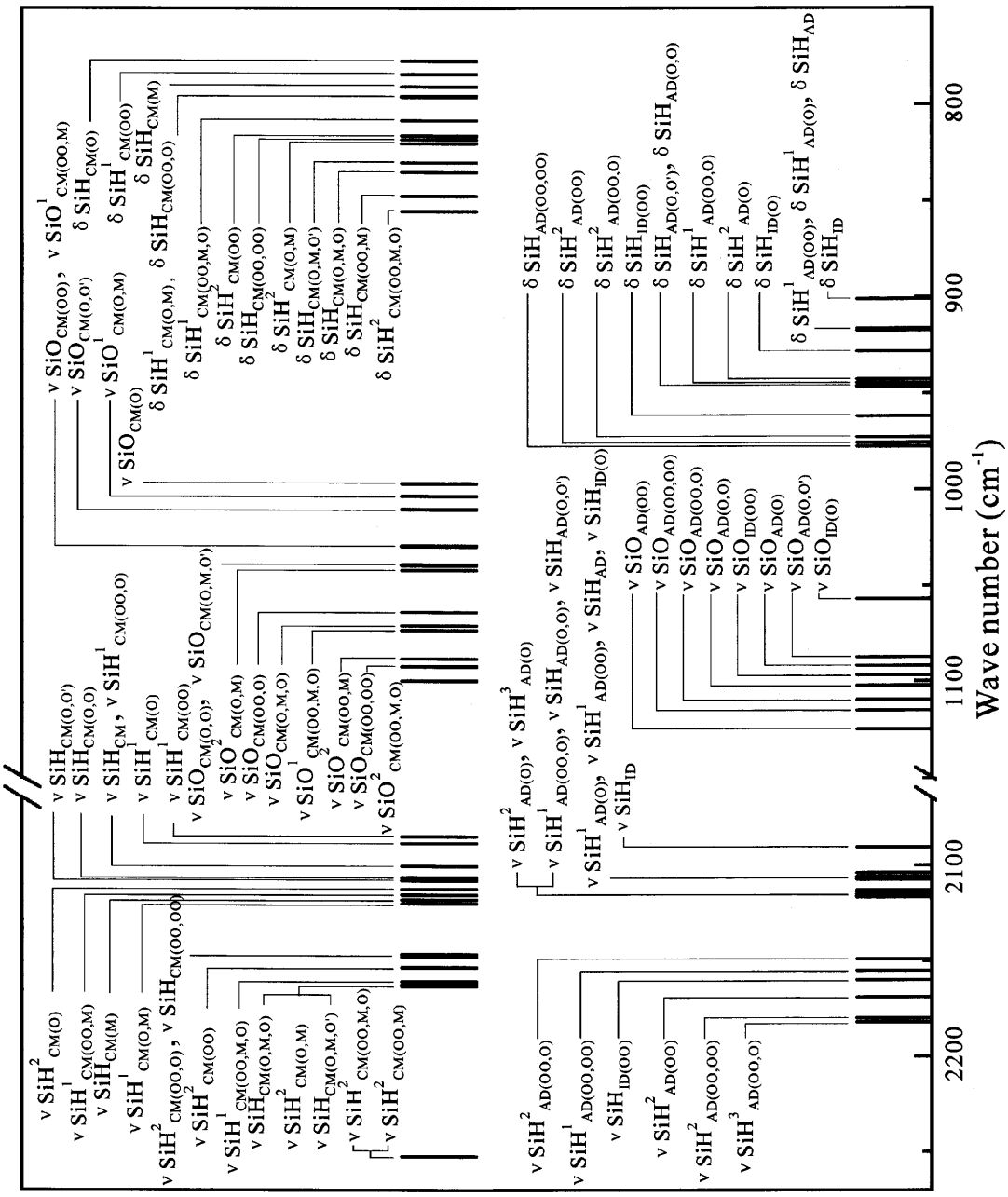

Figure 5.3: Summary of the calculated frequencies for the BML-IRRAS active modes of various silicon species with model cluster structures. Symbols of model clusters are described in the caption of Fig. 5.1. Superscripts indicate the existence of different frequencies for similar vibrational excitations of the same cluster structure.

The species 5.1(i) contributes to both 938 and 982 cm^{-1} Si-H scissoring modes. The 926, 938, 963 and 982 cm^{-1} vibrational modes are almost insensitive to the ET geometry due to their perpendicular dynamic dipole moments. Even at 60 degree incident angle, the δSiH_{ID} peak intensity observed on the H:Si(100)-(3×1) surface by ET geometry [7] is about 1/5 of that observed by the BML-IRRAS [16].

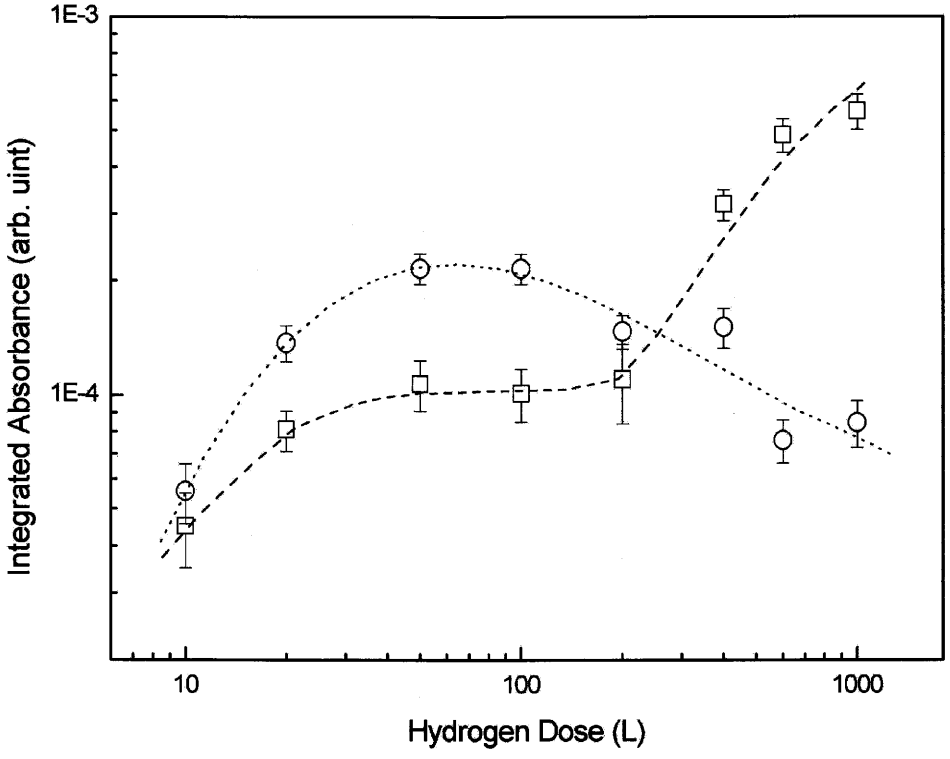

Figure 5.4: Hydrogen dose dependence of the integrated absorbance for the 2114 cm^{-1} ($\nu SiH_{CM(M)} + \nu SiH_{CM(O,M)}$) and 982 cm^{-1} ($\delta SiH_{AD(OO)}$, $\delta SiH_{AD(OO,O)}$ and $\delta SiH_{AD(OO,OO)}$) bands at Tm=373 K.

The small peaks observed in the 990 $\sim$ 1050 cm^{-1} range are assigned from the calculated results shown in Fig. 5.2, to the SiO stretching mode of coupled monohydrides with one to three oxygen atoms at the Si back bonds and/or the Si-Si dimer bond. The peak at 1002 cm^{-1} is assigned to the overlapping of $\nu SiO_{CM(O)}$ (calc. = 997 cm^{-1}) and $\nu SiO^{1}_{CM(O,M)}$ (calc. = 1004 cm^{-1}). However,

Weldon et al. [7] observed ν $SiO_{CM(O)}$ stretch at 967 cm^{-1} experimentally and at 979 cm^{-1} theoretically. Since the similar vibrational peaks of Si-O with oxygen inserted into Si back bond (for example, the calculated ν $SiO_{CM(O,M)}$ for H-Si-O-Si(O)-H is 1013 cm^{-1} by Weldon et al and 1004 cm^{-1} in this work), located at frequencies greater than 1000 cm^{-1}, the calculated frequency at 997 cm^{-1} is considered more appropriate. In the case of thermal oxidation, no clear peaks were observed in this range in the BML-IRRAS measurements. On the other hand, in the case of MIR and ET geometries, strong peaks, $\nu SiO_{CM(M)}$ at 993 cm^{-1} and $\nu SiO_{CM(O,M)}$ at 1042 cm^{-1}, were observed in the case of both thermal and atomic hydrogen-induced oxidation [3, 7].

Concerning this point, since parallel components are dominant in both of these modes, the observed difference between BML-IRRAS and ET or MIR indicates that the dominant CM type species are CM(M) and CM(O,M) in both thermal and atomic hydrogen-induced oxidations. Therefore, the strong peak observed at 2114 cm^{-1} in Fig. 5.2 is assigned to the overlapping of the perpendicular components of $\nu SiH_{CM(M)}$ (calc. = 2118 cm^{-1}) and $\nu SiH_{CM(O,M)}$ (calc. = 2120 cm^{-1}) referring to the calculated results shown in Fig. 5.3. The 2141 cm^{-1} peak observed in the high dose region in Fig. 5.2 can be assigned to the overlapping of the perpendicular components of $\nu SiH_{CM(OO,OO)}$ (calc. = 2148 cm^{-1}) and $\nu SiH_{CM(OO,O)}$ (calc. = 2147 cm^{-1}). Similarly, the 2198 and 2185 cm^{-1} peaks are possibly assigned to the overlapping of the perpendicular components of $\nu SiH^2_{AD(OO,OO)}$ (calc. = 2180 cm^{-1}) and $\nu SiH^3_{AD(OO,O)}$ (calc. = 2182 cm^{-1}), and $\nu SiH^2_{AD(OO)}$ (calc. = 2169 cm^{-1}), respectively. The 2108 cm^{-1} peak may be assigned to the overlapping of $\nu SiH_{CM(O,O')}$ (calc. = 2108 cm^{-1}) and $\nu SiH_{CM(O,O)}$ (calc. = 2106 cm^{-1}). The band observed at $\sim$ 1107 cm^{-1} is assigned to the overlapping of νSiO_{ID} and νSiO_{AD} with one to four oxygen atoms inserted into Si back bonds and νSiO_{CM} with three and four oxygen atoms inserted into Si-Si dimer and/or Si back bonds. By decreasing the temperature to 268 K, although the majority of the features are largely unchanged over the entire temperature range, there are three slight changes in the spectra: (1) the structure consisting of three peaks at 2198, 2185, and 2141 cm^{-1} changes to one broad band with a maximum at 2162 cm^{-1}, (2) the peak position in the broad band at around 1100 cm^{-1} changes from 1107 to 1085 cm^{-1}, and (3) the height of the 982 cm^{-1} peak decreases to

almost the same level as that of the 963 cm^{-1} peak. These changes are explained by considering that the frequency of the oxygen atom migration across the back bonds, that is, the populations of (OO,OO) structures are reduced with decreasing temperature [7]. Considering the effects of the substrate temperature and the surface selection rule, the spectrum observed by Weldon et al at 220 K [7] is consistent with the present results.

Figure 5.4 shows dependence of the integrated absorbance on hydrogen dose D for the 2114 cm^{-1} ($\nu SiH_{CM(M)} + \nu SiH_{CM(O,M)}$) and 982 cm^{-1} (δ $SiH_{AD(OO)}$, δ $SiH_{AD(OO,O)}$ and δ $SiH_{AD(OO,OO)}$) bands in the reaction 2H + H_2O/Si(100)-(2×1) at Tm = 373 K. The 2×1 RHEED pattern starts to become diffuse and disappear at D larger than 100 L. Since the 5 L exposure of water gives the IR spectrum with saturation adsorption features agreeing with the known initial surface structure with H and OH passivating the dangling bonds of the same dimer [3]. Hence it is reasonable to assume in the present experiments that the initial surface species, which react with atomic hydrogen, are H-Si-Si-OH dimer units, some of which have hydrogen bonding interactions with the neighboring dimer units [6]. Therefore, the hydrogen exposure dependence of the 2114 cm^{-1} peak at D less than 100 L is well explained by the reaction H-Si-Si-OH + 2H → H-Si-O-Si-H or H-Si-Si(O)-H + H_2 suggested by Weldon et al [7]. On the other hand, since the 982 cm^{-1} band increases independent on the intensity of the 2114 cm^{-1} peak at D less than 100 L, it is concluded that there exists a new hydrogen atom-induced oxidation mechanism; H-Si-Si-OH + 2H → SiH_2 + $Si(O)H_2$, followed by the formation of the doubly O-inserted SiH_2 through the inter-dimer oxygen atom migration. The increase of 982 cm^{-1} peak with decreasing 2114 cm^{-1} peak at D larger than 100 L suggests that the O-inserted dihydride species are also formed by the hydrogen atom-induced reaction of O-inserted dimer species such as H-Si-O-Si-H + 2H → SiH_2 + $Si(O)H_2$. The observed IRRAS spectra show that double oxygen insertion is clearly favored over single oxygen insertion. This is reasonable from thermo-dynamical viewpoint. The calculated energy of AD(OO) shown in Fig. 5.1(k) is 0.449 eV and 0.438 eV lower than those of AD(O,O) of Fig. Fig. 5.1(g) and AD(O,O') of Fig. 5.1(h), respectively. Also, CM(OO) is 0.561 eV and 0.509 eV more stable than the respective enrgies of CM(O,O) and CM(O,O').

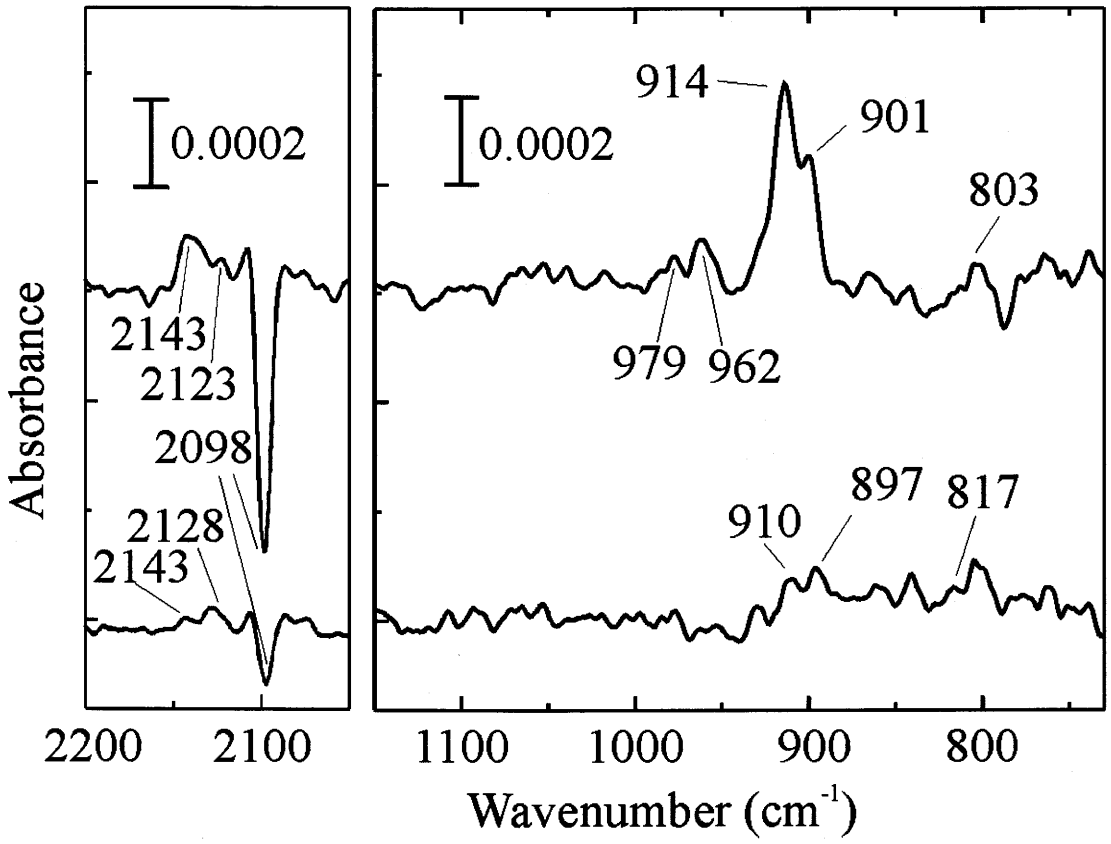

Figure 5.5: Observed BML-IRRAS spectrum of the reaction system H_2O + H/Si(100)-(2×1) at Tm = 373 K for D = 2000 L (upper) and D = 100 L (lower).

Figure 5.5 shows the observed BML-IRRAS spectra for 100 L and 2000 L water exposures to H/Si(100)-(2×1) surface at 373 K. The ideally hydrogen terminated Si(100)-2×1 surface H-Si-Si-H is selected as background. The negative peak at 2098 cm^{-1} indicates that the decomposition of coupled monohydride when the surface is irradiated by water. At low water dose region, the peaks at 897 cm^{-1} and 910 cm^{-1} is assigned to isolated dihydride and adjacent dihydride, respectively. Similarly, the peaks at 901 cm^{-1} and 914 cm^{-1} is assigned to isolated dihydride and adjacent dihydride for high water dose, respectively. Both of these peak position shift to low frequency region. It is caused by low coverage of these species at low dose region. The peak at 2128 (2123 at high dose region) cm^{-1} is assigned to the combination of coupled monodydride stretching vibration with one oxygen inserted to the Si-Si dimer (ν Si-$H_{CM(M)}$ (calc. = 2118 cm^{-1})

and ν Si-$H_{CM(O,M)}$ (calc. = 2120 cm^{-1})). The 2143 cm^{-1} peak is assigned to the overlapping of the perpendicular components of coupled monohydride νSiH with two oxygen atoms inserted to same silicon back bond ($\nu SiH_{CM(OO,OO)}$ (calc. = 2148 cm^{-1}), $\nu SiH_{CM(OO,O)}$ (calc. = 2147 cm^{-1}) and $\nu SiH_{CM(OO)}$ (calc. = 2154 cm^{-1})). The peaks at 962 and 979 cm^{-1} are clear at high water dose region. The peak at 963 cm^{-1} is assigned to the isolated dihydride species (H-$Si(O)_2$-H) with two oxygen atoms in the silicon back bonds. The peak at 982 cm^{-1} is related to the three adjacent dihydride species with two oxygen atoms inserted into the back bonds of the same silicon atom (Fig. 5.1(i), 5.1(k) and 5.1(l)). These two peaks are weak compared to those observed in the H + H_2O/Si(100) reaction system. We have carried out the reaction path analysis for 2H + H_2O/Si(100)-(2×1) and H_2O + H/Si(100)-(2×1) systems and found that SiH_2 + SiH(OH) is a metastable state common in these oxidation reactions. The oxygen insertion reaction, SiH_2 + SiH(OH) → SiH_2 + Si(O)H_2 proceeds by barrier free in the system, 2H + H_2O/Si(100)-(2×1). On the other hand, in the system, H_2O + H/Si(100)-(2×1), however, the oxygen insertion reaction occurs through the tunneling effects. This difference qualitatively agrees with the difference of the observed IRRAS spectra between Fig. 5.2 (doubly oxygen inserted peak is strong) and Fig. 5.5 (upper) (doubly oxygen inserted peak is observed, but very weak).

Figure 5.6 shows IRRAS spectra observed in the reaction system using deuterium instead of hydrogen , 2D + H_2O/Si(100), at Tm = 373 K for D = 100 L and 2000 L. The most important feature is that no Si-H related stretching (2100 ∼ 2200 cm^{-1}) and scissoring (900 ∼ 1000 cm^{-1}) vibrational peaks exist, and, on the other hand, the Si-O stretching vibrational modes are observed at a similar frequency range (∼1072 cm^{-1}) as in the case of hydrogen atom exposures (Figs. 5.2 and 5.5). The band observed at 1525 cm^{-1} is assigned to νSiD_{CM} (symmetric stretching of coupled monodeuteride) [17]. These results support the present assignment with the observed bands in Figs. 5.2 and 5.5, and are explained by that the top hydrogen atoms are replaced by atomic deuterium atoms.

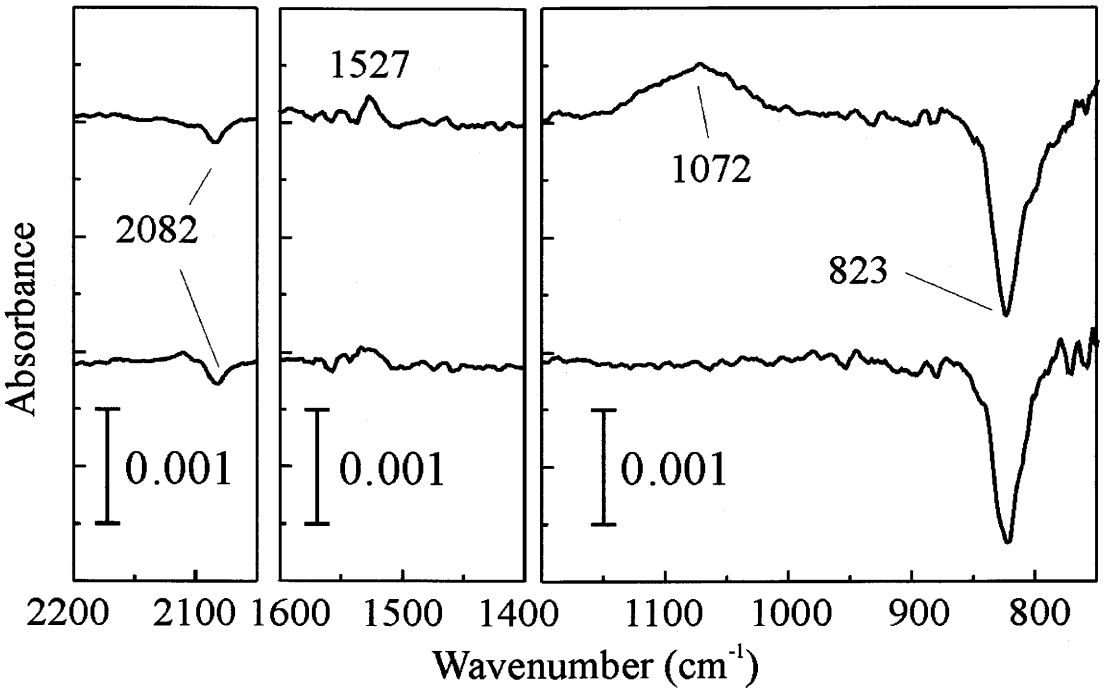

Figure 5.6: Observed BML-IRRAS spectrum of the reaction system D + H_2O/Si(100)-(2×1) at Tm = 373 K for D = 2000 L (upper) and D = 100 L (lower).

5.6 Conclusion

Infrared reflection absorption spectroscopy using buried metal layer substrates (BML-IRRAS) have been employed to study the water related oxidation H + H_2O/Si(100)-(2×1), D + H_2O/Si(100)-(2×1) and H_2O + H/Si(100)-(2×1) systems. Combined with the B3LYP gradient corrected density functional method with the polarized 6-31G** basis set for all atoms, we calculated the IR vibrational frequencies for all possible structural modes. . By comparing the observed peaks with calculations many important peaks are uniquely assigned. The most interesting observations are three pairs of doublet peaks, 901 and 916 cm^{-1}, 926 and 938 cm^{-1}, and 963 and 982 cm^{-1}. These are assigned to δSiH_{ID} and δSiH_{AD} with zero, one and two inserted oxygen atoms at Si back bonds, respectively. And the other peaks of the IR are also clearly assigned. From the studies, we have found that the atomic hydrogen-induced oxidations on water covered Si(100)-

(2×1) surface have different reaction routes depending on the atomic hydrogen dose. At low atomic hydrogen dose region (< 100 L), two types of reaction procedures exist: H-Si-Si-OH + 2H $\longrightarrow$ H-Si-O-Si-H or H-Si-Si(O)-H + H_2 and H-Si-Si-OH + 2H $\longrightarrow$ SiH_2 + $Si(O)H_2$. At high atomic hydrogen dose region (> 100 L), H-Si-O-Si-H + 2H $\longrightarrow$ SiH_2 + $Si(O)H_2$ takes place and followed by further oxygen aggregation, $Si(O)H_2$ + $Si(O)H_2$ $\longrightarrow$ $Si(O)_2H_2$ + SiH_2. The double oxygen insertion is clearly favored over single oxygen insertion confirmed by experimental investigation as well as theoretical calculations. We have carried out the reaction path analysis for 2H + H_2O/Si(100)-(2×1) and H_2O + H/Si(100)-(2×1) systems and found that SiH_2 + SiH(OH) is a metastable state common in these oxidation reactions. The oxygen insertion reaction, SiH_2 + SiH(OH) $\rightarrow$ SiH_2 + $Si(O)H_2$ proceeds by barrier free in the 2H + H_2O/Si(100)-(2×1) system. On the other hand, in the system, H_2O + H/Si(100)-(2×1), however, the oxygen insertion reaction occurs through the tunneling effects.

Bibliography

[1] K. RAGHAVACHARI, Y. J. CHABAL, and L. M. STRUCK, *Chem. Phys. Lett.* **252**, 230 (1996).

[2] R. KONEČNÝ and D. J. DOREN, *J. Chem. Phys.* **106**, 2426 (1997).

[3] M. K. WELDON, B. B. STEFANOV, K. RAGHAVACHARI, and Y. J. CHABAL, *Phys. Rev. Lett.* **79**, 2851 (1997).

[4] B. B. STEFANOV, A. B. GUREVICH, M. K. WELDON, K. RAGHAVACHARI, and Y. J. CHABAL, *Phys. Rev. Lett.* **81**, 3908 (1998).

[5] L. M. STRUCK, J. E. JR., B. E. BENT, G. W. FLYNN, Y. J. CHABAL, S. B. CHRISTMAN, E. E. CHABAN, K. RAGHAVACHARI, G. P. WILLIAMS, K. RADERMACHER, and S. MANTL, *Surf. Sci.* **380**, 444 (1997).

[6] A. B. GUREVICH, B. B. STEFANOV, M. K. WELDON, Y. J. CHABAL, and K. RAGHAVACHARI, *Phys. Rev. B* **58**, 13434 (1998).

[7] M. K. WELDON, K. T. QUEENEY, A. B. GUREVICH, B. B. STEFANOV, Y. J. CHABAL, and K. RAGHAVACHARI, *J. Chem. Phys.* **113**, 2440 (2000).

[8] V. M. BERMUDEZ, *J. Vac. Sci. Technol. A* **10**, 152 (1992).

[9] A. YOSHIGOE, K. MASE, Y. TSUSAKA, T. URISU, Y. KOBAYASHI, and T. OGINO, *Appl. Phys. Lett.* **67**, 2364 (1995).

[10] Y. KOBAYASHI and T. OGINO, *Surf. Sci.* **368**, 102 (1996).

[11] Z.-H. WANG, H. NODA, Y. NONOGAKI, N. YABUMOTO, and T. URISU, *Surf. Sci.* **502** (2002).

[12] R. WALSH, *Acc. Chem. Res.* **14**, 246 (1981).

[13] C. LEE, W. YANG, and R. G. PARR, *Phys. Rev. B* **37**, 785 (1988).

[14] M. J. F. ET AL.

[15] M. CHANDER, Y. Z. LI, J. C. PATRIN, and J. H. WEAVER, *Phys. Rev. B* **48**, 2493 (1993).

[16] H. NODA and T. URISU, *Chem. Phys. Lett.* **326**, 163 (2000).

[17] Y. J. CHABAL and K. RAGHAVACHARI, *Phys. Rev. Lett.* **53**, 282 (1984).

Chapter 6

Summary

The dependence of the line width of the coupled monohydride symmetric stretching vibration on the H-terminated Si(100)-(2×1) surface as a function of temperature and hydrogen exposure has been investigated by BML-IRRAS. Even for nearly ideally H-terminated Si(100) surface, the line width changes significantly depending on the the hydrogen exposure and the exposure temperature. The minimum line width observed on the nearly ideally H-terminated surface at around 670 K and 500 L of the hydrogen exposure agrees or even better than the reported homogeneous line width determined by the dephasing effects. The dependence of the line width broadening on the hydrogen exposure and the temperature on nearly ideal H-terminated regions can not be explained by either dephasing effects or inhomogeneities due to the coexistence of higher hydrides, or contaminations by the residual water. The line width broadening is also not due to the surface roughness induced by the hydrogen etching. We suggest that the line width broadening is essentially caused by subsurface hydrogen.

We have carried out a number of experiments to investigate the presence of subsurface hydrogen and its affect on the infrared line width broadening. The Si(100) surface was initially cleaned by flashing it to high temperature ($\sim$ 1150 K) and exposed to 5000 L atomic deuterium at about 670 K. Then the surface silicon deuterides were completely replaced by exposing 500 L atomic hydrogen at 620 K. The sample was then annealed for one minute at fixed higher temperatures in order to check the reappearance of surface deuterium from silicon bulk by IR at 1525 cm^{-1}. We find that with increasing annealing temperatures, the de-

composition rate of coupled monohydride (νSi-H_{CM}) characterized by 2098 cm^{-1} becomes faster. This is simultaneously followed by the appearance of coupled monodeuteride peak at 1525cm $^{-1}$ which can only be explained by the diffusion of deuterium atoms from silicon bulk to the surface at higher annealing temperatures.

We have also measured the amount of deuterium incorporated into the Si bulk by conventional TPD experiment for the samples prepared by the similar process of deuterium exposure and replacement by hydrogen as described above. The νSi-H_{CM} IR line width, separately measured for 500 L hydrogen exposure, is found to increase from 2.1 cm^{-1} at 673 K to 3.2 cm^{-1} at 598 K which is roughly in proportion to the amount of deuterium atoms incorporated in the Si bulk as determined by TPD measurements. Similarly, by keeping the exposure temperature constant, for example at 673 K, the IR peak width broadening occurs from 2.1 cm^{-1} at 500 L to 2.5 cm^{-1} at 1000 L of hydrogen exposure. We have done several of these measurements to confirm these trends.

The IR and TPD experiments clearly demonstrate that the diffusion of hydrogen atoms does occur into the Si(100) bulk and causes the inhomogeneous broadening of the IR line width.

The interaction of water with hydrogen-terminated Si(100) surface is studied by BML-IRRAS technique. Nearly ideally H-terminated Si(100) surfaces were prepared by exposing the clean Si(100) surface to 500 L hydrogen at 650 K. These surfaces were exposed to controlled amount of water and the changes occurring on the surfaces were monitored by BML-IRRAS as a function of the water exposure. The surface oxidation of Si has been observed due to water adsorption and it is concluded that the nearly ideally H-terminated Si(100) surface is still quite reactive with water. However, it has also been noted that the reactivity of H-terminated surface has diminished due to the passivation effect of the surface hydride layer on Si against the background water in the ultrahigh vacuum.

In the present work, the BML-IRRAS has been used to investigate the atomic hydrogen-induced oxidation on the water-adsorbed Si(100)-(2×1) surface over a wide range of temperatures (268∼373 K) and exposures of atomic hydrogen. A series of bending modes consisting of oxidized and nonoxidized SiH_2, which are not observed or very week by the ET geometry because of its low sensitivity to

the perpendicular component, are observed clearly for the first time, and a new oxidation mechanism is proposed.

Combined with well-documented B3LYP gradient corrected density functional method most IRRAS experimental peaks are uniquely assigned. Three pairs of doublet peaks, 901 and 916 cm^{-1}, 926 and 938 cm^{-1}, and 963 and 982 cm^{-1} are assigned to δSiH_{ID} and δSiH_{AD} with zero, one and two inserted oxygen atoms at Si back bonds, respectively. The small peaks observed at $990 \sim 1050$ cm^{-1} range are assigned to the SiO stretching mode of coupled monohydrides with one to three oxygen atoms at the Si back bonds and/or the Si-Si dimer bond. The other peaks located at high frequency region are also clearly assigned.

From these studies, we have found that the atomic hydrogen-induced oxidations on water covered Si(100)-(2×1) surface have different reaction routes depending on the atomic hydrogen dose. At low atomic hydrogen dose region (< 100 L), H-Si-Si-OH + 2H $\longrightarrow$ H-Si-O-Si-H or H-Si-Si(O)-H + H_2, proposed by Weldon et al. and a new reaction route H-Si-Si-OH + 2H $\longrightarrow$ SiH_2 + $Si(O)H_2$ are main reaction routes. At hydrogen exposures greater than 100 L, H-Si-O-Si-H + 2H $\longrightarrow$ SiH_2 + $Si(O)H_2$ takes place and followed by further oxygen aggregation, $Si(O)H_2$ + $Si(O)H_2$ $\longrightarrow$ $Si(O)_2H_2$ + SiH_2. The observed IRRAS spectra show that double oxygen insertion is favored over single oxygen insertion which also confirmed by theoretical calculations.

Chapter 7

List of Publications

(1) **"IR line width broadening at nearly ideal H-termination region on Si(100)-(2×1) surfaces"**
Z.-H. Wang, H. Noda, Y. Nonogaki, N. Yabumoto, T. Urisu *Surf. Sci.* **502-503** (2002) 86-90
(2) **"Hydrogen Diffusion and Chemical Reactivity with Water on Nearly Ideally H-terminated Si(100) Surface"**
Z.-H. Wang, H. Noda, Y. Nonogaki, N. Yabumoto, T. Urisu *Jpn. J. Appl. Phys.* **41** (2002) 4275-4278
(3) **"Atomic Hydrogen-induced Oxidation on Water-adsorbed Si(100)-(2×1) Surfaces"**
Z.-H. Wang, T. Urisu, S. Nanbu, J. Maki, M. Aoyagi, H. Watanabe, K. Ooi Being submitted for publication at Physical Review Letter.

Presentations at International Conference

(1) **"Hydrogen Diffusion into the Bulk at Nearly Ideal H-Terminated Region on Si(100) Surfaces"**
Z.-H. Wang, H. Noda, Y. Nonogaki, T. Urisu in *14th International Microprocesses and Nanotechnology Conference 2001* in Matsue, on October 31 - November 2, 2001
(2) **"Nearly Ideally Hydrogen-terminated Si(100) Surface and Spectrum Width Broadening Due to Hydrogen Diffusion into the Subsur-**

face"

Z.-H. Wang, H. Noda, Y. Nonogaki, T. Urisu in *10th International Conference on Vibrations at Surface* in Saint Malo-France, on June, 17-21, 2001

Award

"Hydrogen Diffusion into the Bulk at Nearly Ideal H-Terminated Region on Si(100) Surfaces"

MNC 2001 Award for Most Impressive Presentation

Presented at the 14th International Microprocesses and Nanotechnology Conference, 2001 in Matsue, on October 31 - November 2, 2001

Z.-H. Wang, H. Noda, Y. Nonogaki, T. Urisu

Acknowledgment

The research work reported in this thesis has been done under the guidance of Prof. Urisu Tsuneo, Institute for Molecular Science (IMS). I am grateful to him for his encouragement during the course of these investigations. He has been very patient and kind to me when I had troubles in experiments and living life. I express my sincere gratitude to him for providing me personal help and inspiration to complete my thesis work. I always felt that I am working in my hometown, not aboard. He also taught me the experimental skills and the joy of doing surface science experiments precisely. It will always be a great pleasure for me to cherish my association with him.

I would like to thank Heiwa Nagajima Foundation which give me scholarship support. Based on this I can concentrate my research works and studies.

I sincerely thank Dr. Nonogaki Youichi who is an Assistant Professor in our group. He has helped me a lot in many of my experiments and related activities. I have had many experimental and personal discussions with him and got benefited to a great extent. He has always been a bridge between me and the Japanese salesmen in booking experimental instruments.

I would like to thank Dr. Noda Hideyuki who is currently working in Central Research Laboratory of Hitachi Ltd for providing me initial support and help to understand the experimental procedures in the laboratory.

I sincerely thank Dr. Sam Dylan More who now joined Mitsui Ltd for his comments and advise. He always came up with new ideas and discussions.

I would like to thank my very dear friend Dr. G. Ranga Rao, Department of Chemistry, Indian Institute of Technology, Chennai, India, currently a Visiting Professor of IMS, for his comments and advises on my thesis. He has taught me many skills of scientific expression for manuscript and thesis preparation. It has been a nice experience for me to interact with him and learn more about scientific world.

I would like to acknowledge the kind support offered by Dr. Watanabe Hidekazu and Dr. Ooi Kenta of National Institute of Advanced Industrial Science and Technology and Dr. Nanbu Shinkoh, Dr. Maki Jun and Prof. Aoyagi Mutsumi of IMS. But for their help in theoretical calculations, it would have been difficult

for me to arrive at the correct assignments of IR spectra.
It is a pleasure to associate with Dr. Yabumoto Norikuni of NTT Advanced Technology Corporation to carry out TPD experiments. I thank him for valuable discussions.
It has been a great pleasure for me to interact with Prof. Changshun Wang, Visiting Professor and Dr. Yanjun Li of Visiting Scientist of IMS on many occasions in IMS.
My sincere thanks are also due to the doctoral students of Prof. Urisu group, Mr. Fujiki Satoshi, Mr. Takizawa Morio, Mr. Yamamura Shusaku, Mr. Kim Yoon hoon and Mr. Md. Mashuir Rahman. We have been together most of the time in the laboratory doing experiments, discussing things, playing tennis and going out for eating.
I would like to thank sincerely Mrs. Nagasono Hisayo, Secretary of Foreign Affair of IMS, Ms. Nagaii Miho, Staff of the Graduate University for Advanced Studies and Mrs. Shimizu Atsuko, Secretary of Urisu group for helping me in several occasions to fill up important documents related to my research studies and also living in Okazaki. They have always shown keen interest in helping me.
Mr. Yamamoto Yoshihiro and Mrs. Nagada Kayo have been my Japanese teachers in Okazaki International Association (OIA) and taught me a great deal of Japanese language, culture, history and society. I always felt very happy and cheerful to meet them.
The staff of IMS are very special and kind to foreign students. I always felt homely to live in Okazaki and work in IMS because of their "ready to help" approach.
I fondly remember the silent contributions made by my wife, Chenqi, my daughter and my parents. They are my source of happiness, motivation and drive to achieve something worthwhile in life.